

Universidade de São Paulo  
Instituto de Física

## **Estudando a Natureza do Bóson de Higgs**

Matheus Martines de Azevedo da Silva



Orientador: Prof. Dr. Oscar J. P. Éboli.

Dissertação de mestrado apresentada ao Instituto de Física como requisito parcial para a obtenção do título de Mestre em Ciências.

Banca Examinadora:

Prof. Dr. Oscar J. P. Éboli (IF/USP)  
Prof. Dr. Ricardo D'Elia Matheus (IFT/UNESP)  
Prof. Dr. Thiago R. F. P. Tomei (IFT/UNESP)

São Paulo  
2022

**FICHA CATALOGRÁFICA**  
**Preparada pelo Serviço de Biblioteca e Informação**  
**do Instituto de Física da Universidade de São Paulo**

Silva, Matheus Martines de Azevedo da

Estudando a natureza do bóson de Higgs/On the nature of the Higgs boson. São Paulo, 2022.

Dissertação (Mestrado) – Universidade de São Paulo. Instituto de Física. Depto. de Física Matemática.

Orientador: Prof. Dr. Oscar José Pinto Éboli

Área de Concentração: Física de partículas elementares e campos

Unitermos: 1. Bóson de Higgs; 2. Teoria quântica de campos; 3. Teoria de campos; 4. física teórica.

USP/IF/SBI-024/2022

University of São Paulo  
Physics Institute

## **On the nature of the Higgs boson**

Matheus Martines de Azevedo da Silva

Supervisor: Prof. Dr. Oscar J. P. Éboli.

Dissertation submitted to the Physics Institute of the University of São Paulo in partial fulfillment of the requirements for the degree of Master of Science.

Examining Committee:

Prof. Dr. Oscar J. P. Éboli (IF/USP)  
Prof. Dr. Ricardo D'Elia Matheus (IFT/UNESP)  
Prof. Dr. Thiago R. F. P. Tomei (IFT/UNESP)

São Paulo  
2022



---

# ACKNOWLEDGMENTS - AGRADECIMENTOS

Quando me recordo dos últimos dois anos percebo a importância de diversas pessoas ao meu redor que me ajudaram nesta caminhada. Primeiramente, gostaria de agradecer a minha família, em especial ao meus pais e ao meu irmão, por terem tido paciência comigo durante esses anos.

Não posso deixar de agradecer ao Professor Enrico Bertuzzo e à Professora Renata Funchal por terem moldado minha formação.

Também preciso agradecer aos meus amigos Diogo e João Pedro pelas situações divertidas que passamos durante a nossa graduação, e aos meus colegas e amigos de departamento Pedro, Antonio, Gabriel, Gustavo, Ana, Peter e Natália, por tornarem os horários de almoço pós-pandemia sempre agradáveis.

Em particular, gostaria de agradecer meus amigos e colegas Ana Foguel, Gustavo Sadao e Luighi Leal, por todas as discussões sobre física e, sobretudo, ao companheirismo que tivemos ao longo da pandemia.

Finalmente, gostaria de dedicar esse trabalho a duas pessoas que tiveram um papel fundamental neste início da minha carreira acadêmica. Primeiro, à Professora Maria Concepcion Gonzalez-Garcia, que aceitou me orientar durante dois meses que passei em Barcelona, onde tive uma das melhores experiências da minha vida. Por último, ao meu orientador Professor Oscar J. P. Éboli por toda a orientação e ao apoio durante esses dois anos e aos que virão.

O presente trabalho foi realizado com apoio do CNPq, Conselho Nacional de Desenvolvimento Científico e Tecnológico - Brasil, processo 131133/2020-9, e da FAPESP, Fundação de Amparo à Pesquisa do Estado de São Paulo, processo 2020/02250-8.



---

# ABSTRACT

The goal of this project is to study the nature of the Higgs boson, that is, to verify whether the Higgs boson belongs to a  $SU(2)_L$ , as in the Standard Model, or whether it is a singlet under this symmetry, as predicted by dynamical symmetry breaking models. Using the available experimental data, we analyze the Higgs couplings to gauge bosons as well as triple gauge boson couplings in order to test the nature of the Higgs.

**Keywords:** Higgs boson; Large Hadron Collider; Effective Lagrangians.





---

# RESUMO

O objetivo deste projeto é analisar a natureza do bóson de Higgs, a saber, se ele pertence a um dubleto de  $SU(2)_L$  como no modelo padrão, ou se o Higgs é um singleto desta simetria, o que ocorre, por exemplo, em modelos de quebra dinâmica de simetria. Utilizando os dados experimentais disponíveis, analisaremos os acoplamentos do Higgs com bósons vetoriais, bem como os acoplamentos tríplexes de gauge, para testar a natureza do bóson de Higgs.

**Palavras Chave:** Bóson de Higgs; Large Hadron Collider; Lagrangianas efetivas.



---

# LIST OF FIGURES

1.1	Feynman diagrams for the $\phi\phi \rightarrow \phi\phi$ scattering at tree-level. . . . .	19
1.2	Feynman diagrams for the $\phi\phi \rightarrow \phi\phi$ scattering proportional to $\lambda$ and $\lambda^2$ . . . . .	22
1.3	Feynman diagrams for the $\phi\phi \rightarrow \phi\phi$ scattering proportional to $\kappa^2$ . . . . .	22
1.4	Figure extracted from [28]. The matching procedure was done in a scale $\Lambda$ , the RGEs were used to run the Wilson coefficients down to a scale $m_W$ , where the EFT should be use to make precision tests. . . . .	26
2.1	Feynman diagrams for $h \rightarrow \gamma\gamma$ decay. . . . .	39
2.2	Feynman diagrams for $h \rightarrow gg$ decay. . . . .	39
5.1	Distribution of the invariant mass of the $WZ$ system for the $WZ$ pair production from CMS $WZ$ . The yellow region represents the SM signal for $WZ$ pair production, while the remaining regions represent background processes. A few values of the SM prediction together with the effect of the Wilson coefficients from the SMEFT basis are also displayed for comparison. . . . .	71
5.2	Definition of STXS Stage1.2 bins for the ggF production mode. . . . .	73
5.3	Definition of STXS Stage1.2 bins for the VBF production mode. . . . .	74
5.4	Definition of STXS Stage1.2 bins for the VH production mode. . . . .	74
5.5	Definition of STXS Stage1.2 bins for the ttH production mode. . . . .	75
5.6	One dimension marginalized projections of $\Delta\chi^2$ for the Wilson coefficients $c_{WW}$ , $c_2$ , $c_3$ , and $c_{13}$ , as indicated in the panels after marginalizing over the remaining fit parameters. The results are shown for the analysis including only the linear contribution of the Wilson coefficients (red curves) as well as up to quadratic contributions (black curves). . . . .	77
5.7	Two dimension marginalized projections of $\Delta\chi^2$ for the Wilson coefficients $c_{WW}$ , $c_2$ , $c_3$ , and $c_{13}$ , as indicated in the panels after marginalizing over the remaining fit parameters. The results are shown for the analysis including only the linear contribution of the Wilson coefficients (solid curves) as well as up to quadratic contributions (dashed curves). . . . .	78

5.8	Two dimension marginalized projections for the Wilson coefficients $c_2$ , $c_3$ , and $c_{WWW}$ , as indicated in the panels after marginalizing over the remaining fit parameters, including (gray curves) and not (red curves) the coefficient $c_{13}$ . The results are shown for the analysis including only the linear contribution of the Wilson coefficients (solid lines) as well as up to quadratic contributions (dashed lines). . . . .	80
5.9	Normalized Fisher Value for the Wilson coefficients that affect TGV. Results for the analysis where we included only the linear (above) and up to the quadratic (below) contribution of the Wilson coefficients. The entries are normalized in such a way that the sum of the diagonal elements of the Fisher matrix for a specific Wilson coefficient is 100. . . . .	82
5.10	One dimension marginalized projections of $\Delta\chi^2$ for the Wilson coefficients $a_4$ , $a_5$ , $a_{17}$ , $a_B$ , $a_W$ , $a_G$ , and $\Delta a_C$ , as indicated in the panels after marginalizing over the remaining fit parameters. The results are shown for the analysis including only the linear contribution of the Wilson coefficients. . . . .	84
5.11	One dimension marginalized projections for the Yukawa couplings $Y_t^{(1)}$ , $Y_b^{(1)}$ , $Y_\tau^{(1)}$ , and $Y_\mu^{(1)}$ , as indicated in the panels after marginalizing over the remaining fit parameters. The results are shown for the analysis including only the linear contribution of the Wilson coefficients. . . . .	85
5.12	Two dimension marginalized projections for the Wilson coefficients $a_{17}$ , $a_4$ , $a_5$ , $a_B$ , and $a_W$ , as indicated in the panels after marginalizing over the remaining fit parameters. The results are shown for the analysis including only the linear contribution of the Wilson coefficients. . . . .	86
5.13	$\Delta\chi^2$ as a function of the Wilson coefficients $a_4$ , $a_5$ , $a_{17}$ , $a_B$ , $a_W$ , $a_G$ , $Y_t^{(1)}$ , $Y_b^{(1)}$ , $Y_\tau^{(1)}$ , $Y_\mu^{(1)}$ , and $\Delta a_c$ as indicated in the panels after marginalizing over the remaining fit parameters. The red (black) line stands for the analysis considering the linear (and quadratic) contributions of the Wilson coefficients. Results extracted from [8]. . . . .	88
5.14	$1\sigma$ and 95% CL (2dof) allowed regions from the Higgs analysis for the combinations $c^2 a_B + s^2 a_W$ and $s^2 a_B - c^2 a_W$ . The results are shown for the analysis including only the linear contributions of the Wilson coefficients (lighter regions) as well as up to quadratic contributions (darker regions). Results extracted from [8]. . . . .	89
5.15	Normalized Fisher Value for the Wilson coefficients that affect the Higgs couplings. Results for the analysis where we included only the linear anomalous contribution. The entries are normalized in such a way that the sum of the diagonal elements of the Fisher matrix for a specific Wilson coefficient is 100. . . . .	89
5.16	Correlation Matrix for the Higgs Branching Ratios. Results for the analysis where we included only the linear anomalous contribution. . . . .	90
5.17	Correlation Matrix for the Higgs Production Cross-Sections normalized by the total production cross-section. Results for the analysis where we included only the linear anomalous contribution. . . . .	91
5.18	One-dimensional marginalized projection of the $\Delta\chi^2$ for the Higgs branching ratios (BRs). . . . .	92

5.19	Two dimension marginalized projections for the Higgs Branching Ratios $\text{BR}(H \rightarrow ZZ^*)$ , $\text{BR}(H \rightarrow WW^*)$ , and $\text{BR}(H \rightarrow Z\gamma)$ , as indicated in the panels after marginalizing over the remaining fit parameters. . . . .	93
5.20	One- and two- dimensional marginalized projections of the $\Delta\chi^2$ for the Higgs production cross sections as indicated on the panels. . . . .	95
5.21	One dimension projection and two dimensional confidence regions for the SS of $H \rightarrow \mu\mu$ and $H \rightarrow Z\gamma$ . . . . .	96
5.22	One dimension projection for the variables $\Sigma_B$ , $\Sigma_W$ , $\Delta_B$ , and $\Delta_W$ after marginalizing with respect to the fit parameters. The results are shown for the analysis including only the linear contribution for the Wilson coefficients. . . . .	97
5.23	Two dimension confidence region for the variables $\Delta_B$ and $\Delta_W$ after marginalizing with respect to the fit parameters. The results are shown for the analysis including only the linear contribution for the Wilson coefficients. . . . .	98



---

# LIST OF TABLES

2.1	Hypercharge values and representations under the SM gauge symmetry for the leptons, quarks, and the Higgs doublet. . . . .	34
3.1	Dimension-six effective operators from [9] affecting TGCs and Higgs physics. .	43
3.2	Dimension-six effective operators from [9] affecting Higgs physics. . . . .	43
4.1	Hypercharge values and representations under the SM gauge symmetry for the leptons, and quarks. . . . .	56
4.2	HEFT operators affecting TGC . . . . .	63
4.3	NLO Bosonic HEFT operators . . . . .	63
5.1	Data sets used for the TGC analysis . . . . .	70
5.2	Table with the generated processes and the typical selection cuts. More details about the selection can be found in the respective papers together with the definition of the kinematical variables. . . . .	72
5.3	Data used for the Higgs analysis . . . . .	76
5.4	Individual and marginalized 95% CL allowed range for the Wilson coefficients. . . . .	77
5.5	95% C.L. allowed range for the Wilson coefficients after marginalizing with respect to only one parameter. The results are shown only for the analysis including the linear contribution of the Wilson coefficients. The individual fit results are shown in the diagonal entries (gray entries) as well as the results taking into account all the parameters in the last column (gray entries) for comparison. . . . .	79
5.6	95% C.L. allowed range for the Wilson coefficients after marginalizing with respect to only one parameter. The results are shown only for the analysis including up to the quadratic contribution of the Wilson coefficients. The individual fit results are shown in the diagonal entries (gray entries) as well as the results taking into account all the parameters in the last column (gray entries) for comparison. . . . .	79

5.7	Allowed 95% C.L. range for the Wilson coefficients $c_2$ , $c_3$ , and $c_{WWW}$ after marginalizing over the remaining fit parameters. The results are shown including and not the coefficient $c_{13}$ on the fit. . . . .	80
5.8	Approximate best-fit values, uncertainties, and correlation matrix for the analysis including only the linear contribution of the Wilson coefficients $c_2$ , $c_3$ , $c_{13}$ , and $c_{WWW}$ . . . . .	83
5.9	95 % Confidence Level for the parameters in the fit. The analysis was made including only the linear contribution of the Wilson coefficients. . . . .	85
5.10	Data used for the Higgs analysis in [8], but absent in Table 5.3. . . . .	87
5.11	Best-fit values, uncertainties, and correlation matrix for the analysis including only the linear contribution of the Wilson coefficients. . . . .	87



---

# CONTENTS

<b>Acknowledgments - Agradecimientos</b>	<b>1</b>
<b>Abstract</b>	<b>3</b>
<b>Resumo</b>	<b>5</b>
<b>Introduction</b>	<b>13</b>
<b>I Theoretical Framework</b>	<b>15</b>
<b>1 Introduction to Effective Field Theories</b>	<b>17</b>
1.1 Tree-level matching . . . . .	18
1.2 Loop-level matching . . . . .	21
1.3 The EFT concept for renormalization . . . . .	26
1.4 The bottom-up approach . . . . .	28
1.5 Digression about symmetries . . . . .	29
<b>2 The Standard Model</b>	<b>33</b>
2.1 The SM Lagrangian . . . . .	33
<b>3 The Standard Model Effective Field Theory</b>	<b>41</b>
<b>4 The Higgs Effective Field Theory</b>	<b>49</b>
4.1 Non-linear realizations . . . . .	49
4.2 Power Counting for HEFT . . . . .	56
4.2.1 Power Counting for $\chi$ PT . . . . .	57
4.2.2 HEFT Basis . . . . .	58
4.3 The HEFT Lagrangian . . . . .	59
4.4 HEFT vs SMEFT . . . . .	63

<b>II</b>	<b>Analysis Framework</b>	<b>67</b>
<b>5</b>	<b>HEFT constraints</b>	<b>69</b>
5.1	TGC data sets . . . . .	69
5.2	Higgs data sets . . . . .	72
5.3	Results . . . . .	76
5.3.1	Triple gauge coupling constraints . . . . .	76
5.3.2	Higgs constraints . . . . .	83
5.4	Discussion and conclusion . . . . .	92
	<b>Conclusions</b>	<b>99</b>

---

# INTRODUCTION

The discovery of the scalar state consistent with the Standard Model (SM) Higgs boson by the CMS and ATLAS Collaboration [1, 2] was a milestone in particle physics. This event, together with the preceding precision tests, has shown that the SM is the best theory to describe the elementary particles and their electroweak and strong interactions.

Even though the SM is compatible with the observed data collected from the LHC and LEP experiments, it is still not able to explain some open problems in physics. Such as Dark Matter and Dark Energy [3], the strong CP problem [4], the mass generation mechanism for the neutrinos, naturalness [5], etc. All these problems show that the the SM is not the end of the history, and more fundamental theories are yet to be found.

Unfortunately, so far we have not seen any direct or indirect evidence pointing to new physics at the LHC. As a result, if we assume the existence of unknown massive particles, they can be heavy in such a way that our current experiments can not access them. Even so, despite being off-shell, they can lead to modifications in kinematical distributions [6] and one possible framework to encode this information is called Effective Field Theories (EFTs).

Nowadays, we have two EFTs for the electroweak and strong interactions. The first one is called Standard Model Effective Theory (SMEFT), which considers the observed Higgs boson embedded in a  $SU(2)_L$  doublet together with the Goldstone bosons from the electroweak symmetry breaking process. Meanwhile, there is another one called Higgs Effective Field Theory (HEFT). In the latter, the Higgs boson is considered to be a singlet of the SM gauge group and it does not belong to a  $SU(2)_L$  doublet. On the other side, the Goldstone bosons transform according to a non-linear realization of the symmetry. Both of these frameworks are discussed by [7], and phenomenological studies using the SMEFT and the HEFT can be found in [8, 9, 10, 11, 12], [13, 14, 8], respectively.

In this work, we use the HEFT Lagrangian to analyze the available LHC Run 2 data affecting the interactions among the electroweak gauge bosons as well as the Higgs interactions. In particular, we investigate the possible (de)correlations present in these two datasets, which can shed light on how the gauge symmetry is realized at low-energies.

This work is divided in two parts. The first introduces the ideas regarding EFTs, where we use a simple toy model to show that a theory constructed only with the light states and symmetries contains the low-energy information of a more complete theory. Also in the first part, both the SMEFT and the HEFT are discussed, together with their main differences. In the second part, using the newest data concerning triple electroweak gauge interactions and the Higgs interactions, we put constraints on the Wilson coefficients of the HEFT Lagrangian. More details about the content discussed in each chapter can be found in the table of contents.

# **Part I**

## **Theoretical Framework**



---

---

# CHAPTER 1

---

## INTRODUCTION TO EFFECTIVE FIELD THEORIES

Effective Field Theory (EFT) is one of the most powerful tools to perform calculations on theoretical physics. Its range of applications can go from Cosmology [15], Condensed Matter [16] to Particle Physics [7]. It allows one to concentrate only on the relevant degrees of freedom and symmetries for a specific energy scale while ignoring all effects that are irrelevant for the observables in question. Furthermore, the precision of the calculations can be improved as needed in a consistent way. All these aspects of EFTs are to be discussed in this section.

As pointed out before, after the Higgs boson discovery by the ATLAS and the CMS Collaborations in 2012 [1, 2], one of the major goals of the LHC was to find new particles. Nevertheless, none has been found so far. Within the current data, no significant deviations from the Standard Model have been observed [8, 9, 10, 11, 12] and, as a consequence, EFT techniques are needed. If we assume the existence of new particles with masses well above the electroweak scale, the new physics effects, despite being off-shell, can change the tail of kinematic distributions [6]. The EFT is the ideal framework to encode this information since it does not carry any UV assumptions. Moreover, any beyond Standard Model theory can be checked by means of a matching calculation, since one is able to translate the bounds from the EFT to the parameters of the full theory. In this work, a model independent path is taken, which we typically call the *bottom-up* approach. The main point of this section is to illustrate, with the help of a simple toy model, why the EFT contains the low-energy behavior of a more complex and involved theory.

The content of this chapter is divided as follows: starting from Sec. 1.1 we will use a toy model to illustrate the important features of an EFT. Once we have finished, in chapter 2 the

Standard Model is described to fix notation and in chapters 3 and 4 the possible ways to parameterize deviations from the electroweak interactions, the SMEFT and the HEFT, are discussed. But before we get into the world of EFTs, I need to say that the amount of literature on the matter is huge, along the way I will cite the ones that help me the most during this master thesis. In any case, I apologize in advance for all the works I have not acknowledged in the text.

## 1.1 Tree-level matching

The whole idea behind the EFTs is to reproduce the low energy behavior of a more complete theory with only a few ingredients: symmetries and degrees of freedom [17, 18]. To show that, we consider a simple toy model consisting of two real scalar fields,  $\phi$  and  $\Phi$ , with masses  $m$  and  $M$ , respectively, satisfying  $M \gg m$  as well. Moreover, the theory has a  $Z_2$  symmetry that acts only on the light field  $\phi$ . The Lagrangian for the model is given by

$$\mathcal{L}^{\text{FULL}} = \frac{1}{2}\partial_\mu\phi\partial^\mu\phi - \frac{1}{2}m^2\phi^2 + \frac{1}{2}\partial_\mu\Phi\partial^\mu\Phi - \frac{1}{2}M^2\Phi^2 - \frac{\lambda}{4!}\phi^4 - \frac{\kappa}{2}\phi^2\Phi - \frac{g}{2}\phi^2\Phi^2. \quad (1.1)$$

Note that the Lagrangian above is incomplete since we could have a cubic and a quartic interaction for  $\Phi$ , but we decided to set these couplings to zero for the sake of simplicity.

Now we can compute some amplitude and take the low-energy limit since we are interested in making predictions at low-energies. In the following, we discuss the elastic scattering  $\phi\phi \rightarrow \phi\phi$ . The diagrams for this process are shown in Figure 1.1, where we took into account only tree-level diagrams.

The full amplitude for this process is

$$i\mathcal{A}^{\text{FULL}} = -i\lambda - i\kappa^2\left(\frac{1}{s-M^2} + \frac{1}{t-M^2} + \frac{1}{u-M^2}\right), \quad (1.2)$$

if we assume  $s, t, u \sim E^2 \sim m^2$ , we can Taylor expand the expression

$$i\mathcal{A}^{\text{FULL}} = -i\lambda + i\frac{\kappa^2}{M^2}\left(3 + \frac{4m^2}{M^2} + \frac{s^2 + t^2 + u^2}{M^4} + \mathcal{O}\left(\frac{E^6}{M^6}\right)\right), \quad (1.3)$$

$$\simeq -i\lambda + i\frac{3\kappa^2}{M^2}, \quad (1.4)$$

where we used  $s + t + u = 4m^2$  and we truncated the expansion at leading order. Also it is important to remember that the parameter  $\kappa$  has mass dimension, *i.e.*  $[\kappa] = 1$ . Details on how to read the Feynman rules and evaluate the amplitudes can be found in [19, 20].

Looking at equation (1.3), the ratio  $E^2/M^2$  dictates the precision that we want to achieve



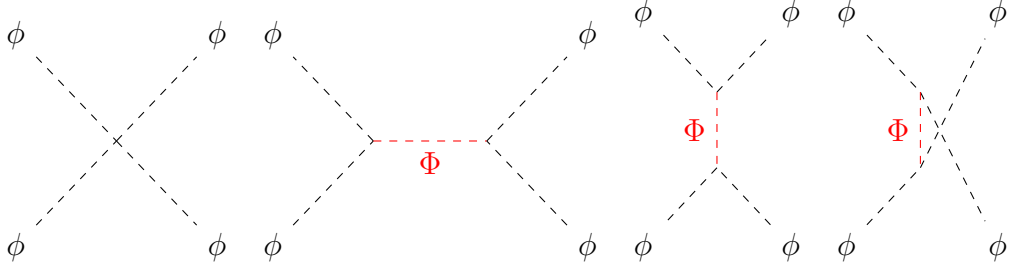


Figure 1.1: Feynman diagrams for the  $\phi\phi \rightarrow \phi\phi$  scattering at tree-level.

in the computation of the amplitude. When we write down our effective Lagrangian we will organize the operators in terms of mass dimensions. The same ratio  $E^2/M^2$  is going to be the parameter controlling the expansion of the effective interactions. In other words, if the amplitude  $\mathcal{A}^{\text{FULL}}$  is computed with precision up to  $\mathcal{O}(E^2/M^2)$  we need to account for effective interactions that give contributions up to the same order. This is typically called the Power Counting. More details about it are discussed in Chapter 4.

We can reproduce the same low energy effects of the full theory by means of an effective Lagrangian that only contains the light particle. Since the full theory has a  $Z_2$  symmetry acting on the light fields, we must impose it in the EFT as well. If we are only interested in the leading order terms, the ones in equation (1.4), the effective Lagrangian that respects the symmetries restrictions is [21]

$$\mathcal{L}_0^{\text{EFF}} = \frac{1}{2} \partial_\mu \phi \partial^\mu \phi - \frac{1}{2} m^2 \phi^2 - \frac{C_0}{4!} \phi^4. \quad (1.5)$$

To find out how to express  $C_0$  in terms of the parameters of the full theory we need to equate the amplitude (1.3) and the one computed with the Lagrangian above,

$$i\mathcal{A}^{\text{EFF}} = i\mathcal{A}^{\text{FULL}}, \quad (1.6)$$

which gives

$$C_0 = \lambda - \frac{3\kappa^2}{M^2}. \quad (1.7)$$

If we want the next leading order term we need to add a few more interactions to our Lagrangian up to dimension six [21],

$$\mathcal{L}_1^{\text{EFF}} = -\frac{1}{6!} \frac{1}{M^2} C_{1,0} \phi^6 - \frac{1}{4} \frac{1}{M^2} C_{1,1} \phi^2 (\partial^2 \phi^2). \quad (1.8)$$

The  $C$ 's are called Wilson coefficients, and here we already made it dimensionless by introducing the term  $1/M^2$ . Note that at this order we could also think about the term  $\partial_\mu \phi^2 \partial^\mu \phi^2$ , but this

is related to the second one in (1.8) by integration by parts, so its contribution can be absorbed in the coefficient  $C_{1,1}$ .

Following the same reasoning from [17], let us check whether the terms in (1.8) can really reproduce the expected behavior we are seeking. First, we can realize that each derivative acting on  $\phi$  scales within the energy regime in which the process is being probed, *i.e.*  $\partial_\mu \sim E$ . Invoking the uncertainty principle, we can notice that  $x_\mu \sim 1/E$  and  $d^4x \sim 1/E^4$ . If we are working with a weakly coupled effective theory it is reasonable to assume the kinetic term to be the leading term in an  $E/M$  expansion. This requirement fixes the scaling of  $\phi$ :

$$\int d^4x \frac{1}{2} \partial_\mu \phi \partial^\mu \phi \sim 1 \rightarrow \phi \sim E. \quad (1.9)$$

Armed up with these rules we can figure out how the terms in (1.8) scale. For example, the first term in the expression scales as:

$$\int d^4x \left\{ -\frac{1}{6!} \frac{1}{M^2} C_{1,0} \phi^6 \right\} \sim \left( \frac{E}{M} \right)^2, \quad (1.10)$$

which has the same order as the next-leading-order term in (1.3) we want to reproduce.

To obtain the values of the new Wilson coefficients in terms of the parameters of the full theory we need to do the same procedure we did before, but up to the order  $(E/M)^2$  with the Lagrangian  $\mathcal{L}_0^{EFF} + \mathcal{L}_1^{EFF}$ . Using the  $\phi\phi \rightarrow \phi\phi$  scattering we can only fix the parameters  $C_0$  and  $C_{1,1}$ :

$$C_0 = \lambda - \frac{3\kappa^2}{M^2}, \quad (1.11)$$

$$C_{1,1} = \frac{1}{2} \frac{\kappa^2}{M^2}. \quad (1.12)$$

To fix the value of the coefficient  $C_{1,0}$  we need to choose a different process in which the corresponding vertex would enter at tree-level. For instance, we could choose the process  $\phi\phi\phi \rightarrow \phi\phi\phi$ .

At this point we see that we can organize the effective Lagrangian in a systematic way, sorting the operators in terms of mass dimensions:

$$\mathcal{L}^{EFF} = \sum_{n=0}^{\infty} \frac{1}{M^{2n}} \sum_{k=0}^{\# \text{ ops}} c_{n,k} \mathcal{O}_{n,k}. \quad (1.13)$$

The index  $n$  represents a specific dimension of the effective operators and the index  $k$  sums over all allowed operators of that dimension. Typically when one is using the effective Lagrangian

to compute observables the series is truncated at order that will give the precision needed.

The process of figuring out how the Wilson coefficients are expressed in terms of the parameters of the full theory by equating amplitudes the way we did is called *Matching* [21]. Note that in the case we studied the parameters of the full theory and the Wilson coefficients do not depend on any scale. This is only the case because we have used tree level diagrams. When loop diagrams come into play we will need to be more careful on this matter. Details about this problem are found in the next section.

When using the EFT attention must be paid to the energy scale where the computation is being performed. Note that the former has a natural cutoff: the mass  $M$ . When the energy of the process under study is reaching the threshold  $M$  all the terms in the expansion (1.13) become important. Hence, we can no longer use it to make perturbative predictions. Whenever this situation occurs it means that the EFT is not a good description anymore and we need to look for a more complete theory.

Before we move on we should point out an alternative strategy to matching: integrating out fields [22]. At tree-level this consists in using the equations of motion to express the heavy field  $\Phi$  in terms of the light field  $\phi$ . Once this is done, the interactions for the field  $\Phi$  are replaced by a series of local interactions with only the light field  $\phi$ . We will not enter in any details about this method, but it has a really interesting interpretation in terms of path integrals that can be found in [23].

## 1.2 Loop-level matching

In the last section we performed a simple matching calculation using only tree-level diagrams and we completely neglected the scale dependence of the couplings. In this section we need to fill in the blanks that have not been clarified yet. For example, at which energy scale the matching procedure should be performed and how we can use the EFT at low energies once the matching has been done.

Again, we will make use of our toy model to evaluate the loop contributions for the  $\phi\phi \rightarrow \phi\phi$  scattering, but now only turning on the following interactions:

$$\mathcal{L}_{\text{Int}}^{\text{FULL}} = -\frac{1}{4}\kappa\phi^2\Phi^2 - \frac{\lambda}{4!}\phi^4. \quad (1.14)$$

The diagrams entering in this process are displayed in Figures 1.2 and 1.3.

The evaluation of loop diagrams is more difficult. One needs to regulate the integrals to keep the divergences under control and define the renormalization procedure [24]. Here we

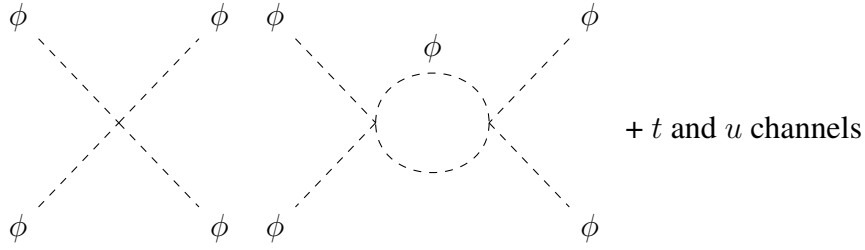


Figure 1.2: Feynman diagrams for the  $\phi\phi \rightarrow \phi\phi$  scattering proportional to  $\lambda$  and  $\lambda^2$ .

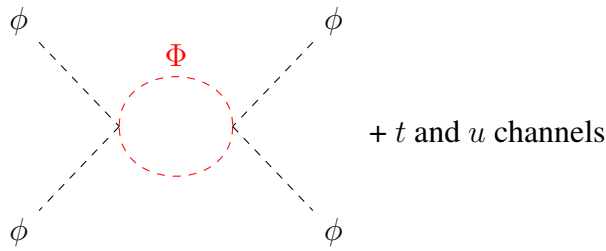


Figure 1.3: Feynman diagrams for the  $\phi\phi \rightarrow \phi\phi$  scattering proportional to  $\kappa^2$ .

are going to use Dimensional Regularization (DR) [25, 26, 24, 21, 20] and we will define our counterterms in the minimum subtraction scheme ( $\overline{\text{MS}}$ ) [21, 20]. Although DR is very abstract with respect to the physical interpretation in comparison to other dimensionful regularization procedures, it does not break any symmetries in all steps of the computation [25] and it also respects the Power Counting [7]. First, we need to evaluate the diagrams in the full theory, and then we will move on to the EFT. Once we have reached this point, we need to be consistent: the conventions used in one must be the same as in the other.

Starting by evaluating the  $s$ -channel proportional to the  $\lambda^2$  contribution, after applying the Feynman rules [27, 19] and the Feynman trick to combine the denominators [21, 19], the amplitude reads

$$i\mathcal{A}_s^{FULL} = \frac{\lambda^2}{2} \int_0^1 dx \int \frac{d^4 l}{(2\pi)^4} \frac{1}{(l^2 - \Delta^2)^2}, \quad (1.15)$$

where the factor  $1/2$  is a symmetry factor and  $\Delta^2 = x(x-1)p^2 + m^2$ , with  $p^2$  being the total four momentum coming from the initial particles. In order to make the calculations easier, we will perform the matching at the threshold limit, which means that the initial and final particles have  $p_i^\mu = (m, \vec{0})$ .

The DR idea consists in deviating the dimension of the integral by a little amount  $\epsilon$  in such a way that we can track down the divergent terms when we take the limit  $\epsilon \rightarrow 0$ . Changing to

$d = 4 - 2\epsilon$  dimensions, the amplitude becomes

$$\begin{aligned}
i\mathcal{A}_s^{FULL} &= \frac{\lambda^2}{2} \mu^{2\epsilon} \int_0^1 dx \int \frac{d^d l}{(2\pi)^d} \frac{1}{(l^2 - \Delta^2)^2}, \\
&= \frac{\lambda^2}{2} \frac{1}{16\pi^2} \int_0^1 dx \left\{ \frac{1}{\epsilon} + \log \frac{\tilde{\mu}^2}{m^2} - \log [4x(x-1) + 1] \right\}, \\
&= \frac{i\lambda^2}{32\pi^2} \left\{ \frac{1}{\epsilon} + \log \frac{\tilde{\mu}^2}{m^2} + 2 \right\},
\end{aligned} \tag{1.16}$$

where we used the formula (3.19) from [21] and defined  $\tilde{\mu} = 4\pi e^{-\gamma_E} \mu^2$ . Note that  $\mu$  is an nonphysical scale introduced to correct the dimensions of the integral. The calculations for the  $t$  and  $u$  channels give similar results, aside from the exclusion of the last factor 2, since in the threshold limit we have  $\Delta^2 = m^2$ . The total amplitude proportional to  $\lambda^2$  is then

$$i\mathcal{A}_{\lambda^2} = \frac{3i\lambda^2}{32\pi^2} \left\{ \frac{1}{\epsilon} + \log \frac{\tilde{\mu}^2}{m^2} + \frac{2}{3} \right\}. \tag{1.17}$$

The evaluation of the diagrams proportional to  $\kappa^2$  are identical, we only need to exchange  $m$  for  $M$ . For the  $s$ -channel, the  $\Delta^2$  reads,

$$\Delta^2 = M^2 \left\{ 4x(x-1) \frac{m^2}{M^2} + 1 \right\} \simeq M^2, \tag{1.18}$$

so the factor 2 in the  $s$ -channel can be dropped. The total amplitude proportional to  $\kappa^2$  is

$$i\mathcal{A}_{\kappa^2} = \frac{3i\kappa^2}{32\pi^2} \left\{ \frac{1}{\epsilon} + \log \frac{\tilde{\mu}^2}{M^2} \right\}. \tag{1.19}$$

Both amplitudes (1.17) and (1.19) contain divergent terms, so we need to define our counterterms in a way to eliminate them. Our bare parameter  $\lambda^o$  is related to the renormalized one  $\lambda^r$  through the use of the counterterm  $Z$ :

$$\lambda^o = Z\lambda^r, \tag{1.20}$$

when working with a perturbative model the counterterm takes the form [21]

$$Z = 1 + \mathcal{O}(\lambda^r, \kappa^r). \tag{1.21}$$

The  $\overline{\text{MS}}$  scheme tantamounts to letting the counterterm absorb only the divergent piece of the

amplitude. In our case, this implies

$$Z = 1 + \frac{3\lambda}{32\pi^2} \frac{1}{\epsilon} + \frac{3}{32\pi^2} \frac{\kappa^2}{\lambda} \frac{1}{\epsilon}. \quad (1.22)$$

One important feature about the  $\overline{\text{MS}}$  scheme is that the non-physical scale  $\tilde{\mu}^2$  can be understood as the renormalization scale. For a comprehensive discussion on the matter see [20]. From now on,  $\tilde{\mu}^2$  is also the renormalization scale of the theory, and the parameters  $\lambda$  and  $\kappa$  depend on it. Also, we will assume that the parameter  $\kappa$  has been properly renormalized, see [21] for details of the calculation.

Now we can write down the full amplitude for the  $\phi\phi \rightarrow \phi\phi$  scattering at next leading order:

$$i\mathcal{A}^{\text{FULL}} = -i\lambda(\tilde{\mu}) + i\frac{3}{32\pi^2}(\lambda(\tilde{\mu}))^2 \left\{ \log \frac{\tilde{\mu}^2}{m^2} + \frac{2}{3} \right\} + i\frac{3}{32\pi^2}(\kappa(\tilde{\mu}))^2 \log \frac{\tilde{\mu}^2}{M^2}. \quad (1.23)$$

Note that the amplitude is free of divergent terms and all the couplings depend on the running scale  $\tilde{\mu}$ . Another important aspect to observe is the appearance of the logarithm terms. Both of them depend on different mass scales. If we choose a renormalization scale  $\tilde{\mu}$  close to one of the masses,  $m$  for example, the first of them is going to be under control while the other will be a large one, since we have a hierarchy of scales, *i.e.*  $M \gg m$ .

The emergence of logs is an inevitable consequence of the loop calculations. We need to be careful with them because they can spoil perturbation theory before its time if we do not treat it properly [20]. The procedure in which we can resum the large logs and restore the perturbation aspect of the theory is by means of the Renormalization Group Equations (RGE) [20, 27]. As pointed out by [21], not even the RGE will solve the problem we have encountered in (1.23), because the differential equations for both parameters do not depend on the mass  $M$ . Hence, they will not be able to decouple the heavy particle effect as we move to low energies. Here is the time that the EFT approach comes in handy.

To solve the problem we need to perform the matching with an EFT that only contains the light particle  $\phi$ . For the case in question we only need one interaction:

$$\mathcal{L}_{\text{int}}^{\text{EFT}} = -\frac{C}{4!}\phi^4, \quad (1.24)$$

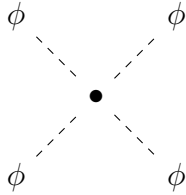
where  $C$  is the Wilson coefficient. Since now the couplings depend on the running scale we must be clear about the scale where the matching is being done. To this purpose, let us define it as  $\tilde{\mu}_M$ .

To perform the matching at one-loop we will use an iterative approach. As a starting value

for the Wilson coefficient, we use the leading order matching relation,

$$C(\tilde{\mu}_M) = \lambda(\tilde{\mu}_M), \quad (1.25)$$

and the discrepancy among the EFT and the full-theory amplitude can be eliminated by introducing an additional tree-level diagram in the EFT equal to



$$= i\mathcal{A}^{\text{Match}} = -iC^{\text{Match}}(\tilde{\mu}_M) = i[\mathcal{A}^{\text{Full}} + \mathcal{A}_{\text{c.t.}}^{\text{Full}}] - i[\mathcal{A}^{\text{EFT}} + \mathcal{A}_{\text{c.t.}}^{\text{EFT}}], \quad (1.26)$$

where c.t. stands for the counterterms contributions and  $C^{\text{Match}}$  encodes the one-loop corrections to the Wilson coefficient. Note that the EFT amplitude is the same one as for the full theory, except that we do not include the contributions from the diagrams in Figure (1.3). Then, if we use the relation (1.25) in (1.26) the one-loop corrections to the Wilson coefficient come only from the diagrams with the heavy particle in the loop [21]:

$$C^{\text{Match}}(\tilde{\mu}_M) = -\frac{3}{32\pi^2}(\kappa(\tilde{\mu}_M))^2 \log \frac{\tilde{\mu}_M^2}{M^2}. \quad (1.27)$$

It is crucial to realize that although the loop expansion in the full theory depends on terms of the form  $\log \mu^2/m^2$ , the matching coefficient does not. That is how the EFT matching solve the problem we have encountered before: as long as we choose  $\tilde{\mu}_M \sim M$  we do not have to worry about large logarithms in the matching coefficients.

Now we can update our leading matching relation from (1.25) to

$$C(\tilde{\mu}_M) = \lambda(\tilde{\mu}_M) - \frac{3}{32\pi^2}(\kappa(\tilde{\mu}_M))^2 \log \frac{\tilde{\mu}_M^2}{M^2}. \quad (1.28)$$

Again, it depends only on the mass  $M$ , and we do not have problems with large logarithms as long as we take the matching scale close to the cutoff.

When we are working with EFTs our goal is to make predictions at low energies, which means that we need to use the RGEs to run the parameter  $C$  from the matching scale  $\tilde{\mu}_M$  down to a lower scale  $\tilde{\mu}_L$ . Since we are just giving a brief introduction to the EFT ideas we will not enter into details on how to derive the RGEs, for that we refer the reader to [20, 27, 21]. Here

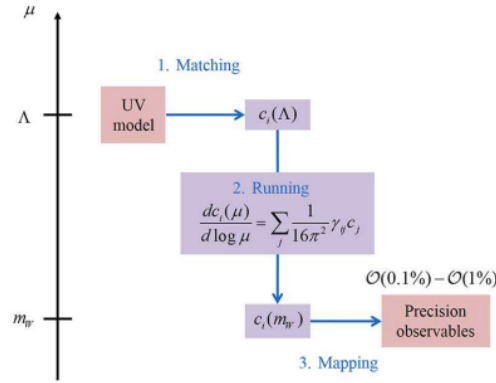


Figure 1.4: Figure extracted from [28]. The matching procedure was done in a scale  $\Lambda$ , the RGEs were used to run the Wilson coefficients down to a scale  $m_W$ , where the EFT should be used to make precision tests.

we just state the RGE for the Wilson coefficient:

$$\frac{dC}{d \log \tilde{\mu}^2} = \frac{3}{32\pi^2} C^2. \quad (1.29)$$

Once the RGE is solved for the boundary condition (1.28) we can evolve the coupling down to the scale  $\tilde{\mu}_L$ . Finally, including the one-loop contributions, our low-energy amplitude is given by

$$i\mathcal{A}^{EFT} = -iC(\tilde{\mu}_L) + i\frac{3}{32\pi^2} C(\tilde{\mu}_L)^2 \left\{ \log \frac{\tilde{\mu}_L^2}{m^2} + \frac{2}{3} \right\}. \quad (1.30)$$

No logarithms depending on  $M$  appear.

Right now we have everything we need to understand the full picture. First, we need to perform the matching at scale  $\tilde{\mu}_M$  close to the cutoff in such a way to avoid the large logarithms in the matching coefficients. Once this has been done, we can use the RGEs inside the EFT to evolve the Wilson coefficients down to an energy scale  $\tilde{\mu}_L$ . Finally, when we are at low energies we can use our EFT to make precision tests. This procedure is known as *Matching, Running and Mapping* [28], and it is schematically described in Figure (1.4).

### 1.3 The EFT concept for renormalization

In the previous sections we performed the matching procedure to obtain the values of the Wilson coefficients in terms of the parameters of the full theory at tree-level and also at loop-level. Once the matching is done, we can compute amplitudes at low-energies with our EFT. Moreover, the calculation can be systematically improved by adding more interactions. In our



toy model, it means that we need to add higher dimensional operators. But one may be concerned about working with non-renormalizable theories where we have to deal with UV divergences.

In the traditional sense, a theory is said to be renormalizable if at any order in perturbation theory divergences from loop integrals can be absorbed in a finite set of parameters [24]. But the EFT concept of renormalization is more relaxed: a theory must be renormalizable order by order in its expansion parameters [17]. Let us try to illustrate what we mean with this last statement.

Consider a real scalar field  $\phi$  and the following interactions

$$\mathcal{L}_{\text{Int}}^{\text{EFT}} = -\lambda\phi^4 + \frac{c}{M^2}\phi^6. \quad (1.31)$$

Here we are considering that the Lagrangian is invariant under the transformation  $\phi \rightarrow -\phi$  and  $M$  is playing the role of the mass of the heavy particle we integrated out to generate the EFT. The first divergence we could think of comes from the four point function and it can be absorbed by the counterterm  $\delta_\lambda$  of the coupling  $\lambda$ :

$$\sim \lambda^2 \quad \text{Renormalized by:} \quad = \delta_\lambda \phi^4.$$

The second comes from the six-point function, note that its amplitude is proportional to  $\lambda c/M^2$  and it can be absorbed by the coupling  $c$ :

$$\sim \lambda \frac{c}{M^2} \quad \text{Renormalized by:} \quad = \frac{\delta_c}{M^2} \phi^6.$$

The last divergent diagram comes from the eight-point function, it is proportional to  $c^2/M^4$ . No parameter of the Lagrangian (1.31) can absorb this divergence. To do so, we would have to add

a interaction proportional to  $\phi^8$ :

$\sim \lambda \frac{c^2}{M^4}$  Renormalized by:  $\sim \phi^8$ .

This is the point where our Power Counting enters to save the day. Since we are ordering the operators in terms of mass dimension and we are keeping only interactions up to  $1/M^2$ , in any amplitude we should only add terms up to the same order, which means that terms proportional to  $1/M^4$  must not be included. As a consequence, this implies that we do not need to add a  $\phi^8$  interaction, because loop divergences renormalized only by it will not be taken into account.

This is what we meant by a renormalizable theory order by order in the expansion parameters. Here we discovered another aspect about EFTs: they are naturally renormalizable once we are consistent with our Power Counting. In a way this reflects the importance of the Power Counting for an EFT, because without it we are not able to use it in a consistent way.

## 1.4 The bottom-up approach

On the preceding sections we discussed some important features about EFTs. First, we discuss how to perform the matching at tree-level, and then we moved to the loop-level matching. In the latter, we saw the importance of EFT techniques to solve the problem of large logarithms introduced through loop effects, and how the heavy particle mass decouples once the matching and running of the Wilson coefficients is done. Lastly, we also saw the EFT concept for renormalization, which pointed out that, even though we are working with non-renormalizable interactions, we can still make predictions thanks to the Power Counting.

The path we have taken up to this section is typically called the *top-down* approach [18, 29]. We had a complete UV model to begin with and we worked out an EFT that could reproduce its predictions at low-energies. In fact, the matching procedure even told us what were the interactions among the light fields that were turned on in the EFT and how the respective Wilson coefficients depended on the parameters of the full theory.

In contrast, when one wishes to be as model independent as possible, the EFT can be built in another way. Knowing the light particles and the symmetries restrictions, we can construct an EFT by establishing interactions among the light fields that preserve the symmetries. To make

sense of the construction, the Power Counting for the operators must be clear. In the example we have studied, the operators were organized in terms of mass dimension, but there may be other possibilities, *e.g.* a derivative expansion for chiral theories. This strategy is called the *bottom-up* approach [29]. In this case, there is no matching procedure, which tells us that the Wilson coefficients are free parameters and their values are only obtained when contrasting the theory with data.

The *bottom-up* approach is the path we will take in this work. All the discussion we made in this section was to motivate that with only a few ingredients, symmetries and degrees of freedom, we can build an EFT. Any UV model that contains those light particles and respects the same set of symmetries at low energies can be matched to the former. In a way, we can see the *bottom-up* approach as the inverse path of that we have taken: we first write down an EFT, then we constrain the Wilson coefficients with the largest dataset possible, and, if it is of one's desire, the constraints obtained can be translated to any UV model through a matching calculation.

## 1.5 Digression about symmetries

Before we move on we would like to make some comments on how symmetries can be realized at low-energies. This discussion is going to be important for the next sections. Unfortunately, to make this comment we need to change our toy model. Let us consider a complex scalar field  $\phi$  that respects a global  $U(1)$  symmetry.

The full Lagrangian for the model takes the form

$$\mathcal{L} = \partial_\mu \phi^* \partial^\mu \phi - \frac{\lambda}{4} (\phi^* \phi - v^2)^2. \quad (1.32)$$

Note that the model presents a Spontaneous Symmetry Breaking (SSB) pattern [30], since the field configuration that minimizes the classical energy is not zero, *i.e.*  $\langle \phi^* \phi \rangle = v^2$ . In order to make perturbative predictions we need to expand the Lagrangian around the true vacuum of the theory. Rewriting the field as  $\phi = v + \tilde{\phi}$ , we end up with

$$\mathcal{L} = \partial_\mu \tilde{\phi}^* \partial^\mu \tilde{\phi} - \frac{\lambda}{4} (v(\tilde{\phi} + \tilde{\phi}^*) + \tilde{\phi}^* \tilde{\phi})^2. \quad (1.33)$$

To make the particle content more clear it is useful to write the field in terms of its real and

imaginary parts,  $\tilde{\phi} = \frac{1}{\sqrt{2}}(\tilde{\phi}_R + i\tilde{\phi}_L)$ . The leading terms of the Lagrangian get

$$\mathcal{L} = \frac{1}{2}\partial_\mu\tilde{\phi}_R\partial^\mu\tilde{\phi}_R + \frac{1}{2}\partial_\mu\tilde{\phi}_L\partial^\mu\tilde{\phi}_L - \frac{\lambda v^2}{2}\tilde{\phi}_R^2 + \dots \quad (1.34)$$

From (1.34) we see that we have a massive particle  $\tilde{\phi}_R$  with mass  $m_R^2 = \lambda v^2$  and massless one  $\tilde{\phi}_L$ .

Since we have a hierarchy of masses we can ask ourselves what would be the low-energy EFT for only the light field  $\tilde{\phi}_L$ . The first question we must address is how the symmetry acts at low-energies on the light degree of freedom. Since  $U(1) \simeq SO(2)$ , we can arrange the real and imaginary fields in a doublet, and the phase transformation  $\phi \rightarrow e^{i\theta}\phi$  can be written as

$$\begin{pmatrix} \phi_R \\ \phi_L \end{pmatrix} \rightarrow \begin{pmatrix} \cos\theta & -\sin\theta \\ \sin\theta & \cos\theta \end{pmatrix} \begin{pmatrix} \phi_R \\ \phi_L \end{pmatrix}. \quad (1.35)$$

This means that the two fields mix with each other and our EFT will break the doublet structure. More important, after the SSB the  $U(1)$  symmetry is not a manifest symmetry in the Lagrangian anymore. Even though it seems we can not learn anything from the symmetries of the full theory, they can still help us in the EFT construction.

The trick to recognize how the symmetry acts on the light state is by doing a field redefinition. Instead of decomposing the field into its real and imaginary parts, we can rewrite it as

$$\phi = \left(v + \frac{\chi}{\sqrt{2}}\right)e^{\frac{i\xi}{\sqrt{2}v}}. \quad (1.36)$$

In this parametrization it is clear that the field  $\chi$  is a singlet of the symmetry while  $\xi$  under  $\phi \rightarrow e^{i\theta}\phi$  transformation goes to

$$\xi \rightarrow \xi + \sqrt{2}v\theta. \quad (1.37)$$

In particular, this transformation already tells us that  $\xi$  is going to be the light state since a mass term for it would break the symmetry. Indeed, when we use (1.36), the Lagrangian in (1.32) takes the form

$$\mathcal{L} = \frac{1}{2}\partial_\mu\chi\partial^\mu\chi + \frac{1}{2}\partial_\mu\xi\partial^\mu\xi - \frac{1}{2}\lambda v^2\chi^2 + \dots, \quad (1.38)$$

where only  $\chi$  acquires a mass.

Actually, the Lagrangian above clarifies that  $\xi$  is the Nambu-Goldstone boson of the SSB [31]. The transformation (1.37) is said to be a *non-linear* realization of the symmetry, because when one is dealing with non-abelian gauge symmetries the transformation of the Nambu-

Goldstone bosons is highly non-linear [23].

Now we know how the symmetry acts on the light state and in principle we could build our EFT, but since the  $\xi$ 's transformation is a non homogeneous shift the construction is not straight forward. As we will see with more detail later on, to write down an EFT for the Nambu-Goldstone boson one can build functions of it that transform linearly under the symmetry. In our case, this is accomplished by defining  $U = e^{i\xi/v}$ , which transforms as  $U \rightarrow e^{i\sqrt{2}\theta}U$ . Our leading order EFT Lagrangian written in terms of  $U$  is

$$\mathcal{L}^{EFT} = \frac{v^2}{2} \partial_\mu U^\dagger \partial^\mu U = \frac{1}{2} \partial_\mu \xi \partial^\mu \xi + \dots, \quad (1.39)$$

where in the second equality we just kept the kinetic term.

In the following sections, one of the possible EFTs to describe the electroweak interactions is also a non-linear realization of the SM symmetry group. When we get there, we will need to generalize this construction to non-abelian gauge theories.



---

---

# CHAPTER 2

---

## THE STANDARD MODEL

The Standard Model (SM) is a theory describing the electroweak and strong interactions among all the elementary particles we know so far [32, 33, 34]. It was created with a mass generation mechanism based on the idea of SSB of a gauge theory, *i.e.* the Higgs Mechanism [35, 36]. So far, the theory has been found to be compatible with data. This was first shown by the precision measurements made by LEP [37, 38]. Later on, in 2012, the ATLAS and the CMS Collaborations observed a scalar state consistent with the Higgs boson [1, 2]. Since then, the LHC Collaborations have not seen any significant deviation from the SM predictions. This section is devoted to introduce the SM in a concise way, with emphasis on the Higgs and on the triple electroweak gauge bosons interactions.

### 2.1 The SM Lagrangian

The SM is a chiral theory based on the symmetry breaking pattern  $SU(2)_L \times U(1)_Y \times SU(3)_C \rightarrow U(1)_{EM} \times SU(3)_C$ , where  $U(1)_{EM}$  stands for the electromagnetism gauge group. The  $L$  is there as reminder that the  $SU(2)_L$  symmetry only acts on the left-handed fermions and on the Higgs doublet. The  $Y$  is called hypercharge and its value for each particle is fixed in a way to give the correct electric charge. Lastly, the  $C$  stands for color and the  $SU(3)_C$  describes the strong interactions amid the quarks. To build up the Lagrangian we are going to use the *bottom-up* approach, that is, once we describe the particle content we will write down all possible interactions allowed by the symmetries. In the SM Lagrangian we only need the operators with mass dimension less or equal than four.

Starting with the leptons, the left-handed particles ( $e_L, \mu_L, \tau_L, \nu_{eL}, \nu_{\mu L}, \nu_{\tau L}$ ) are arranged in a doublet to transform under  $SU(2)_L$  in the fundamental representation, while the right-handed ones ( $e_R, \mu_R, \tau_R$ ) are singlets. Here, we will not take into account the right-handed neutrinos. There are three generations of lepton doublets, ordered by the mass of its second component:

$$L^i = \begin{pmatrix} \nu_{eL} \\ e_L \end{pmatrix}, \begin{pmatrix} \nu_{\mu L} \\ \mu_L \end{pmatrix}, \begin{pmatrix} \nu_{\tau L} \\ \tau_L \end{pmatrix}. \quad (2.1)$$

The right-handed leptons are also ordered by their mass:

$$e_R^i = \{e_R, \mu_R, \tau_R\}. \quad (2.2)$$

Following the same notation as [7], the covariant derivative acting on the lepton doublets is given by

$$D_\mu L^i = \left( \partial_\mu + igW_\mu^a \frac{\sigma^a}{2} + ig' B_\mu Y_L \right) L^i, \quad (2.3)$$

where  $W_\mu^a$ 's and  $B_\mu$  are the  $SU(2)_L$  and  $U(1)$  gauge bosons with  $g$  and  $g'$  being their gauge couplings, respectively. The  $\sigma^a$ 's denote the Pauli matrices and the  $Y$  represents the hypercharge, which is the same for all the generations. In Table 2.1 we displayed the hypercharge values and the representations under the gauge symmetry of the leptons, quarks, and the Higgs doublet.

Field	$SU(3)_C$	$SU(2)_L$	$U(1)_Y$
$L^i$	<b>1</b>	<b>2</b>	-1/2
$Q^i$	<b>3</b>	<b>2</b>	1/6
$e_R^i$	<b>1</b>	<b>1</b>	-1
$u_R^i$	<b>3</b>	<b>1</b>	2/3
$d_R^i$	<b>3</b>	<b>1</b>	-1/3
$H$	<b>1</b>	<b>2</b>	1/2

Table 2.1: Hypercharge values and representations under the SM gauge symmetry for the leptons, quarks, and the Higgs doublet.

The covariant derivatives for the right-handed leptons are similar, but they do not transform under  $SU(2)_L$ :

$$D_\mu e_R^i = \left( \partial_\mu + ig' B_\mu Y_R \right) e_R^i, \quad (2.4)$$

where  $Y_R$  represents the hypercharge, which is the same over all generations.

In the SM, the Higgs boson together with Goldstone bosons from the SSB process belong to a  $SU(2)_L$  doublet, generically denoted as  $H$ , with hypercharge 1/2. A mass term for the leptons (and also for the quarks) can not be written in the Lagrangian since it violates the symmetry. In



contrast, Yukawa terms with the Higgs doublet are allowed. Keeping that in mind, the leptonic sector of the SM Lagrangian takes the form

$$\mathcal{L}_{\text{Lepton}}^{\text{SM}} = \bar{L}^i \not{\partial} L^i + \bar{e}_R^i \not{\partial} e_R^i - \left[ y^i \bar{e}_R^i H^\dagger L^i + \text{h.c.} \right], \quad (2.5)$$

where we have taken the lepton Yukawa matrix to be diagonal.

The quark sector is displayed in a similar way. The left-handed particles are paired up into  $SU(2)_L$  doublets:

$$Q^i = \begin{pmatrix} u_L \\ d_L \end{pmatrix}, \begin{pmatrix} c_L \\ s_L \end{pmatrix}, \begin{pmatrix} t_L \\ b_L \end{pmatrix}. \quad (2.6)$$

The right-handed quarks are indexed as follows

$$u_R^i = \{u_R, c_R, t_R\}, \quad (2.7)$$

$$d_R^i = \{d_R, s_R, b_R\}. \quad (2.8)$$

The covariant derivatives acting on the left-handed and right-handed quarks are similar to the ones in (2.3-2.4), but now we need to add the gluons since they are charged under  $SU(3)_C$ :

$$D_\mu Q^i = \left( \partial_\mu + \imath g_s T^A G_\mu^A + \imath g W_\mu^a \frac{\sigma^a}{2} + \imath g' B_\mu Y_Q \right) Q^i, \quad (2.9)$$

$$D_\mu u_R^i = \left( \partial_\mu + \imath g_s T^A G_\mu^A + \imath g' B_\mu Y_u \right) u_R^i, \quad (2.10)$$

$$D_\mu d_R^i = \left( \partial_\mu + \imath g_s T^A G_\mu^A + \imath g' B_\mu Y_d \right) d_R^i, \quad (2.11)$$

where  $G_\mu^A$  represent the gluons,  $g_s$  is gauge coupling for  $SU(3)_C$ , and the  $T^A$  are denoting their generators, which can be represented by the Gell-Mann matrices. As before, the  $Y$ 's stand for hypercharge and they are the same among all generations. The quark sector of the SM Lagrangian is given by

$$\mathcal{L}_{\text{Quark}}^{\text{SM}} = \bar{Q}^i \not{\partial} Q^i + \bar{u}_R^i \not{\partial} u_R^i + \bar{d}_R^i \not{\partial} d_R^i - \left[ y_{ij}^d \bar{Q}^i H d_R^j + y_{ij}^u \bar{Q}^i \tilde{H} u_R^j + \text{h.c.} \right], \quad (2.12)$$

where  $\tilde{H} = \imath \sigma_2 H^*$  and it transforms under  $SU(2)_L$  in the fundamental representation with hypercharge  $-1/2$ .

We also need to add the kinetic term of the gauge bosons. In terms of the field strengths, they are organized as follows

$$\mathcal{L}_{\text{Gauge}}^{\text{SM}} = -\frac{1}{4} G_{\mu\nu}^A G^{A\mu\nu} - \frac{1}{4} W_{\mu\nu}^a W^{a\mu\nu} - \frac{1}{4} B_{\mu\nu} B^{\mu\nu}. \quad (2.13)$$

The field strength can be generically written as

$$F_{\mu\nu}^a = \partial_\mu F_\nu^a - \partial_\nu F_\mu^a + gf^{abc}F_\mu^b F_\nu^c, \quad (2.14)$$

with  $T^a$  denoting the generators of the gauge group,  $F_\mu^a$  the gauge bosons, and  $f^{abc}$  representing the group structure constant. For the abelian  $U(1)_Y$ , we have  $f^{abc} = 0$ .

Finally, the only piece missing is the scalar sector of the Lagrangian:

$$\mathcal{L}_{\text{Scalar}}^{\text{SM}} = (D_\mu H)^\dagger (D^\mu H) - \lambda \left( H^\dagger H - \frac{1}{2}v^2 \right)^2, \quad (2.15)$$

where  $v$  stands for the vacuum expectation value (vev) of the electroweak symmetry breaking (EWSB) process. The covariant derivative takes the same form as (2.3) except we must change  $Y_L$  for  $1/2$ . After the SSB, the Higgs doublet acquires a non-vanishing vev,  $\langle H^\dagger H \rangle = v^2/2$ , and, in the unitary gauge, it takes the following form [20, 7]:

$$H = \frac{1}{\sqrt{2}} \begin{pmatrix} 0 \\ v + h \end{pmatrix}. \quad (2.16)$$

Once we have plugged the vev contribution in the Higgs kinetic term we can read the masses of the electroweak gauge bosons:

$$\mathcal{L}_{\text{Scalar, mass}}^{\text{SM}} = \frac{v^2}{8} \left\{ g^2 \left( W_\mu^1 W^{1\mu} + W_\mu^2 W^{2\mu} \right) + \left( g' B_\mu - g W_\mu^3 \right)^2 \right\}. \quad (2.17)$$

First, it is useful to make the definitions:

$$W_\mu^1 = \frac{1}{\sqrt{2}} \left( W_\mu^+ + W_\mu^- \right), \quad (2.18)$$

$$W_\mu^2 = \frac{i}{\sqrt{2}} \left( W_\mu^+ - W_\mu^- \right), \quad (2.19)$$

where  $W_\mu^+$  and  $W_\mu^-$  represent the charged gauge bosons under  $U(1)_{\text{EM}}$ . Their mass term reads

$$\mathcal{L}_{\text{Scalar, mass-charged}} = \frac{g^2 v^2}{4} W^{+\mu} W_\mu^- \equiv m_W^2 W^{+\mu} W_\mu^-. \quad (2.20)$$

The remaining terms in (2.17) give rise to the neutral gauge bosons under  $U(1)_{\text{EM}}$ . To read the physical fields we need to diagonalize the mass matrix among the fields  $W_\mu^3$  and  $B_\mu$  in equation

(2.17):

$$\mathcal{L}_{\text{Scalar, mass-neutral}} = \frac{v^2}{8} \begin{pmatrix} W_\mu^3 & B_\mu \end{pmatrix} \begin{pmatrix} g^2 & -gg' \\ -gg' & g'^2 \end{pmatrix} \begin{pmatrix} W_\mu^3 \\ B_\mu \end{pmatrix}, \quad (2.21)$$

$$= \frac{v^2}{8} \begin{pmatrix} W_\mu^3 & B_\mu \end{pmatrix} \frac{1}{\sqrt{g^2 + g'^2}} \begin{pmatrix} g & g' \\ -g' & g \end{pmatrix} \begin{pmatrix} g^2 + g'^2 & 0 \\ 0 & 0 \end{pmatrix} \frac{1}{\sqrt{g^2 + g'^2}} \begin{pmatrix} g & -g' \\ g' & g \end{pmatrix} \begin{pmatrix} W_\mu^3 \\ B_\mu \end{pmatrix}. \quad (2.22)$$

By making the following definitions

$$\cos \theta = \frac{g}{\sqrt{g^2 + g'^2}}, \quad (2.23)$$

$$\sin \theta = \frac{g'}{\sqrt{g^2 + g'^2}}, \quad (2.24)$$

where  $\theta$  denotes the weak angle, the expression (2.22) gets

$$\mathcal{L}_{\text{Scalar, mass-neutral}} = \frac{v^2}{8} \begin{pmatrix} W_\mu^3 & B_\mu \end{pmatrix} \begin{pmatrix} \cos \theta & \sin \theta \\ -\sin \theta & \cos \theta \end{pmatrix} \begin{pmatrix} \frac{g^2}{\cos^2 \theta} & 0 \\ 0 & 0 \end{pmatrix} \begin{pmatrix} \cos \theta & -\sin \theta \\ \sin \theta & \cos \theta \end{pmatrix} \begin{pmatrix} W_\mu^3 \\ B_\mu \end{pmatrix}, \quad (2.25)$$

$$= \frac{g^2 v^2}{8 \cos^2 \theta} Z_\mu Z^\mu \equiv \frac{1}{2} m_Z^2 Z_\mu Z^\mu, \quad (2.26)$$

where the physical fields were defined through the rotation:

$$Z_\mu = \cos \theta W_\mu^3 - \sin \theta B_\mu, \quad (2.27)$$

$$A_\mu = \sin \theta W_\mu^3 + \cos \theta B_\mu, \quad (2.28)$$

This means that we have a massive gauge boson  $Z_\mu$  and a massless  $A_\mu$ . The latter represents the photon.

Previously, we saw that due to the Higgs Mechanism the SM can allow three massive gauge bosons and a massless one. The same mechanism is also responsible for generating the fermion masses by means of the Yukawa interactions.

At this point, we have written all the terms in the SM Lagrangian and we can finally put them all together:

$$\mathcal{L}^{\text{SM}} = \mathcal{L}_{\text{Lepton}}^{\text{SM}} + \mathcal{L}_{\text{Quark}}^{\text{SM}} + \mathcal{L}_{\text{Gauge}}^{\text{SM}} + \mathcal{L}_{\text{Scalar}}^{\text{SM}}. \quad (2.29)$$

A lot of interesting consequences can be found in the Lagrangian above. We will not go into

detail in all of them, but it is going to be useful for us later on to read out the Higgs interactions and the triple gauge couplings (TGCs).

The TGCs in terms of the Lorentz structure of the physical fields can be written as [13]

$$\mathcal{L}_{WWV} = -ig_{WWV} \left\{ g_1^V \left( W_{\mu\nu}^+ W^{-\mu} V^\nu - W_\mu^+ V_\nu W^{-\mu\nu} \right) + \kappa_V W_\mu^+ W_\nu^- V^{\mu\nu} + \frac{\lambda_V}{m_W^2} W_{\mu\nu}^+ W^{-\nu\rho} V_\rho^\mu \right\}, \quad (2.30)$$

with  $V = \{Z, \gamma\}$  being one of the neutral gauge bosons,  $g_{WW\gamma} = e$ ,  $g_{WWZ} = g \cos \theta$ , and  $W_{\mu\nu}^\pm$  and  $V_{\mu\nu}$  refer exclusively to the kinematic part of the gauge field strengths. Note that the last term in the Lagrangian above can not be generated by the SM Lagrangian since it has a canonical mass dimension equal to six. We are only introducing this term here because, as we will see later on, this interaction is generated by a dimension-six effective operator. The SM predictions for the couplings above are

$$g_1^Z = \kappa_Z = \kappa_\gamma = 1, \quad (2.31)$$

$$\lambda_\gamma = \lambda_Z = 0 \quad (2.32)$$

When one is working with effective field theories these couplings are modified in the presence of new operators. The only coupling that remain the same is  $g_1^\gamma = 1$ , which is enforced by the electromagnetic gauge invariance. The Lagrangian in (2.30) tells us that the SM gives rise to  $WW\gamma$  and  $WWZ$  interactions, indicating that this couplings can be probed by Vector Boson Fusion (VBF) or by Vector Boson Production (VBP).

At tree-level, the Higgs couples with the massive fermions and with the massive gauge bosons. These interactions can be summarized in the Lagrangian

$$\mathcal{L}_{\text{Higgs}} = g_{ZZh} Z^\mu Z_\mu h + g_{WWh} W_\mu^+ W^{-\mu} h + \sum_{f=\tau,b,t} \left\{ g_f h \bar{f}_L f_R + \text{h.c.} \right\}. \quad (2.33)$$

In the SM, the Higgs couplings are proportional to the masses of the particles it couples with. For instance, the parameters in (2.33) are

$$g_{ZZh} = \frac{m_Z^2}{v}, \quad (2.34)$$

$$g_{WWh} = \frac{2m_W^2}{v}, \quad (2.35)$$

$$g_f = \frac{m_f}{v}. \quad (2.36)$$

The Higgs can also interact with the massless gauge bosons through loop-effects. In particular, the  $H\gamma\gamma$ ,  $HZ\gamma$ , and  $Hgg$  interactions [39], where  $g$  stands for gluons, will play an important

role for the Higgs production and decays modes. The diagrams for these process are displayed in Figures 2.1 and 2.2. The Feynman diagrams for  $h \rightarrow Z\gamma$  decay are equal to the ones for the  $h \rightarrow \gamma\gamma$  decay.

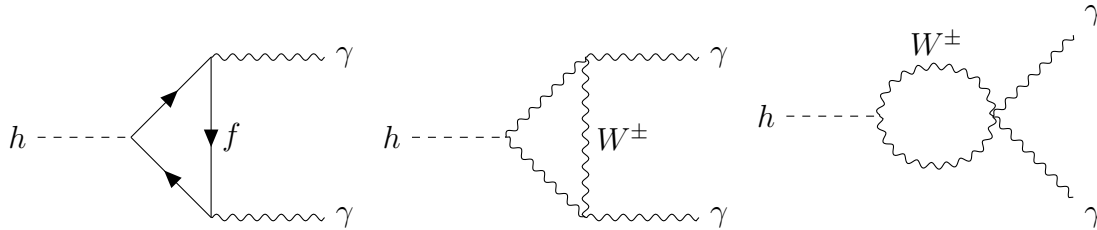


Figure 2.1: Feynman diagrams for  $h \rightarrow \gamma\gamma$  decay.

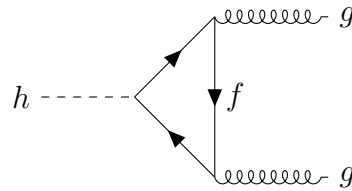


Figure 2.2: Feynman diagrams for  $h \rightarrow gg$  decay.



---

---

## CHAPTER 3

---

# THE STANDARD MODEL EFFECTIVE FIELD THEORY

The Standard Model Effective Field Theory (SMEFT) is a generalization of the SM. It shares the same set of symmetries and particle content as the latter. Most important, it also assumes that the Higgs-like boson is embedded in a  $SU(2)_L$  doublet so the gauge symmetry  $SU(2)_L \times U(1)_Y$  is linearly realized. The only relaxed SM condition is concerning the number of interactions: the SMEFT allows operators with dimension greater than four. This last assumption comes from the belief that unknown particles are heavier than any SM particle and the current experiments can not access them. As a consequence, their low-energy effects can be tracked down by local interactions among the SM degrees of freedom suppressed by some characteristic new physics scale [7].

As discussed in the first chapter, EFTs are a consistent framework to encode possible deviations from the SM predictions, specially the ones accessible by the ATLAS and CMS experiments. In the context of particle physics, the SMEFT has been the most used EFT. Moreover, once we have set the bounds on the Wilson coefficients they can be translated to any model through a *Matching* calculation instead of having to derive them for each model separately. In particular, the assumptions made here are very plausible since we have not seen any direct or indirect signals indicating new physics. Nonetheless, even if new particles are discovered the SMEFT can still be useful to describe swaths of data below the characteristic energy of the new physics sector.

When working with the SMEFT, the Lagrangian is written as follows

$$\mathcal{L}_{\text{SMEFT}} = \mathcal{L}_{\text{SM}} + \mathcal{L}^{(5)} + \mathcal{L}^{(6)} + \mathcal{L}^{(7)} + \dots, \quad (3.1)$$

where the series is sorted in terms of canonical mass dimensions of the operators, which means that each term of the expansion above has a set of  $n_d$  interactions with the same dimension:

$$\mathcal{L}^{(d)} = \sum_{i=1}^{n_d} \frac{f_i^{(d)}}{\Lambda^{d-4}} \mathcal{O}_i^{(d)} \quad \text{for } d > 4. \quad (3.2)$$

We denoted the effective operators by  $\mathcal{O}_i^{(d)}$  and they are suppressed by a characteristic new physics scale  $\Lambda$ . The first term in the expansion,  $\mathcal{L}^{(5)}$ , only contains one interaction, which gives a majorana mass for the neutrinos and it also violates lepton number [40]. Since the LHC is blind to neutrino physics and its Wilson coefficient is highly constrained by data [41], the first anomalous effects for the LHC physics emerge at dimension six, *i.e.*  $\mathcal{L}^{(6)}$ .

One must pay attention to only take into account effective interactions whose combinations do not vanish in the  $S$ -matrix for a given order in the  $\Lambda$  expansion. This situation typically happens when operators are related by the equations of motion (EOM). In this case, the EOM can also be employed to remove the redundant interactions as shown by [42]. The minimum set with only non-redundant interactions is called basis. The common ones used in the literature are the Warsaw [43], the HISZ [44, 45], and the SILH [46] basis.

To illustrate a few subtleties with the SMEFT, we will continue the discussion with the basis presented in [9]. In there, a global fit was performed using data from electroweak precision, TGC's, and Higgs observables. Assuming the conservation of total baryon and lepton number, C and P, and no tree-level sources flavor violation, they had 21 relevant independent operators for their analysis. The basis contains the bosonic operators from HISZ basis [44, 45], keeping the operators  $\mathcal{O}_B$  and  $\mathcal{O}_W$  in exchange for a few operators involving fermions. Here we are only interested in a subset of operators that affects the TGC's and Higgs physics. We emphasize that our list of operators is not complete, but the discussion we are about to make is very general. The operators affecting TGC's are shown in Table 3.1 and the ones affecting the Higgs physics are displayed in Table 3.2. The operators in Table 3.1 also affect the Higgs interactions with the electroweak gauge bosons (HVV). Moreover, the operator  $\mathcal{O}_{BW}$  also affects TGC, but it is highly constrained by the electroweak precision data and it can be neglected in the TGC analysis [9]. Lastly, the operators in Table 3.2 are not the only ones affecting Higgs physics, the operators we did not include are displayed in [9].

When writing the operators above we follow the same definition as [9]: we defined  $\hat{B}^{\mu\nu} \equiv$



$\mathcal{O}_B = (D_\mu H)^\dagger \hat{B}^{\mu\nu} (D_\nu H)$	$\mathcal{O}_W = (D_\mu H)^\dagger \hat{W}^{\mu\nu} (D_\nu H)$	$\mathcal{O}_{WWW} = \text{Tr} \left[ \hat{W}_\mu^\nu \hat{W}_\nu^\rho \hat{W}_\rho^\mu \right]$
--	--	--

Table 3.1: Dimension-six effective operators from [9] affecting TGCs and Higgs physics.

$\mathcal{O}_{H,1} = (D_\mu H)^\dagger H H^\dagger (D^\mu H)$	$\mathcal{O}_{H,2} = \frac{1}{2} \partial^\mu (H^\dagger H) \partial_\mu (H^\dagger H)$	$\mathcal{O}_{tG} = (\bar{Q}_3 \sigma^{\mu\nu} \frac{\lambda^a}{2} u_3) \tilde{H} G_\mu^a \nu$
$\mathcal{O}_{GG} = H^\dagger H G_{\mu\nu}^a G^{a\mu\nu}$	$\mathcal{O}_{BB} = H^\dagger \hat{B}^{\mu\nu} \hat{B}^{\mu\nu} H$	$\mathcal{O}_{WW} = H^\dagger \hat{W}^{\mu\nu} \hat{W}^{\mu\nu} H$
$\mathcal{O}_{eH,ii} = (H^\dagger H) (\bar{L}_i H e_{R,i}) \quad i = 2, 3$	$\mathcal{O}_{uH,33} = (H^\dagger H) (\bar{Q}_3 \tilde{H} u_{R,3})$	$\mathcal{O}_{dH,33} = (H^\dagger H) (\bar{Q}_3 H d_{R,3})$
$\mathcal{O}_{BW} = H^\dagger \hat{B}^{\mu\nu} \hat{W}_{\mu\nu} H$		

Table 3.2: Dimension-six effective operators from [9] affecting Higgs physics.

$i(g'/2)B^{\mu\nu}$ ,  $\hat{W}^{\mu\nu} = i(g/2)\sigma^a W^{a\mu\nu}$ , and when including a sub-index it refers to the fermionic generation. We can construct our phenomenological SMEFT Lagrangian with the operators above, dividing it into three pieces. The first one is the SM Lagrangian  $\mathcal{L}_{SM}$ , the second one is made from the operators in Table 3.1:

$$\mathcal{L}_{\text{SMEFT}}^{\text{TGC}} = \frac{f_{WWW}}{\Lambda^2} \mathcal{O}_{WWW} + \frac{f_W}{\Lambda^2} \mathcal{O}_W + \frac{f_B}{\Lambda^2} \mathcal{O}_B, \quad (3.3)$$

and the last one is made from operators in Table 3.2:

$$\begin{aligned} \mathcal{L}_{\text{SMEFT}}^{\text{H}} &= \frac{f_\mu}{\Lambda^2} \frac{m_\mu}{v} \mathcal{O}_{eH,22} + \frac{f_\tau}{\Lambda^2} \frac{m_\tau}{v} \mathcal{O}_{eH,33} + \frac{f_b}{\Lambda^2} \frac{m_b}{v} \mathcal{O}_{dH,33} + \frac{f_t}{\Lambda^2} \frac{m_t}{v} \mathcal{O}_{uH,33} + \text{h.c.} \\ &- \frac{\alpha_s}{8\pi} \frac{f_{GG}}{\Lambda^2} \mathcal{O}_{GG} + \frac{f_{BB}}{\Lambda^2} \mathcal{O}_{BB} + \frac{f_{WW}}{\Lambda^2} \mathcal{O}_{WW} + \frac{f_{H,1}}{\Lambda^2} \mathcal{O}_{H,1} + \frac{f_{H,2}}{\Lambda^2} \mathcal{O}_{H,2} + \frac{f_{BW}}{\Lambda^2} \mathcal{O}_{BW} \\ &+ \frac{f_{tG}}{\Lambda^2} \mathcal{O}_{tG}. \end{aligned} \quad (3.4)$$

We can write our Lagrangian with these three terms as

$$\mathcal{L}_{\text{SMEFT}} = \mathcal{L}_{\text{SM}} + \mathcal{L}_{\text{SMEFT}}^{\text{TGC}} + \mathcal{L}_{\text{SMEFT}}^{\text{H}}. \quad (3.5)$$

In Table 3.1, all three operators generate deviations from the SM predictions for the TGCs. Also, no anomalous interaction among the neutral gauge bosons will emerge. This only happens when we take into account dimension-eight operators [47]. The couplings of the Lorentz structures from (2.30) need to be updated to accommodate the anomalous contributions. In the unitary gauge, the couplings of the Lorentz structures in terms of the Wilson coefficients now

read [48]

$$g_1^Z = 1 + \frac{f_W m_Z^2}{\Lambda^2} \frac{1}{2} \quad (3.6)$$

$$\kappa_\gamma = 1 + \left( \frac{f_W}{\Lambda^2} + \frac{f_B}{\Lambda^2} \right) \frac{m_W^2}{2} \quad (3.7)$$

$$\kappa_Z = 1 + \left( \frac{f_W}{\Lambda^2} - \frac{f_B}{\Lambda^2} \tan^2 \theta \right) \frac{m_W^2}{2} \quad (3.8)$$

$$\lambda_\gamma = \lambda_Z = \frac{f_{WWW}}{\Lambda^2} \frac{3g^2 m_W^2}{2} \quad (3.9)$$

It is interesting to observe that we have corrections for the SM predictions in the coefficients  $g_1^Z$ ,  $\kappa_\gamma$ , and  $\kappa_Z$ . Also, new interactions not present in the SM have appeared due to the introduction of the operator  $\mathcal{O}_{WWW}$ . Those correspond to the couplings  $\lambda_\gamma$  and  $\lambda_Z$ . It is good to keep in mind that the operators  $\mathcal{O}_B$  and  $\mathcal{O}_W$  modify the couplings of the Higgs with the electroweak gauge bosons as well.

All operators in Table 3.2 affect the couplings of the Higgs with the fermions or the couplings of the Higgs with the gauge bosons. In special, the operators  $\mathcal{O}_{H,1}$  and  $\mathcal{O}_{H,2}$  affect all the SM Higgs couplings. The effective operator  $\mathcal{O}_{tH}$  modifies the Higgs production through gluon fusion. Lastly, all the operators from the second line in the table affect the Higgs-gauge bosons interactions, while the ones in the third line affect the Higgs-fermions interactions.

When one is working with the SMEFT, it is convenient to make a few modifications in the Lagrangian to implement the model into Monte-Carlo event generators, *e.g.* normalized kinetic terms, normalized masses, no kinetic mixing among the physical degrees of freedom, etc. These changes can be performed since we have the freedom to make field redefinitions and they are clear once we have put the theory in the unitary gauge.

As an example, let us carry out the necessary Lagrangian modifications to perform calculations up to  $\mathcal{O}(\Lambda^{-2})$  in the unitary gauge. Starting with the operator  $\mathcal{O}_{BB}$ , after we have plugged the vev, the kinetic term normalization of the gauge boson  $B_\mu$  goes to

$$-\frac{1}{4} B_{\mu\nu} B^{\mu\nu} + \frac{f_{BB}}{\Lambda^2} \mathcal{O}_{BB} = -\frac{1}{4} \left\{ 1 + \frac{g'^2 f_{BB} v^2}{\Lambda^2} \right\} B_{\mu\nu} B^{\mu\nu} + \dots, \quad (3.10)$$

the dots represent all the terms from  $\mathcal{O}_{BB}$  that do not affect the gauge boson kinetic term. To ensure its canonical normalization, we need to rescale the field by

$$B_\mu \rightarrow \left( 1 - \frac{g'^2 f_{BB} v^2}{\Lambda^2} \right) B_\mu. \quad (3.11)$$

In principle, this would affect all the neutral gauge boson interactions, but since  $B_\mu$  only appears

in the covariant derivatives we can rescale its gauge coupling  $g'$  in a way to leave the covariant derivative unchanged:

$$g' \rightarrow \left(1 + \frac{g'^2 f_{BB} v^2}{4 \Lambda^2}\right) g'. \quad (3.12)$$

The same process has to be done with the operators  $\mathcal{O}_{WW}$  and  $\mathcal{O}_{GG}$ . This means that the impact of these operators are completely absorbed in the definition of the fields and gauge couplings. As a result, they have no effect on the pure gauge sector, only on the Higgs-gauge bosons interactions.

The operator  $\mathcal{O}_{BW}$  introduces a mixing among the fields  $W_\mu^3$  and  $B_\mu$  that requires some attention. Now, the neutral gauge bosons kinetic terms are given by

$$\begin{aligned} & -\frac{1}{4} B_{\mu\nu} B^{\mu\nu} - \frac{1}{4} W_{\mu\nu}^3 W^{3\mu\nu} + \frac{f_{BW}}{\Lambda^2} \mathcal{O}_{BW} = \\ & -\frac{1}{4} B_{\mu\nu} B^{\mu\nu} - \frac{1}{4} W_{\mu\nu}^3 W^{3\mu\nu} - \frac{gg' f_{BW}}{8 \Lambda^2} v^2 B_{\mu\nu} W^{3\mu\nu} + \dots \end{aligned} \quad (3.13)$$

The diagonal and canonical kinetic term can be achieved through the rotation [49]

$$\begin{pmatrix} B_\mu \\ W_\mu^3 \end{pmatrix} \rightarrow \begin{pmatrix} 1 & -\frac{f}{2} \\ -\frac{f}{2} & 1 \end{pmatrix} \begin{pmatrix} B_\mu \\ W_\mu^3 \end{pmatrix}, \quad (3.14)$$

where we defined  $f \equiv \frac{1}{4} gg' \frac{f_{BW}}{\Lambda^2} v^2$ . As consequence, the mass matrix (2.22) for the neutral gauge bosons is modified:

$$\begin{aligned} (g' B_\mu - g W_\mu)^2 & \rightarrow (W_\mu^3 \quad B_\mu) \begin{pmatrix} 1 & -\frac{f}{2} \\ -\frac{f}{2} & 1 \end{pmatrix} \frac{1}{\sqrt{g^2 + g'^2}} \begin{pmatrix} g & g' \\ -g' & g \end{pmatrix} \times \\ & \begin{pmatrix} g^2 + g'^2 & 0 \\ 0 & 0 \end{pmatrix} \times \\ & \frac{1}{\sqrt{g^2 + g'^2}} \begin{pmatrix} g & -g' \\ g' & g \end{pmatrix} \begin{pmatrix} 1 & -\frac{f}{2} \\ -\frac{f}{2} & 1 \end{pmatrix} \begin{pmatrix} W^{3\mu} \\ B^\mu \end{pmatrix}. \end{aligned} \quad (3.15)$$

The matrix can be diagonalized by the rotation [50]:

$$\begin{pmatrix} W_\mu^3 \\ B_\mu \end{pmatrix} = \frac{1}{\sqrt{g^2 + g'^2}} \begin{pmatrix} g & g' \\ -g' & g \end{pmatrix} \begin{pmatrix} 1 & -\frac{f g'^2 - g^2}{2 g^2 + g'^2} \\ \frac{f g'^2 - g^2}{2 g^2 + g'^2} & 1 \end{pmatrix} \begin{pmatrix} Z_\mu \\ A_\mu \end{pmatrix}, \quad (3.16)$$

The rightmost matrix is a rotation up to order  $\mathcal{O}(\Lambda^{-2})$ . Moreover, we can also write it as

$$\begin{pmatrix} W_\mu^3 \\ B_\mu \end{pmatrix} = \begin{pmatrix} \cos \theta & \sin \theta \\ -\sin \theta & \cos \theta \end{pmatrix} \begin{pmatrix} Z_\mu \\ A_\mu \end{pmatrix}. \quad (3.17)$$

where the angle  $\theta$  is shifted:

$$\tan \theta = \frac{g'}{g} + \frac{1}{2} \left(1 - \frac{g'^2}{g^2}\right) f. \quad (3.18)$$

Once we have implemented this rotation in the Lagrangian, the  $Z$  boson mass is corrected due to the presence of the anomalous coupling:

$$\frac{1}{2} m_Z^2 Z_\mu Z^\mu = \frac{v^2}{8} \left( g'^2 + g^2 + \frac{1}{8} g^2 g'^2 \frac{f_{BW}}{\Lambda^2} v^2 \right) Z_\mu Z^\mu. \quad (3.19)$$

And it also has an impact in the covariant derivative [50]:

$$D_\mu = \partial_\mu + iQg \sin \theta A_\mu \left[1 - \frac{1}{2} \cot \theta f\right] + i \frac{g}{\cos \theta} Z_\mu \left(\frac{\sigma_3}{2} - Q \sin^2 \theta\right) \left[1 + \frac{1}{2} \tan \theta f\right] + \dots, \quad (3.20)$$

the  $Q = \sigma_3/2 + Y$  is the electric charge and the angle  $\theta$  is defined in the equation (3.18). The dots denote the gluon and the  $W^\pm$  terms, which are unaffected by the operator  $\mathcal{O}_{BW}$ . As shown in the equation above, the presence of the anomalous operator introduces net modifications in the  $\gamma$  and  $Z$  couplings. In the first, it just leads to a universal rescaling of the electric charge, while in the latter it depends on the field's charge.

It is also important to see how the Higgs-fermionic operators affect the SM Yukawa couplings. As an example, let us take the one that affects the bottom quark Yukawa coupling, the operator  $\mathcal{O}_{dH,33}$ . The important terms in the SMEFT Lagrangian are

$$\begin{aligned} & - \frac{\sqrt{2} m_b}{v} \bar{Q}^3 H d_R^3 + \frac{f_b m_b}{\Lambda^2} \mathcal{O}_{dH,33} + \text{h.c.} = \\ & - m_b \left(1 - \frac{v^2}{2\sqrt{2}} \frac{f_b}{\Lambda^2}\right) \bar{b} b - \frac{m_b}{v} \left(1 - \frac{3v^2}{2\sqrt{2}} \frac{f_b}{\Lambda^2}\right) \bar{b} b h + \dots, \end{aligned} \quad (3.21)$$

where  $h$  denotes the physical Higgs boson and the dots refer to terms which do not affect the SM interactions. Not only the Yukawa interaction with the Higgs boson is affected but the mass term also is. Usually it is preferable to have canonical mass terms, so we shift the mass of the particle and leave all the anomalous effect in the Yukawa vertex. This can be done by

$$m_b \rightarrow \left(1 + \frac{v^2}{2\sqrt{2}} \frac{f_b}{\Lambda^2}\right) m_b. \quad (3.22)$$

After the redefinition, the Lagrangian takes a simpler form

$$-m_b \bar{b}b - \frac{m_b}{v} \left(1 - \frac{v^2}{\sqrt{2}} \frac{f_b}{\Lambda^2}\right) \bar{b}b h + \dots \quad (3.23)$$

Note that this change is equivalent to leaving the anomalous effect in the fermionic propagator and, when we are computing amplitudes which contain the propagator of the particle, we just expand it up to  $\mathcal{O}(\Lambda^{-2})$ . The redefinition in (3.22) is usually preferable because Monte-Carlo event generators can not expand the Wilson coefficients in the propagator. The only program that knows how to do it is the SMEFTsim [50], but it is only available for the Warsaw basis.

As was pointed out before, the effective operators  $\mathcal{O}_{H,1}$  and  $\mathcal{O}_{H,2}$  affect the Higgs kinetic terms:

$$\frac{1}{2} \partial_\mu h \partial^\mu h + \frac{f_{H,1}}{\Lambda^2} \mathcal{O}_{H,1} + \frac{f_{H,2}}{\Lambda^2} \mathcal{O}_{H,2} = \frac{1}{2} \left[1 + v^2 \left(\frac{1}{2} \frac{f_{H,1}}{\Lambda^2} + \frac{f_{H,2}}{\Lambda^2}\right)\right] \partial_\mu h \partial^\mu h + \dots, \quad (3.24)$$

a simple rescaling fixes the normalization:

$$h \rightarrow \left[1 - \frac{v^2}{2} \left(\frac{f_{H,2}}{\Lambda^2} + \frac{1}{2} \frac{f_{H,1}}{\Lambda^2}\right)\right] h. \quad (3.25)$$

This shift introduces an overall rescaling of all the SM Higgs interactions. Moreover, the operator  $\mathcal{O}_{H,1}$  also introduces anomalous corrections to the  $Z$  boson mass as a consequence of the term

$$\mathcal{O}_{H,1} = \frac{g^2 v^4}{16 \cos^2 \theta} Z_\mu Z^\mu + \dots \quad (3.26)$$

Here one can proceed in the same way we did for the Yukawas couplings: we renormalize the mass to leave the anomalous effect in all SM  $Z$  interactions.

These are basically all the field and coupling redefinitions we must pay attention to when working with this subset of effective operators. As it was shown in [9], some of these modifications can lead to a change of sign of the SM couplings and, as a consequence, degenerate regions in the parameter space are allowed. This happens, for example, to the Yukawa coupling of the tau lepton and bottom quark.

To finish, we state here the Higgs interactions with the SM gauge-boson pairs in the unitary gauge considering the effective operators from Tables 3.1 and 3.2 [51]:

$$\begin{aligned} \mathcal{L}^{\text{HVV}} = & g_{Hgg} h G_{\mu\nu}^a G^{a\mu\nu} + g_{H\gamma\gamma} h A_{\mu\nu} A^{\mu\nu} + g_{HZ\gamma}^{(1)} A_{\mu\nu} Z^\mu \partial^\nu h + g_{HZ\gamma}^{(2)} h A_{\mu\nu} Z^{\mu\nu} \\ & + g_{HZZ}^{(1)} Z_{\mu\nu} Z^\mu \partial^\nu h + g_{HZZ}^{(2)} h Z_{\mu\nu} Z^{\mu\nu} + g_{HZZ}^{(3)} h Z_\mu Z^\mu \\ & + g_{HWW}^{(1)} (W_{\mu\nu}^+ W^{-\mu} \partial^\nu h + \text{h.c.}) + g_{HWW}^{(2)} h W_{\mu\nu}^+ W^{-\mu\nu} + g_{HWW}^{(3)} h W_\mu^+ W^{-\mu}, \end{aligned} \quad (3.27)$$

where  $V_{\mu\nu} = \partial_\mu V_\nu - \partial_\nu V_\mu$ , with  $V = A, Z, W$ , and  $G$ . The couplings from the Lagrangian above can be expressed in terms of the Wilson coefficients as follows

$$\begin{aligned}
g_{Hgg} &= -\frac{\alpha_s f_{GG} v}{8\pi \Lambda^2}, \\
g_{H\gamma\gamma} &= -\left(\frac{g^2 v s^2}{2\Lambda^2}\right) \frac{f_{BB} + f_{WW} - f_{BW}}{2}, \\
g_{HZ\gamma}^{(1)} &= \left(\frac{g^2 v}{2\Lambda^2}\right) \frac{s(f_W - f_B)}{2c}, \\
g_{HZ\gamma}^{(2)} &= \left(\frac{g^2 v}{2\Lambda^2}\right) \frac{s[2s^2 f_{BB} - 2c^2 f_{WW} + (c^2 - s^2) f_{BW}]}{2c}, \\
g_{HZZ}^{(1)} &= \left(\frac{g^2 v}{2\Lambda^2}\right) \frac{c^2 f_W + s^2 f_B}{2c^2}, \\
g_{HZZ}^{(2)} &= -\left(\frac{g^2 v}{2\Lambda^2}\right) \frac{s^4 f_{BB} + c^4 f_{WW} + c^2 s^2 f_{BW}}{2c^2}, \\
g_{HZZ}^{(3)} &= \left(\frac{g^2 v}{4c^2}\right) \left[1 + \frac{v^2}{4\Lambda^2} \left(3f_{H,1} - 2f_{H,2} - \frac{2g^2 g'^2}{g^2 + g'^2} f_{BW}\right)\right], \\
g_{HWW}^{(1)} &= \left(\frac{g^2 v}{2\Lambda^2}\right) \frac{f_W}{2}, \\
g_{HWW}^{(2)} &= -\left(\frac{g^2 v}{2\Lambda^2}\right) f_{WW}, \\
g_{HWW}^{(3)} &= -\left(\frac{g^2 v}{2}\right) \left[1 - \frac{v^2}{4\Lambda^2} (f_{H,1} + 2f_{H,2})\right],
\end{aligned} \tag{3.28}$$

where we defined  $s = \sin \theta$  and  $c = \cos \theta$  for simplicity, and  $\theta$  is the same angle from (3.18). As we pointed out before, the operators  $\mathcal{O}_W$  and  $\mathcal{O}_B$  also affect the Higgs couplings with the electroweak gauge bosons.

---

---

# CHAPTER 4

---

## THE HIGGS EFFECTIVE FIELD THEORY

In the previous section we saw one possible EFT used to describe the electroweak and strong interactions. The goal of this section is to present another one based on the idea of Chiral Lagrangians [52]. The latter has been extensively used in QCD at low energies, where it was able to describe the interactions among mesons and baryons [52, 17]. At this energy range, QCD leaves the perturbative regime and an EFT approach is required. When these ideas are applied for the electroweak interactions, the EFT is called Higgs effective field theory (HEFT) [7].

Differently from the SMEFT, the HEFT does not consider the Higgs boson as part of a  $SU(2)_L$  doublet, instead it is just a singlet under the SM gauge symmetry. To describe this EFT, we must review a few concepts about group theory, specially about the Callan, Coleman, Wess and Zumino (CCWZ) construction [53, 54]. In the following, the discussion is based on [55], but other good reviews about the matter are found in [52, 56].

### 4.1 Non-linear realizations

To start, consider a Lie Group  $G$  that acts on the manifold  $M$

$$x \rightarrow gx, \quad x \in M, \quad g \in G. \quad (4.1)$$

Also, a subgroup  $H$  of  $G$  contains only transformations that leave the origin of  $M$  invariant:

$$h0 = 0, \quad h \in H. \quad (4.2)$$

The physical picture is a SSB of  $G$  to  $H$  with  $0$  playing the role of the vacuum of the theory. Our goal here is to characterize all possible non-linear realizations of the group  $G$  on the manifold  $M$ . In other words, we need to classify all the theories consistent with the SSB pattern.

Below we state two theorems that will allow us to accomplish our goal. For their proof, we refer the reader to [53, 55].

**Theorem I:** When one performs a field redefinition the content of the theory changes, but provided the transformation has a Jacobian that equals to one at the origin, the outcome of the  $S$ -matrix will remain the same.

**Theorem II:** If  $H$  is the subgroup of  $G$  leaving the origin invariant, then it is always possible to choose coordinates on  $M$  such that:

$$hy = D(h)y \quad \forall h \in H, \quad (4.3)$$

where  $D(h)$  is a linear representation of  $H$ .

For **Theorem I** we can have some intuition. The field redefinitions are equivalent to a change of coordinates on the manifold  $M$ . The theorem is telling us that the results of our computations must be independent of the type of coordinates we are using. Hence, the observables are unaffected by field redefinitions. All field redefinitions satisfying the **Theorem I** condition are called allowed ones.

The generators of  $G$  are denoted by  $(A_i, V_i)$ , where  $A_i$  and  $V_i$  represent the generators of the coset  $G/H$  and of the subgroup  $H$ , respectively. Any element of  $G$  can be decomposed as [55]

$$g_0 = e^{\xi A} e^{uV}, \quad (4.4)$$

where we defined  $\xi A = \xi_l A_l$  and  $uV = u_i V_i$  for simplicity. To find a non-linear realization, the trick is to promote the parameters  $\xi$ 's to coordinates of the manifold  $M$  and interpret them as the Goldstone bosons of the SSB. In order to fulfill the set of coordinates, we can introduce a vector  $\psi$  that transforms linearly under the subgroup  $H$

$$\psi \rightarrow D(h)\psi. \quad (4.5)$$



Moreover, for every element  $g \in G$  we can write the relation

$$\begin{aligned} ge^{\xi A} &= e^{\beta A} e^{uV} e^{\xi A}, \\ &= e^{\xi^g A} e^{u^g V}, \end{aligned} \quad (4.6)$$

with  $\xi_l^g = \xi_l^g(\xi)$  and  $u_l^g = u_l^g(\xi)$ . It is always possible to find such equality since the multiplication of two group elements also belongs to the group [57].

The transformations in (4.6) and in (4.5) for  $\xi^i$  and  $\psi$ , respectively,

$$\xi \rightarrow \xi^g(\xi), \quad (4.7)$$

$$\psi \rightarrow D(e^{u_i^g V_i})\psi. \quad (4.8)$$

provide a non-linear realization of the group  $G$ , which is called the standard one. This realization is said to be non-linear because the generators of  $G$  do not commute.

So far we only found a specific parametrization of the elements of  $M$ . First, we promote the parameters  $\xi$  associated with the generators of the coset space  $G/H$  to coordinates in the manifold. Then, we filled out the set by adding a vector  $\psi$  that transforms linearly under the unbroken group  $H$ . Lastly, we noticed that the way the coordinates transform characterize a non-linear realization of the symmetry. We remember the reader that any other possible parametrization can be put in the one we choose by an allowed field redefinition. Also, it is possible to find  $\psi$  transforming linearly under  $H$  due to **Theorem II**.

When we restrict the transformation  $g$  to the subgroup  $H$ , the Goldstone bosons transform linearly. For  $h \in H$ , the relation (4.6) becomes

$$he^{\xi A} = he^{\xi A} h^{-1} h = e^{\xi^g A} e^{u^g V}. \quad (4.9)$$

As a result, the coordinates transform as

$$e^{\xi A} \rightarrow he^{\xi A} h^{-1}, \quad (4.10)$$

$$\psi \rightarrow D(h)\psi. \quad (4.11)$$

As an example, let us apply this formalism to our simple model from Sec. 1.5. There we considered a complex scalar field  $\phi$  respecting an abelian global symmetry  $U(1)$ . The symmetry was spontaneously broken due to the presence of a non-vanishing vev  $\langle \phi \phi^* \rangle = v^2/2$ . Here, we denote  $G = U(1)$  and the broken generator by  $Y$ . After the SSB we have no symmetry left.

Applying the expression (4.6) to this case, we have

$$e^{i\xi_g Y} = g e^{i\xi Y} \quad (4.12)$$

$$= e^{i\theta Y} e^{i\xi Y}, \quad (4.13)$$

and we can recover the transformation for the Goldstone boson from Sec. 1.5

$$\xi \rightarrow \xi + \theta. \quad (4.14)$$

In this case we just have a shift because we are dealing with an abelian group.

Next, let us use the SM gauge group as an example. We know that the SSB pattern is  $SU(2)_L \times U(1)_Y \rightarrow U(1)_{EM}$ . The generator of the unbroken group is denoted by  $Q = Y + T^3$ , where  $Y$  is the hypercharge and  $T^3$  is the third generator of  $SU(2)_L$ . The generators of the coset space  $SU(2)_L \times U(1)_Y / U(1)_{EM}$  are denoted by  $T^i$ , which can be expressed in terms of the Pauli matrices by  $T^i = \sigma^i / 2$ . The  $SU(2)_L$  generators satisfy the following algebra [55]

$$[T^i, T^j] = i\epsilon^{ijk} T^k. \quad (4.15)$$

Using what we learned in equation (4.6), the Goldstone bosons  $\xi^i$  transform under  $g \in SU(2)_L \times U(1)_Y$  following the relation below

$$\begin{aligned} g e^{i\xi^i T^i} &= e^{i\beta_i T^i} e^{i\alpha Q} e^{i\xi^i T^i}, \\ &= e^{i\xi_g^i T^i} e^{i\alpha_g Q}. \end{aligned} \quad (4.16)$$

Note that this transformation rule is highly non-linear and to obtain a closed form for it is far from simple. Nevertheless, when we restrict the transformation to the unbroken subgroup  $U(1)_{EM}$  it gets simpler

$$e^{i\alpha Q} e^{i\xi^i T^i} = e^{i\alpha Q} e^{i\xi^i T^i} e^{-i\alpha Q} e^{i\alpha Q}, \quad (4.17)$$

$$= e^{i\xi_g^i T^i} e^{i\alpha Q}. \quad (4.18)$$

In turn, the  $\xi^i$ 's transform as follows

$$e^{i\xi_g^i T^i} = e^{i\alpha Q} e^{i\xi^i T^i} e^{-i\alpha Q}. \quad (4.19)$$

For infinitesimal transformations, the equation above leads to

$$\xi^i \rightarrow \xi^i + \alpha \epsilon^{ik3} \xi^k + \mathcal{O}(\alpha^2, \xi^2). \quad (4.20)$$

The rule above is similar to the one that we saw in the abelian case, except that now it also depends on the group constant structure since we are dealing with non-abelian theories.

At this point we have accomplished our goal. Just as a recap, our initial intention was to find all possible theories consistent with the SSB pattern. In the end, we only found one in (4.8), which we called the standard one. But, any other possible non-linear realization can be put in the latter by an allowed field redefinition. In other words, the problem of characterizing all non-linear realizations has been solved.

Now we must move on and construct a Lagrangian for the theory. One can use the transformations in (4.8) and define covariant derivatives for the field as it was done by [58]. Even if we are working with global symmetries the covariant derivatives will be local since the transformations in (4.8) depend on the field  $\xi$ . Another strategy used by [55] is to create functions of the Goldstone bosons fields that transform linearly under the symmetry. To do so, consider a linear representation  $\mathcal{D}(g)$  of  $G$  containing in its decomposition the representation  $D(h)$ . We define the field  $\Phi$  by

$$\Phi = \mathcal{D}(e^{\xi A})\psi. \quad (4.21)$$

Under (4.8), this combination goes to

$$\begin{aligned} \Phi' &= \mathcal{D}(e^{\xi^g A})\mathcal{D}(e^{u^g V})\psi, \\ &= \mathcal{D}(ge^{\xi A}e^{-u^g V})\mathcal{D}(e^{u^g V})\psi, \\ &= \mathcal{D}(g)\mathcal{D}(e^{\xi A})\mathcal{D}(e^{-u^g V})\mathcal{D}(e^{u^g V})\psi, \\ &= \mathcal{D}(g)\mathcal{D}(e^{\xi A})\psi, \\ &= \mathcal{D}(g)\Phi, \end{aligned} \quad (4.22)$$

where in the second line we used the rule in (4.6). Next, we can apply this strategy to the electroweak interactions.

As before, the generators are the ones in (4.15). First, consider a singlet  $h$  under  $U(1)_{EM}$ , which plays the role of the Higgs boson. This field is embedded into a doublet representation  $\mathcal{D}$  with hypercharge  $Y = 1/2$ :

$$\phi = \begin{pmatrix} 0 \\ h \end{pmatrix}. \quad (4.23)$$

A generic doublet  $\psi$  transforms under the representation  $\mathcal{D}$  as follows

$$\psi \rightarrow \mathcal{D}(g)\psi = e^{i\vec{\alpha}\cdot\frac{\vec{\sigma}}{2}} e^{i\alpha_Y Y} \psi, \quad (4.24)$$

where  $\alpha$  and  $\alpha_Y$  are the local parameters of the  $SU(2)_L$  and  $U(1)_Y$  groups, respectively. Restricting the transformation to the unbroken group  $U(1)_{EM}$ , one can recognize that  $\phi$  is indeed a singlet under the unbroken group.

Now we need to define the field  $\Phi$ . Following the prescription from (4.22), we end up with

$$\Phi = \mathcal{D}(e^{i\vec{\xi}\cdot\vec{Y}})\phi = e^{i\vec{\xi}\cdot\frac{\vec{\sigma}}{2}}\phi, \quad (4.25)$$

with  $\vec{Y}$  denoting the generators of  $SU(2)_L \times U(1)_Y / U(1)_{EM}$ . From the definition above it also follows that  $\Phi$  transforms as a doublet with hypercharge  $Y = 1/2$ :

$$\begin{aligned} \Phi &\rightarrow \mathcal{D}(e^{i\vec{\xi}^g\cdot\vec{Y}})e^{i\alpha Q}\phi, \\ &= \mathcal{D}(g)e^{i\vec{\xi}\cdot\frac{\vec{\sigma}}{2}}e^{-i\alpha Q}\phi, \\ &= e^{i\vec{\alpha}\cdot\frac{\vec{\sigma}}{2}}e^{i\alpha_Y Y}e^{i\vec{\xi}\cdot\frac{\vec{\sigma}}{2}}\phi, \\ &= e^{i\vec{\alpha}\cdot\frac{\vec{\sigma}}{2}}e^{i\alpha_Y \frac{1}{2}}\Phi, \end{aligned} \quad (4.26)$$

where in the second and third line we used that  $\phi$  is a singlet under  $U(1)_{EM}$ .

For us it is more convenient to work with a bi-doublet instead of a doublet. To this purpose, we define

$$\tilde{\Phi} = i\sigma_2\Phi^* = e^{i\vec{\xi}\cdot\frac{\vec{\sigma}}{2}} \begin{pmatrix} h \\ 0 \end{pmatrix}. \quad (4.27)$$

Using  $\sigma_a^2 = 1$  and  $\sigma_2\sigma_a^*\sigma_2 = -\sigma_a$ , one can show that  $\tilde{\Phi}$  transforms as a doublet with hypercharge  $Y = -1/2$ . With the fields in  $\Phi$  and  $\tilde{\Phi}$  we can write the bi-doublet as

$$M = (\tilde{\Phi}\Phi) = he^{i\vec{\xi}\cdot\frac{\vec{\sigma}}{2}}, \quad (4.28)$$

which under a  $SU(2)_L \times U(1)_Y$  transformation goes to

$$M \rightarrow g_L M g_R^\dagger, \quad (4.29)$$

where the matrices  $g_L$  and  $g_R$  are given by

$$g_L = e^{i\vec{\alpha} \cdot \frac{\vec{\sigma}}{2}}, \quad (4.30)$$

$$g_R = e^{i\alpha_Y \frac{\sigma_3}{2}}. \quad (4.31)$$

To leave the Goldstone bosons with the proper dimension we construct the matrix  $U$

$$U = e^{i \frac{\vec{\xi} \cdot \vec{\sigma}}{f}}, \quad (4.32)$$

where  $f$  is a dimensional parameter introduced to fix  $\xi$ 's dimensions and the factors of 2 were absorbed in the definition of the fields. Using this notation, the transformation in (4.29) can be written as

$$h \rightarrow h, \quad (4.33)$$

$$U \rightarrow g_L U g_R^\dagger. \quad (4.34)$$

From the equations above, one can see that  $h$  is a singlet of the SM gauge group, while the Goldstone bosons transform non-linearly among themselves. But, the matrix  $U$  transforms linearly as shown in (4.34). This is the major difference of the HEFT from the SM and the SMEFT. Here, we do not consider the observed Higgs boson in a doublet mixing with the Goldstone bosons of the SSB in the EFT construction.

Using the matrix  $U$  we can construct the leading order HEFT Lagrangian. Before moving forward, we need to define its covariant derivative [7, 8]:

$$D_\mu U(x) \equiv \partial_\mu U + i g \frac{g_a}{2} W_\mu^a U - i \frac{g'}{2} B_\mu \sigma_3, \quad (4.35)$$

where  $W_\mu^a$  and  $B_\mu$  are the gauge bosons for the  $SU(2)_L$  and  $U(1)_Y$ , respectively, with the gauge couplings  $g$  and  $g'$ .

The particle content is the same one as the SM, with a slight difference. Now we also consider the right-handed particles in a doublet structure, but they still are chargeless under  $SU(2)_L$ :

$$Q_R^i = \begin{pmatrix} u_R \\ d_R \end{pmatrix}, \begin{pmatrix} c_R \\ s_R \end{pmatrix}, \begin{pmatrix} t_R \\ b_R \end{pmatrix}, \quad (4.36)$$

$$L_R^i = \begin{pmatrix} 0 \\ e_R \end{pmatrix}, \begin{pmatrix} 0 \\ \mu_R \end{pmatrix}, \begin{pmatrix} 0 \\ \tau_R \end{pmatrix}, \quad (4.37)$$

To account for the different charge of each component under  $U(1)_Y$ , they generically transform as

$$\psi_R \rightarrow e^{i\alpha_T \left( Y + \frac{\sigma_3}{2} \right)} \psi_R. \quad (4.38)$$

For the electron the value  $Y$  has to be  $-1/2$ , for example. Their covariant derivative changes to

$$D_\mu \psi_R = \left( \partial_\mu + ig_s T^A G_\mu^A + ig' B_\mu \left( \frac{\sigma^3}{2} + Y_\psi \right) \right) \psi_R, \quad (4.39)$$

where the  $SU(3)_C$  only exists for the quarks, for the leptons it must be dropped. A table with the hypercharge of each particle can be found in Table 4.1.

$\psi$	$SU(2)_L$	$Y$
$Q_L$	<b>2</b>	1/6
$Q_R$	<b>1</b>	1/6
$L_L$	<b>2</b>	-1/2
$L_R$	<b>1</b>	-1/2

Table 4.1: Hypercharge values and representations under the SM gauge symmetry for the leptons, and quarks.

Before we write down the Lagrangian we must summarize the criteria we will employ to classify the leading order (LO) and next-leading order (NLO) operators. To this purpose, in Sec. 4.2 we discuss the Power Counting applied to the HEFT.

## 4.2 Power Counting for HEFT

In Sec. 1.3, we illustrated the importance of the Power Counting in our simple toy model. We showed that it makes the EFT able to make predictions in a consistent way. A precise definition of Power Counting is given in [7], which we state below.

A Power Counting must have two features:

1. Describe how the Lagrangian terms scales in a consistent manner with the dimensionful quantities in the theory; and
2. give a prescription to order the interactions in the Lagrangian in a way that we are able to estimate its relative physical impact on a measurement, so the precision of the calculations can be well defined.

In the SMEFT, the Power Counting is in canonical mass dimension. An operator built with total mass dimension  $d$  should be multiplied by a factor  $\Lambda^{4-d}$ , where  $\Lambda$  represents the new

physics scale. The Lagrangian is organized in terms of a  $\Lambda$  expansion. The leading terms correspond to the ones with  $\Lambda^0$  which gives the SM Lagrangian, the next-leading terms contain operators with dimension  $d = 5, 6$ , and so on.

In contrast, the HEFT has a scalar sector constructed out of Chiral Perturbation theory ( $\chi$ PT) and, at the same time, it has fermions and the transverse components of the gauge bosons, whose interactions can be organized in terms of canonical dimensions. The presence of these two distinct interactions makes the HEFT Power Counting complex. To understand it, first we review in Sec. 4.2.1 the Power Counting for Chiral Lagrangians, and in Sec. 4.2.2 we summarize the criteria chosen by [7] to define the NLO operators.

### 4.2.1 Power Counting for $\chi$ PT

Previously, we used  $\chi$ PT to write down an EFT for the electroweak interactions. We realized that the Goldstone bosons  $\xi^i$  transform in a non-linear way, and we found to be more useful to work with functions of the fields  $\xi^i$  that transform linearly under the symmetry. In particular, we constructed the matrix  $U$

$$U = e^{i \frac{\vec{\xi} \cdot \vec{\sigma}}{f}}, \quad (4.40)$$

which transforms as

$$U \rightarrow g_L U g_R^\dagger, \quad (4.41)$$

with  $g_L$  and  $g_R$  defined in equations (4.30) and (4.31), respectively.

Let us assume for a second that the scalar sector is all there is for the electroweak interactions, and we are working at energies well below the Higgs boson mass. Moreover, let us consider that the symmetry  $SU(2)_L \times U(1)_Y$  is global instead of local. To describe the physics in this situation, we can write a leading order Lagrangian of the form

$$\mathcal{L}_2 = \frac{f^2}{4} \text{Tr}\{\partial_\mu U^\dagger \partial^\mu U\}, \quad (4.42)$$

where the factor  $f^2/4$  was chosen to leave the Goldstone bosons with canonical kinetic terms.

Since the matrix  $U$  is dimensionless, we can organize the effective interactions as an expansion in derivatives:

$$\mathcal{L} = \mathcal{L}_2 + \mathcal{L}_4 + \mathcal{L}_6 + \dots, \quad (4.43)$$

where  $\mathcal{L}_d$  has operators with  $d$  derivatives.

As discussed in [7], the derivative expansion is a way to systematically renormalize the theory. When we are ordering the interactions in terms of the number of derivatives, we are using

Weinberg's power counting approach [59]. The latter leads to the following way of organizing the interactions: each order of the EFT must contain at least all the operators that are required as counterterms for the one-loop renormalization of the previous order.

For example, all the operators required as counterterms to absorb the one-loop divergences from  $\mathcal{L}_2$  contain four-derivatives, therefore are in  $\mathcal{L}_4$ . To show this result, we can count the number of powers of momentum for an amplitude as follows. An amplitude with  $L$  loops and containing  $N_d$  vertices with  $d$  derivatives scale with  $D$  powers of momentum, given by [59]

$$D = 2L + 2 + \sum_d (d - 2)N_d. \quad (4.44)$$

If we apply this formula for diagrams containing one loop,  $L = 1$ , and with interactions carrying only two derivatives,  $d = 2$ , we get  $D = 4$ . Which means that all the interactions required as counterterms are in  $\mathcal{L}_4$ . For the case of two loops with only interactions with  $d = 2$  or at one loop with one interaction with  $d = 4$ , we obtain  $D = 6$ . This shows that theories constructed with  $\chi$ PT are renormalizable at fixed order in the momentum expansion [7, 59]. This is different from what we saw in Sec. 1.3, where a theory following a power counting based on mass dimension like the SMEFT is renormalizable at fixed order in the  $1/\Lambda$  expansion.

## 4.2.2 HEFT Basis

As discussed by [7, 13], the HEFT can be understood as a fusion of two theories. The first one is constructed out of  $\chi$ PT corresponding to the Higgs bosons and the Goldstone bosons of the EWSB. Meanwhile, the other is associated with the transverse components of the gauge bosons and to the fermions, which can be seen as a linear realization of the symmetry group. This makes the task of finding a precise HEFT counting very complex.

To see these contradictions, let us summarize the observation made by [7]. Consider the operator  $\mathcal{P}_{WWW} = \frac{4\pi\epsilon_{abc}}{\Lambda^2} W_\mu^{a\nu} W_\nu^{b\rho} W_\rho^{c\mu}$ . On one hand, according to Weinberg's counting rule, this effective operator has a chiral dimension equals to six. Thus, it should be an operator at next-next-leading order. On the other hand, since it only contains transverse gauge fields, it should not follow a chiral counting but a SMEFT counting instead, which would make it a next-leading-order term. The different counting rules give contradictory estimates in this case because they are built from different assumptions.

Here, to define the NLO operators we follow the same approach from [7]. They argue that instead of basing the theory on a sophisticated counting rule, which is not valid in full generality, the selection can be made based on the following strategy. A NLO operator should satisfy at least one of the criteria below:



1. It is necessary for reabsorbing 1-loop divergences originating from  $\mathcal{L}_0$ .
2. It presents the same suppression as the operators in the first class and receives finite 1-loop contributions.
3. It is classified as a NLO operator in at least one of the counting principles.

The class of operators satisfying the condition 1 are the ones required to absorb the divergences emerging from the chiral interactions since they can not be absorbed by operators from  $\mathcal{L}_0$ . One operator satisfying the condition number 2 is  $\bar{\psi}_L \sigma^{\mu\nu} U \psi_R X_{\mu\nu}$ , with  $X_{\mu\nu}$  denoting a generic field strength tensor, which correspond to a dipole interaction. The last assumption allows us to include operators important in at least one scenario, preserving the generality of the HEFT. For instance, this is the case for the operator  $\mathcal{P}_{WWW}$ .

In [13], after applying the EOMs to remove redundant interactions, neglecting right-handed neutrinos, and allowing CP violating interactions, the basis contains 148 operators. The ones we will use in our analysis are presented in the next section, assuming that CP is conserved and also neglecting the inclusion of flavour changing interactions. Contrasting with the Warsaw basis, which has 59 operators assuming baryon number conservation, it is clear that the HEFT allow more interactions since it has less symmetry restrictions than the SMEFT.

### 4.3 The HEFT Lagrangian

Finally, the leading order HEFT Lagrangian is given by [7, 13]

$$\begin{aligned}
\mathcal{L}_o = & -\frac{1}{4} G_{\mu\nu}^\lambda G^{\lambda\mu\nu} - \frac{1}{4} W_{\mu\nu}^a W^{a\mu\nu} - \frac{1}{4} B_{\mu\nu} B^{\mu\nu} + \\
& + \frac{1}{2} \partial_\mu h \partial^\mu h - \frac{v^2}{4} \text{Tr} \left[ D_\mu U D^\mu U \right] \mathcal{F}_C(h) - V(h) + \\
& + i \bar{Q}_L \not{D} Q_L + i \bar{L}_L \not{D} L_L + i \bar{Q}_R \not{D} Q_R + i L_R \not{D} L_R + \\
& - \frac{v}{\sqrt{2}} \left( \bar{Q}_L U \mathcal{Y}_Q(h) Q_R + \text{h.c.} \right) - \frac{v}{\sqrt{2}} \left( \bar{L}_L U \mathcal{Y}_L(h) L_R + \text{h.c.} \right).
\end{aligned} \tag{4.45}$$

In the first line we have the gauge bosons field strengths. Moving to the second line, we have the Higgs and Goldstone bosons kinetic terms and the Higgs potential. The Goldstone bosons kinetic term is also responsible for the  $W^\pm$  and  $Z$  masses. The function  $\mathcal{F}_C(h)$  is expanded in terms of the ratio  $h/v$ , defined as

$$\mathcal{F}_C(h) = 1 + 2a_C \frac{h}{v} + b_C \frac{h^2}{v^2} + \dots, \tag{4.46}$$

with the dots accounting for higher powers of  $h/v$ . The third and fourth line contains the fermions' kinetic and Yukawa terms, respectively, where we suppressed the family indices. Also, the Yukawas' interactions  $\mathcal{Y}_{Q(L)}(h)$  take a similar form of the function  $\mathcal{F}_C$ :

$$\mathcal{Y}_Q(h) = \text{diag}\left(Y_U^{(0)} + Y_U^{(1)}\frac{h}{v} + \dots, Y_D^{(0)} + Y_D^{(1)}\frac{h}{v} + \dots\right), \quad (4.47)$$

$$\mathcal{Y}_L(h) = \text{diag}\left(0, Y_l^{(0)} + Y_l^{(1)}\frac{h}{v} + \dots\right), \quad (4.48)$$

where we assumed the Yukawa interactions to be diagonal.

In the following we define the NLO operators. First, it is convenient to define the chiral vector and scalar fields

$$V_\mu = (D_\mu U)U^\dagger, \quad (4.49)$$

$$T = U\sigma_3U^\dagger, \quad (4.50)$$

transforming in the adjoint representation of  $SU(2)_L$ ,

$$V_\mu \rightarrow g_L V_\mu g_L^\dagger, \quad (4.51)$$

$$T \rightarrow g_L T g_L^\dagger. \quad (4.52)$$

Also, in order to see which interactions are turned on by the effective operators it is useful to keep in mind that, in the unitary gauge, the chiral scalar and vector fields are given by

$$T = \sigma_3 \quad (4.53)$$

$$V_\mu = igW_\mu^+ t^+ + igW_\mu^- t^- + i\frac{gg'}{e}Z_\mu\frac{\sigma_3}{2}, \quad (4.54)$$

where we used the same definitions of the physical fields in equations (2.19) and (2.28). Moreover, we defined the matrices  $t^+$  and  $t^-$  in terms of the  $SU(2)_L$  generators by

$$t^+ = \frac{1}{\sqrt{2}}(T^1 + iT^2), \quad (4.55)$$

$$t^- = \frac{1}{\sqrt{2}}(T^1 - iT^2). \quad (4.56)$$

In the unitary gauge, the Goldstone bosons become the longitudinal components of the  $W^\pm$  and  $Z$  gauge bosons, leaving the matrix  $U$  equals to the identity.

In our analysis, only operators affecting TGCs and the Higgs couplings are taken into account. Here we will only list the ones we need in our study. For a list of all the operators in the

basis we refer the reader to [13]. The operators affecting TGCs are listed in Table 4.2, while the ones affecting the Higgs coupling are listed in Table 4.3.

From the Table 4.2, the operators  $\mathcal{P}_2$ ,  $\mathcal{P}_3$ , and  $\mathcal{P}_{WWW}$  lead to the same triple gauge boson interactions as the operators  $\mathcal{O}_B$ ,  $\mathcal{O}_W$ , and  $\mathcal{O}_{WWW}$  in the SMEFT basis. Due to this relation, these SMEFT operators are said to be their linear siblings. In contrast, the operator  $\mathcal{P}_{13}$  leads to an interaction that can not be reproduced by any dimensional-six operator in our SMEFT basis. As in the SMEFT, the HEFT has no source of anomalous interaction among the neutral gauge bosons at this order. As a convention, the Wilson coefficients affecting TGCs will be denoted by  $c$  and the ones affecting the Higgs interactions will be denoted by  $a$ .

The Wilson coefficients for the operators in Table 4.2 for  $\mathcal{F} = 1$  are denoted by

$$\{c_2, c_3, c_{13}, c_{WWW}\}. \quad (4.57)$$

In terms of the Lorentz structures from (2.30), they modify the following couplings

$$g_1^Z = 1 + \frac{g}{4\pi \cos^2 \theta} c_3, \quad (4.58)$$

$$\kappa_z = 1 + \frac{g}{4\pi} \left( c_3 + 2c_{13} - 2 \tan \theta c_2 \right), \quad (4.59)$$

$$\kappa_\gamma = 1 + \frac{g}{4\pi} \left( c_3 + 2c_{13} + 2 \frac{c_2}{\tan \theta} \right), \quad (4.60)$$

$$\lambda_Z = \lambda_\gamma = \frac{6\pi g v^2}{\Lambda^2} c_{WWW}. \quad (4.61)$$

Note that we have the same corrections to the SM predictions as we had in the SMEFT, plus one more source of deviation in the couplings  $\kappa_Z$  and  $\kappa_\gamma$  due to the presence of the operator  $\mathcal{P}_{13}$ .

The last set of operators important to us affect the Higgs couplings with the fermions and with the gauge bosons. First, we need to point out that the coefficient  $a_C$  from equation (4.46) takes the following form

$$a_C = 1 + \Delta a_C. \quad (4.62)$$

When  $\Delta a_C = 0$  the electroweak gauge bosons couplings with the Higgs are the same as in the SM. Basically,  $\Delta a_C$  is accounting for deviations from the SM predictions, and here it is considered to be in the same order as the NLO operators. Also, in our analysis we have enough information to account for deviations in the Yukawa couplings of the bottom, tau, muon, and top fermions. Moreover, we included the NLO bosonic operators shown in Table 4.3.

The functions  $\mathcal{F}$  are parametrized as follows

$$\mathcal{F}_i(h) = 1 + 2\tilde{a}_i \frac{h}{v}. \quad (4.63)$$

If  $c_i$  represents the Wilson coefficients of the operator  $\mathcal{P}_i$ , it appears multiplying all terms in  $\mathcal{F}$ . For convenience, we define

$$c_i \tilde{a}_i \rightarrow a_i, \quad (4.64)$$

which means that the parameters fitted in our Higgs analysis are denoted by

$$\{a_4, a_5, a_B, a_W, a_G, a_{17}\}. \quad (4.65)$$

From Table 4.3, the operators  $\mathcal{P}_4, \mathcal{P}_5, \mathcal{P}_B, \mathcal{P}_W$ , and  $\mathcal{P}_G$  give the same HVV interactions as the SMEFT operators  $\mathcal{O}_B, \mathcal{O}_W, \mathcal{O}_{BB}, \mathcal{O}_{WW}$ , and  $\mathcal{O}_{GG}$ , respectively. The same discussion we did for the linear siblings in the previous section is valid here.  $\mathcal{P}_{17}$  is the only HEFT operator with no linear sibling. The latter leads to interactions of the Higgs with the neutral electroweak gauge bosons.

In the unitary gauge, the couplings of the Lorentz structures from (3.27) in terms of the Wilson coefficients of the HEFT basis are given by [13]

$$\begin{aligned} g_{Hgg} &= -\frac{1}{2v} a_G, \\ g_{H\gamma\gamma} &= -\frac{1}{2v} (s^2 a_W + c^2 a_B), \\ g_{HZ\gamma}^{(1)} &= -\frac{g^S}{4c} \left( a_5 + 2\frac{c}{s} a_4 + 2a_{17} \right), \\ g_{HZ\gamma}^{(2)} &= \frac{sc}{v} (a_B - a_W), \\ g_{HZZ}^{(1)} &= \frac{g}{4\pi v} \left( 2\frac{s}{c} a_4 - a_5 - a_{17} \right), \\ g_{HZZ}^{(2)} &= -\frac{1}{2v} (s^2 a_B + c^2 a_W), \\ g_{HZZ}^{(3)} &= m_Z^2 (\sqrt{2} G_F)^{1/2} (1 + \Delta a_C), \\ g_{HWW}^{(1)} &= -\frac{1}{4\pi v} a_5, \\ g_{HWW}^{(2)} &= \frac{1}{v} a_W, \\ g_{HWW}^{(3)} &= 2m_W^2 (\sqrt{2} G_F)^{1/2} (1 + \Delta a_C), \end{aligned} \quad (4.66)$$

where  $G_F$  is the Fermi constant, and we defined  $\sin \theta = s$  and  $\cos \theta = c$ .

$\mathcal{P}_2(h) = \frac{\imath}{4\pi} B^{\mu\nu} \text{Tr} \left( T[V_\mu, V_\nu] \right) \mathcal{F}_2$	$\mathcal{P}_3(h) = \frac{\imath}{4\pi} \text{Tr} \left( W^{\mu\nu} [V_\mu, V_\nu] \right) \mathcal{F}_3$
$\mathcal{P}_{13}(h) = \frac{\imath}{4\pi} \text{Tr} \left( TW_{\mu\nu} \right) \text{Tr} \left( T[V_\mu, V_\nu] \right) \mathcal{F}_{13}$	$\mathcal{P}_{WWW}(h) = \frac{4\pi\epsilon_{abc}}{\Lambda^2} W_\mu^{a\nu} W_\nu^{b\rho} W_\rho^{c\mu} \mathcal{F}_{WWW}$

Table 4.2: HEFT operators affecting TGC

$\mathcal{P}_4(h) = \frac{\imath}{4\pi} B_{\mu\nu} \text{Tr}(TV^\mu) \partial^\nu \mathcal{F}_4$	$\mathcal{P}_5(h) = \frac{\imath}{4\pi} \text{Tr}(W_{\mu\nu} V^\mu) \partial^\nu \mathcal{F}_5$
$\mathcal{P}_B(h) = -\frac{1}{4} B_{\mu\nu} B^{\mu\nu} \mathcal{F}_B$	$\mathcal{P}_W(h) = -\frac{1}{4} W_{\mu\nu}^a W^{a\mu\nu} \mathcal{F}_W$
$\mathcal{P}_G(h) = -\frac{1}{4} G_{\mu\nu}^a G^{a\mu\nu} \mathcal{F}_G$	$\mathcal{P}_{17}(h) = \frac{\imath}{4\pi} \text{Tr}(TW_{\mu\nu}) \text{Tr}(TV^\mu) \partial^\nu \mathcal{F}_{17}$

Table 4.3: NLO Bosonic HEFT operators

## 4.4 HEFT vs SMEFT

At this point, we showed two possible EFTs used to describe the LHC data. The SMEFT, sometimes referred to as the linear parametrization, makes the same low-energies assumptions as of the SM, except it allows higher dimension operators. Also referred to as the non-linear parameterization, the HEFT assumes a non-linear realization of the SM gauge symmetry, where we constructed its Lagrangian using the CCWZ formalism. In these section we discuss how we can ascertain which scenario is realized at low-energies.

As we have mentioned in the previous sections, since in the non-linear parametrization we do not consider the Higgs boson as part of a  $SU(2)_L$  doublet, the building blocks to construct Lagrangian invariants are different in both cases. In the HEFT, we do not have a symmetry restriction ensuring relations among the Goldstone bosons and the Higgs boson. As a consequence, interactions that were correlated in the SMEFT Lagrangian due to this relation become uncorrelated in the HEFT.

As an example, in the linear parametrization, the operator  $\mathcal{O}_B$  leads to TGC and HVV interactions in the unitary gauge:

$$\begin{aligned}
\mathcal{O}_B = & \frac{ie g^2}{8} A_{\mu\nu} W^{-\mu} W^{+\nu} (v+h)^2 - \frac{ie^2 g}{8 \cos \theta_W} Z_{\mu\nu} W^{-\mu} W^{+\nu} (v+h)^2 \\
& - \frac{eg}{4 \cos \theta_W} A_{\mu\nu} Z^\mu \partial^\nu h (v+h) + \frac{e^2}{4 \cos^2 \theta_W} Z_{\mu\nu} Z^\mu \partial^\nu h (v+h).
\end{aligned} \tag{4.67}$$

The expansion above shows which interactions are correlated. For instance, the interactions  $\gamma - W - W$  and  $\gamma - Z - h$  are related because they share the same Wilson coefficient.

Meanwhile, in the non-linear parametrization, the same set of anomalous interactions are

given by the operators  $\mathcal{P}_2$  and  $\mathcal{P}_4$ :

$$4\pi g' \mathcal{P}_2(h) = 2ie g^2 A_{\mu\nu} W^{-\mu} W^{+\mu} \mathcal{F}_2(h) - 2 \frac{ie^2 g}{\cos \theta_W} Z_{\mu\nu} W^{-\mu} W^{+\nu} \mathcal{F}_2(h), \quad (4.68)$$

$$4\pi g' \mathcal{P}_4(h) = -\frac{eg}{\cos \theta_W} A_{\mu\nu} Z^\mu \partial^\nu \mathcal{F}_4(h) + \frac{e^2}{\cos^2 \theta_W} Z_{\mu\nu} Z^\mu \partial^\nu \mathcal{F}_4(h). \quad (4.69)$$

If we write  $\mathcal{F}_i = (1 + \tilde{a}_i h/v)^2$  we do not have the same correlation as before unless  $a_4 = 2c_2$ . In particular, the  $\gamma - W - W$  interaction is not related to the  $\gamma - Z - h$  one since they have different Wilson coefficients. The same discussion applies to the linear operator  $\mathcal{O}_W$  and the non-linear ones  $\mathcal{P}_3$  and  $\mathcal{P}_5$ .

Following [14, 13, 8] we can construct four specific combinations of the variables  $c_2$ ,  $c_3$ ,  $a_4$  and  $a_5$  which are useful to study the decorrelations present in the TGC and Higgs datasets:

$$\begin{aligned} \Sigma_B &\equiv \frac{1}{\pi g t_\theta} (2c_2 + a_4), & \Sigma_W &\equiv \frac{1}{2\pi g} (2c_3 - a_5), \\ \Delta_B &\equiv \frac{1}{\pi g t_\theta} (2c_2 - a_4), & \Delta_W &\equiv \frac{1}{2\pi g} (2c_3 + a_5). \end{aligned} \quad (4.70)$$

For simplicity we denoted  $t_\theta = \tan \theta$ . In the SMEFT, two of these combinations are zero due to the gauge invariance and the Higgs doublet nature:

$$\Delta_B = \Delta_W = 0. \quad (4.71)$$

While the remaining two are directly proportional to the Wilson coefficients of the operators  $\mathcal{O}_B$  and  $\mathcal{O}_W$ :

$$\begin{aligned} \Sigma_B &= v^2 \frac{f_B}{\Lambda^2}, \\ \Sigma_W &= v^2 \frac{f_W}{\Lambda^2}, \end{aligned} \quad (4.72)$$

with  $f_B$  and  $f_W$  being their Wilson coefficients, respectively. In contrast, the HEFT operators can lead to independent modifications to these four variables. Hence, their study is a way to investigate how the gauge symmetry is realized at low energies.

Just to summarize, let us recap what we saw in this chapter. First, we reviewed how to use the non-linear representations of a SSB pattern to construct an EFT with minimum IR assumptions. Later, we applied this approach to the electroweak interactions and we built up the HEFT Lagrangian. Lastly, we saw how to search for signals that can distinguish whether the gauge symmetry is linearly realized or not. In the next part, we will use the HEFT framework

to analyze the LHC Run 2 data concerning the TGCs and Higgs interactions.





## **Part II**

# **Analysis Framework**



---

---

# CHAPTER 5

---

## HEFT CONSTRAINTS

### 5.1 TGC data sets

As we saw in previous sections, the TGCs amid the electroweak gauge bosons are sensible to new physics effects. In Chapter 2 we saw their SM predictions and in Chapters 3 and 4 these couplings receive corrections due to the presence of effective operators. The SMEFT framework has three dimensional-six operators from the basis presented in [9] responsible for these modifications:  $\mathcal{O}_B$ ,  $\mathcal{O}_W$ , and  $\mathcal{O}_{WW}$ . While the HEFT has four:  $\mathcal{P}_2$ ,  $\mathcal{P}_3$ ,  $\mathcal{P}_{WWW}$ , and  $\mathcal{P}_{13}$ . Here, we will use the HEFT framework, so the operators used in our analysis are the ones from Table 4.2.

In our study we used the electroweak diboson data from the LHC Run 2. More specifically, we looked for shifts from the SM prediction in the diboson production of  $WZ$ ,  $WW$ , and  $W\gamma$  pairs as well as the vector boson fusion in the production of  $Z$ 's ( $Zjj$ ). The data sets used in our analysis are displayed in Table 5.1. In total, we had 73 data points, that is, counting the bins from all distributions we had 73 observables. As an example, in Figure (5.1) we display the  $M(WZ)$  distribution from CMS  $WZ$  used to constrain the Wilson coefficients in our analysis.

To contrast the theory with data we need the theoretical predictions. They were simulated using MADGRAPH5\_AMC@NLO [67] with the UFO files for our effective Lagrangian generated with FEYNRULES [68, 69]. For the parton shower and hadronization we employed PYTHIA8 [70], and for the detector effects we employed DELPHES [71]. We applied the same selection cuts discussed in the respective articles using C or Python with the module LHCReader [72]. The strategy to perform the simulation is the following. First, we need to reproduce

Name	Channel	Distribution	# bins	Data set	Int. Lum.
ATLAS $WW$	$WW \rightarrow e^\pm \mu^\pm + \cancel{E}_T(0j)$	$m_T$	17 (15)	ATLAS 13 TeV	$36 \text{ fb}^{-1}$ [60]
ATLAS $WW + \text{jets}$	$WW \rightarrow e^\pm \mu^\pm + \cancel{E}_T(1j)$	$\frac{d\sigma}{dm_{l+l^-}}$	10	ATLAS 13 TeV	$139 \text{ fb}^{-1}$ [61]
ATLAS $WZ$	$WZ \rightarrow l^+ l^- l^{(\prime)\pm}$	$m_T^{WZ}$	6	ATLAS 13 TeV	$36.1 \text{ fb}^{-1}$ [62]
ATLAS $Zjj$	$Zjj \rightarrow l^+ l^- jj$	$\frac{d\sigma}{d\phi}$	12	ATLAS 13 TeV	$139 \text{ fb}^{-1}$ [63]
CMS $W\gamma$	$W\gamma \rightarrow l\nu\gamma$	$\frac{d^2\sigma}{dp_T d\phi}$	12	CMS 13 TeV	$137.1 \text{ fb}^{-1}$ [64]
CMS $WZ$	$WZ \rightarrow l^+ l^- l^\pm$	$M(WZ)$	7	CMS 13 TeV	$137.2 \text{ fb}^{-1}$ [65]
CMS $WW 0j$	$WW \rightarrow l^+ l^- + 0/1j$	$M(l^+ l^-)$	11	CMS 13 TeV	$35.9 \text{ fb}^{-1}$ [66]

Table 5.1: Data sets used for the TGC analysis

the SM signal. For that we simulate the same process as the experimental Collaborations taking into account the same selections cuts. Once we have managed to reproduce the distribution for the SM signal we can move on and simulate the effects of the anomalous contributions. We must point out that, while the Collaborations typically perform the simulations at Next-Leading Order (NLO) in QCD, we only perform the simulation at Leading Order (LO). For each bin of the distribution, we compute the ratio among the SM signal provided by the Collaborations and ours. We use this ratio to correct our SM prediction and also the simulation of the effective operators bin-wise. We do not simulate the background processes, we use the same predictions as of the Collaborations. In Table 5.2 we display the how we generated the processes and the selection cuts applied in each analysis. When we needed to run Delphes to simulate the detector effects, we use the default CMS or ATLAS card provided by the program.

Excluding the data set CMS  $WW 0j$ , all the remaining ones followed a Gaussian distribution [73]. Whenever available, we used the information about the correlation matrix and uncertainties for the bins. When they were not, we obtained this information by fine-tuning the covariance matrix up to the point that our confidence regions for some Wilson coefficients matched the ones provided by the Collaborations. The data set CMS  $WW 0j$  followed a Poisson distribution where the systematical uncertainties were accounted through pulls [74]. The latter was also unavailable and we used the same procedure we applied to obtain the covariance matrices.

For the Gaussian distributed datasets, the  $\chi^2$  takes the following form

$$\chi^2 = \sum_{i,j} (N_{\text{data}}^i - N_{\text{theory}}^i) V_{ij}^{-1} (N_{\text{data}}^j - N_{\text{theory}}^j), \quad (5.1)$$

with  $N_{\text{data}}^i$  and  $N_{\text{theory}}^i$  denoting the observed number of events and the theory prediction for the bin  $i$ , respectively, and  $V_{ij}$  represents the covariance matrix among the bins. Meanwhile, for the

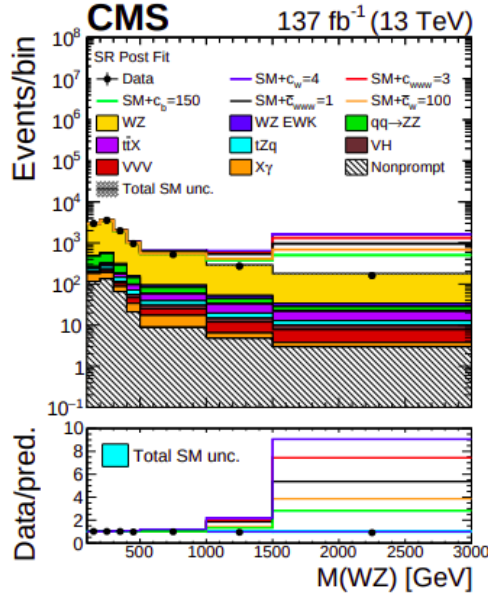


Figure 5.1: Distribution of the invariant mass of the  $WZ$  system for the  $WZ$  pair production from CMS  $WZ$ . The yellow region represents the SM signal for  $WZ$  pair production, while the remaining regions represent background processes. A few values of the SM prediction together with the effect of the Wilson coefficients from the SMEFT basis are also displayed for comparison.

Poisson distributed datasets, the expression for the  $\chi^2$  is

$$\chi^2 = 2 \sum_i \left\{ \tilde{N}_{\text{theory}}^i - \tilde{N}_{\text{data}}^i + \tilde{N}_{\text{data}}^i \log \left( \frac{\tilde{N}_{\text{data}}^i}{\tilde{N}_{\text{theory}}^i} \right) \right\} + \xi_0^2 + \xi_1^2 + \xi_2^2, \quad (5.2)$$

with,

$$\begin{aligned} \tilde{N}_{\text{theory}}^i &= N_{\text{signal}}^i \left( 1 - \xi_0 a \sigma_{\text{sys}}^i \right) + N_{\text{backg}}^i \left( 1 - \xi_2 c \sigma_{\text{sys}}^i \right), \\ \tilde{N}_{\text{data}}^i &= N_{\text{theory}}^i \left( 1 - \xi_1 b \right), \end{aligned} \quad (5.3)$$

where  $N_{\text{signal}}^i$ ,  $N_{\text{backg}}^i$ , and  $N_{\text{data}}^i$  denote the signal, the background, and the observed number of events in the bin  $i$ , the  $\xi$ 's represent the pulls, and the remaining quantities  $a$ ,  $b$ ,  $c$ , and  $\sigma_{\text{sys}}^i$  are obtained by fine-tuning the uncertainties as we described in the previous paragraph.

In general, the number of events takes the the following form

$$N^i = N_{\text{SM}}^i + \sum_j c_j N_{\text{Int},j}^i + \sum_{l \geq m} c_l c_m N_{\text{BSM},lm}^i, \quad (5.4)$$

with  $N^i$  denoting the number of events for the bin  $i$ , and with  $c$  denoting the Wilson coeffi-

Dataset	Process in MadGraph	Selection cuts
ATLAS $WW$	$p p > e^+ \nu_e \mu^- \nu_{\mu}$ $p p > e^- \nu_e \mu^+ \nu_{\mu}$	$N_{\text{b-tagged jets}} = 0, p_T^{l_1,2} = 45, 30$ $m_{ll}^T > 50.0$
ATLAS $WW + \text{jets}$	$p p > e^+ \nu_e \mu^- \nu_{\mu} j$ $p p > e^- \nu_e \mu^+ \nu_{\mu} j$	$N_{\text{jets}} > 0, p_T^l > 27,  \eta^l  < 2.5$ $p_T^j > 30,  y^j  < 4.5, m_{ll} > 85$
ATLAS $WZ$	$p p > l^+ l^- l \nu$ $l^+ = e^+ \mu^+, l^- = e^- \mu^-, \nu = \nu_e \nu_{\mu} \nu_e \nu_{\mu}$	$ \eta^l  < 2.5, p_T^Z > 15, p_T^W > 20$ $ m_{ll}^Z - m_Z  < 10$
ATLAS $Zjj$	$p p > z > e^+ e^- j j \text{ QCD}=0$ $p p > z > \mu^+ \mu^- j j \text{ QCD}=0$	One pair OSSF (Opposite Sign Same Flavor) $p_T^l > 27,  \eta^l  < 2.5, 81 < m_{ll} < 101$ $m_{ll}^T > 20, N_{\text{jets}} > 2, p_j^T > 25,$ $ y^j  < 4.4, \Delta R(j, l) > 0.4$
CMS $W\gamma$	$p p > l \nu a$ $p p > l \nu a j$ $l = e^+ e^- \mu^+ \mu^-, \nu = \nu_e \nu_{\mu} \nu_e \nu_{\mu}$	$p_T^l > 80,  \eta^L  < 2.5, p_T^\gamma > 80$ $ \eta^\gamma  < 2.5, \Delta R(l, \gamma) > 0.7, \text{MET} > 40$ Veto on events with $70 < m_{l\gamma} < 100$
CMS $WZ$	$p p > l^+ l^- \nu l$ $p p > l^+ l^- \nu l j$	OSSF, $\text{MET} > 30, \Delta R(j, l) > 0.4$ $p_T^l > 25,  m_{ll}^Z - m_Z  < 15,$ $N_{\text{b-tagged jets}} = 0, m_{l_1 l_2 l_3} > 100$
CMS $WW 0j$	$p p > e^+ \nu_e \mu^- \nu_{\mu}$ $p p > e^- \nu_e \mu^+ \nu_{\mu}$	$\text{MET} > 20, p_T^{l_1} > 25, p_T^{l_2} > 20,$ $ \eta^l  < 2.5, m_{ll} > 20, m_{ll}^T > 30$

Table 5.2: Table with the generated processes and the typical selection cuts. More details about the selection can be found in the respective papers together with the definition of the kinematical variables.

icients. The first term on the right-hand side denotes the leading-order HEFT prediction, which is the same as the SM one, the second term denotes the interference among the the SM and the anomalous contributions, while the last the denotes the purely anomalous contribution. When the fit is perform up to linear order in the Wilson coefficients the last term must be dropped.

Taking into account all the distributions, we have a  $\chi^2$  function depending on four Wilson coefficients,

$$\chi_{\text{TGC}}^2(c_2, c_3, c_{WWW}, c_{13}). \quad (5.5)$$

Also, we neglected anomalous interaction among the gauge bosons and fermions for simplicity.

## 5.2 Higgs data sets

To obtain the constraints for the bosonic operators in Table 4.3 and also for the Higgs-fermionic interactions we need datasets that can probe the Higgs couplings. In this work we use two types of them. The first one is the total Signal Strength (SS), which is the observed rate

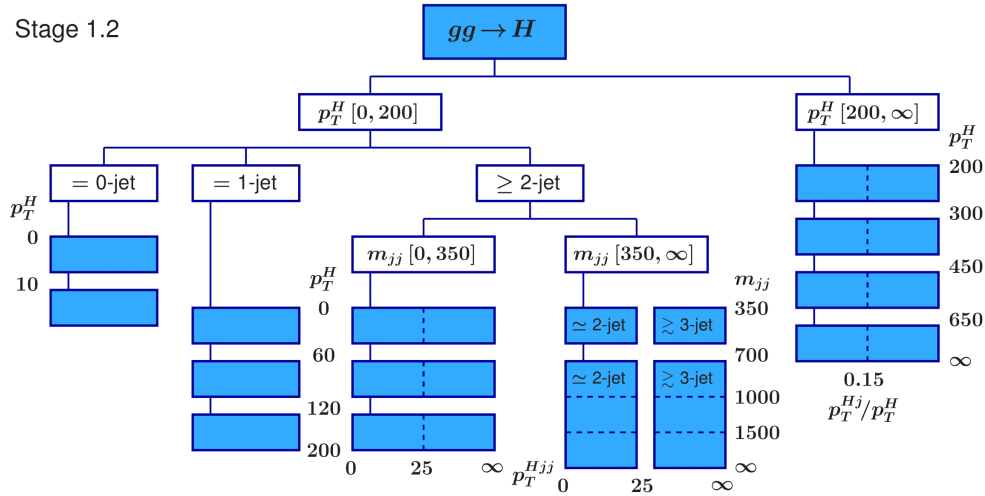


Figure 5.2: Definition of STXS Stage 1.2 bins for the ggF production mode.

normalized by the SM prediction:

$$\mu_i^f = \frac{\sigma_i \cdot \text{Br}^f}{(\sigma_i \cdot \text{Br}^f)_{\text{SM}}}, \quad (5.6)$$

where  $\sigma_i$  is the Higgs production cross-section in the channel  $i$ , while  $\text{BR}_f$  is the Branching Ratio for the Higgs decay mode  $f$ . For a list of the Higgs production and decay modes we refer the reader to [75]. Due to the narrow-width approximation [76], the total cross-section is parametrized in terms of the production cross-section times the branching ratio.

The second one, the Simplified Template Cross Sections (STXS), is the set of Higgs kinematic distributions. This template was created to measure different regions of the phase-space minimizing the theory dependence while at the same time maximizing the sensitivity of the measurements. For a detail discussion of this framework see [75]. The exclusive regions of the phase space are called bins. The bins for the Higgs production by gluon fusion are defined in Figure (5.2), by Vector Boson Fusion (VBF) are in Figure (5.3), by associated production (VH) in Figure (5.4), and production with top-quarks (ttH) in Figure (5.5).

Either way, if we are dealing with the SS or with the STXS, we need to parametrize the measurements in terms of the variable  $\mu_i^f$  as defined in equation (5.6). The SM prediction for them is equal to 1, while the effective operators introduce modifications to the cross-section,

$$\sigma^i = \sigma_{\text{SM}}^i + \sigma_{\text{Int}}^i + \sigma_{\text{BSM}}^i, \quad (5.7)$$

and to Higgs decay widths,

$$\Gamma^f = \Gamma_{\text{SM}}^f + \Gamma_{\text{Int}}^f + \Gamma_{\text{BSM}}^f, \quad (5.8)$$

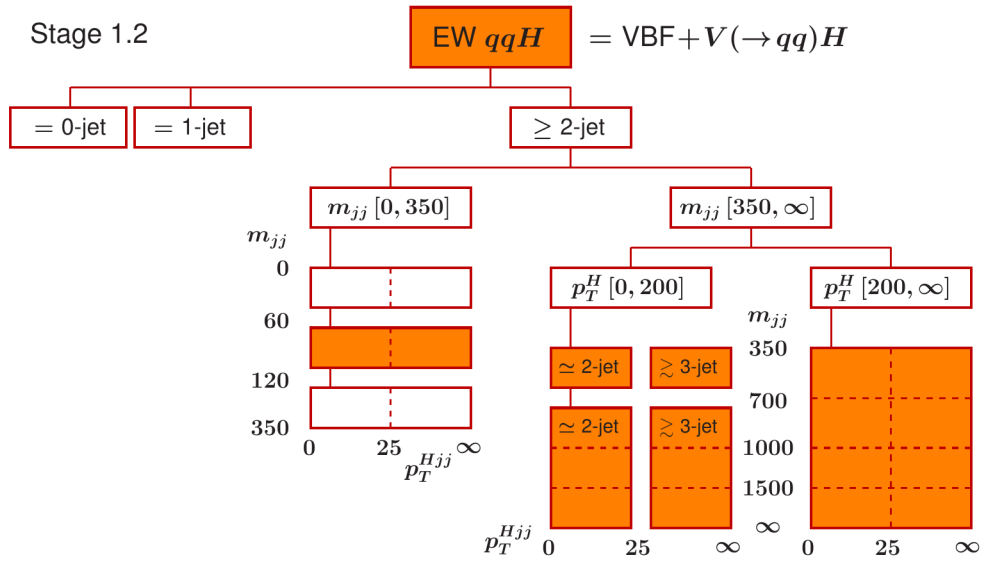


Figure 5.3: Definition of STXS Stage1.2 bins for the VBF production mode.

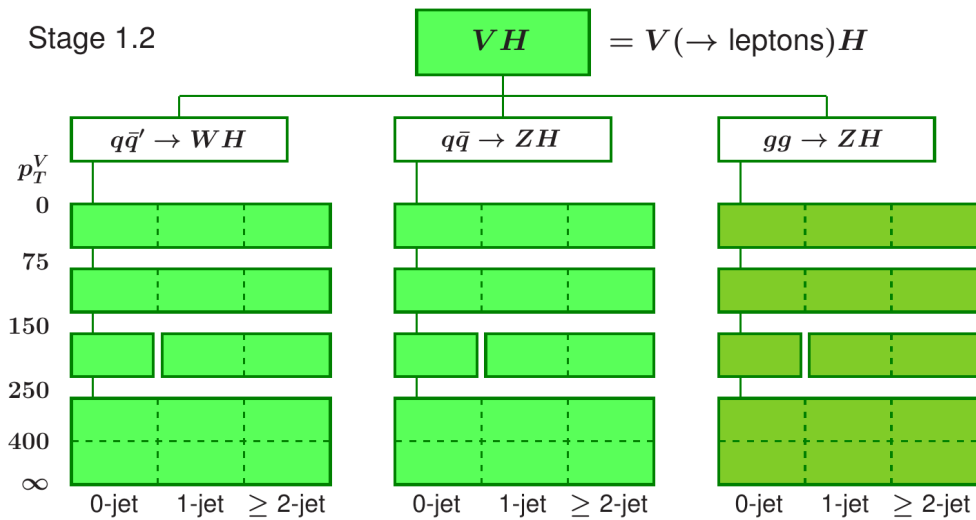


Figure 5.4: Definition of STXS Stage1.2 bins for the VH production mode.



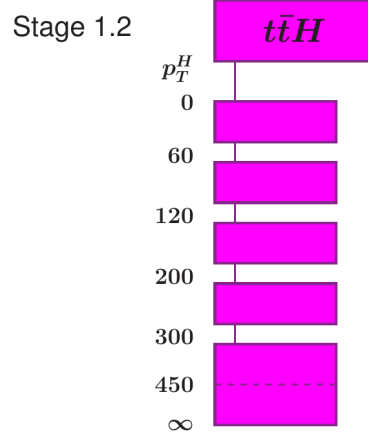


Figure 5.5: Definition of STXS Stage 1.2 bins for the  $t\bar{t}H$  production mode.

where the subscripts Int and BSM denotes interference with the SM and purely BSM contribution, respectively. As a result, the variable  $\mu_i^f$  goes to

$$\mu_i^f = 1 + \sum_j \left( A_j^i + D_j^f + F_j \right) c_j + \sum_{j,k} \left( A_j^i D_k^f + A_j^i F_k + D_j^f F_k + B_{jk}^i + E_{jk}^f + G_{jk} \right) c_j c_k + \mathcal{O}(c^3), \quad (5.9)$$

with

$$\sum_j A_j^i c_j \equiv \frac{\sigma_{\text{int}}^i}{\sigma_{\text{SM}}^i}, \quad \sum_{j \geq k} B_{jk}^i c_j c_k \equiv \frac{\sigma_{\text{BSM}}^i}{\sigma_{\text{SM}}^i}, \quad (5.10)$$

$$\sum_j D_j^f c_j \equiv \frac{\Gamma_{\text{int}}^f}{\Gamma_{\text{SM}}^f}, \quad \sum_{j \geq k} E_{jk}^f c_j c_k \equiv \frac{\Gamma_{\text{BSM}}^f}{\Gamma_{\text{SM}}^f}, \quad (5.11)$$

$$\sum_j F_j c_j \equiv -\frac{\Gamma_{\text{int}}}{\Gamma_{\text{SM}}}, \quad \sum_{j \geq k} G_{jk} c_j c_k \equiv -\frac{\Gamma_{\text{BSM}}}{\Gamma_{\text{SM}}}. \quad (5.12)$$

The  $\Gamma$ 's without upper indices denotes the total decay width and the  $c$ 's denote the Wilson coefficients. When the fit is carried only taking into account the linear contribution of the Wilson coefficients the last term in (5.9) is dropped.

In Table 5.3 we summarize the data we take into account, specifying its STXS or SS format. As pointed out in [8], the correlations among CMS STXS data for the different final states is not publicly available. These are expected to be important for the  $\gamma\gamma$  and  $llll$ . For that reason, here we do not include all the CMS STXS data available, the ones we decided to keep are shown in Table 5.3.

We evaluated the theoretical predictions for the Higgs production by gluon fusion in the channels tagged as STXS in Table 5.3 using MADGRAPH\_AMC@NLO [84] with the SMEFT@NLO

Name	Channel	Distribution	# bins	Data set	Int. Lum.
ATLAS-053	$H \rightarrow \gamma\gamma, ZZ, b\bar{b}(VH)$	STXS	43	ATLAS at 13 TeV	$139 \text{ fb}^{-1}$ [77]
CMS-010	$H \rightarrow \tau^+\tau^-(ggH, VBF)$	STXS	11	CMS at 13 TeV	$137 \text{ fb}^{-1}$ [78]
CMS-017	$H \rightarrow W^+W^-(VH)$	STXS	4	CMS at 13 TeV	$137 \text{ fb}^{-1}$ [79]
ATLAS-027	$H \rightarrow \tau^+\tau^-, W^+W^-, b\bar{b}(VBF, ttH + tH)$	SS	7	ATLAS at 13 TeV	$36.1\text{-}139 \text{ fb}^{-1}$ [80]
ATLAS- $\mu\mu$	$H \rightarrow \mu^+\mu^-$	SS	1	ATLAS at 13 TeV	$139 \text{ fb}^{-1}$ [81]
ATLAS- $Z\gamma$	$H \rightarrow \gamma Z$	SS	1	ATLAS at 13 TeV	$139 \text{ fb}^{-1}$ [82]
CMS-019	$H \rightarrow \gamma Z$	SS	1	CMS at 13 TeV	$139 \text{ fb}^{-1}$ [83]

Table 5.3: Data used for the Higgs analysis

UFO files [85]. The STXS Stage1.2 classification was performed with RIVET [86]. In order to merge the bins from the STXS data we developed a Python module called PySTXS that is about to be released.

Our analysis is made with a  $\chi^2$  function that depends on 11 Wilson coefficients

$$\chi_{\text{Higgs}}^2(\Delta a_c, a_4, a_5, a_{17}, a_B, a_W, a_G, Y_t^{(1)}, Y_b^{(1)}, Y_\tau^{(1)}, Y_\mu^{(1)}). \quad (5.13)$$

Let us notice that we could have included more operators defined in [13], specially the ones that lead to anomalous interaction among the gauge bosons and fermions, but these are highly constrain by the electroweak precision observables [8] and are neglected in our study.

## 5.3 Results

As we shown in the Chapter 4, the non-linear parametrization of the gauge bosons allows for independent statistical analysis of the datasets affecting TGC and the ones affecting the Higgs interactions since the couplings impacting these two sectors are not connected. First, we summarize the TGC constraints, and then we move to the Higgs constraints. A more complete analysis regarding the Higgs datasets can be found in [8], but here we will summarize some important results from there.

### 5.3.1 Triple gauge coupling constraints

The statistical analysis was made taking into account only the linear contribution of the Wilson coefficients as well as up to quadratic contributions. As we mentioned earlier, we neglected possible anomalous interactions of the gauge bosons with fermions, and we focus on the constraints for the operators  $\mathcal{P}_2, \mathcal{P}_3, \mathcal{P}_{13}$ , and  $\mathcal{P}_{WWW}$ . The one dimensional projections of  $\Delta\chi_{\text{TGC}}^2$  for the Wilson coefficients are shown in Figure 5.6 while the two dimensional confi-

dence regions are shown in Figure 5.7. The 95% Confidence Level (C.L.) allowed range for the Wilson coefficients are displayed in Table 5.4. The results are shown together with the confidence interval when we only consider one Wilson coefficient in the fit while setting the others to zero.

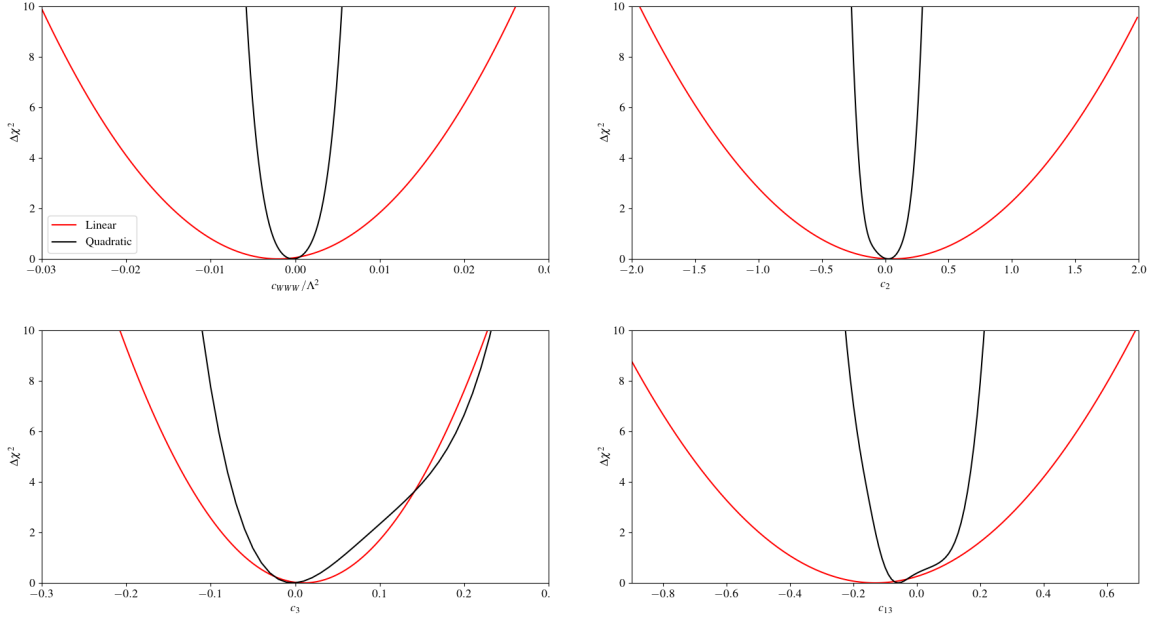


Figure 5.6: One dimension marginalized projections of  $\Delta\chi^2$  for the Wilson coefficients  $c_{WWW}$ ,  $c_2$ ,  $c_3$ , and  $c_{13}$ , as indicated in the panels after marginalizing over the remaining fit parameters. The results are shown for the analysis including only the linear contribution of the Wilson coefficients (red curves) as well as up to quadratic contributions (black curves).

Coefficients	95% C.L. range			
	Linear		Quadratic	
	Individual	Marginalized	Individual	Marginalized
$c_2$	[-0.89, 0.52]	[-1.18, 1.28]	[-0.21, 0.23]	[-0.21, 0.23]
$c_3$	[-0.11, 0.08]	[-0.13, 0.15]	[-0.08, 0.16]	[-0.08, 0.15]
$c_{13}$	[-0.38, 0.16]	[-0.64, 0.38]	[-0.13, 0.15]	[-0.16, 0.16]
$c_{WWW}/\Lambda^2$	[-0.020, 0.014]	[-0.019, 0.015]	[-0.0044, 0.0041]	[-0.0043, 0.0040]

Table 5.4: Individual and marginalized 95% CL allowed range for the Wilson coefficients.

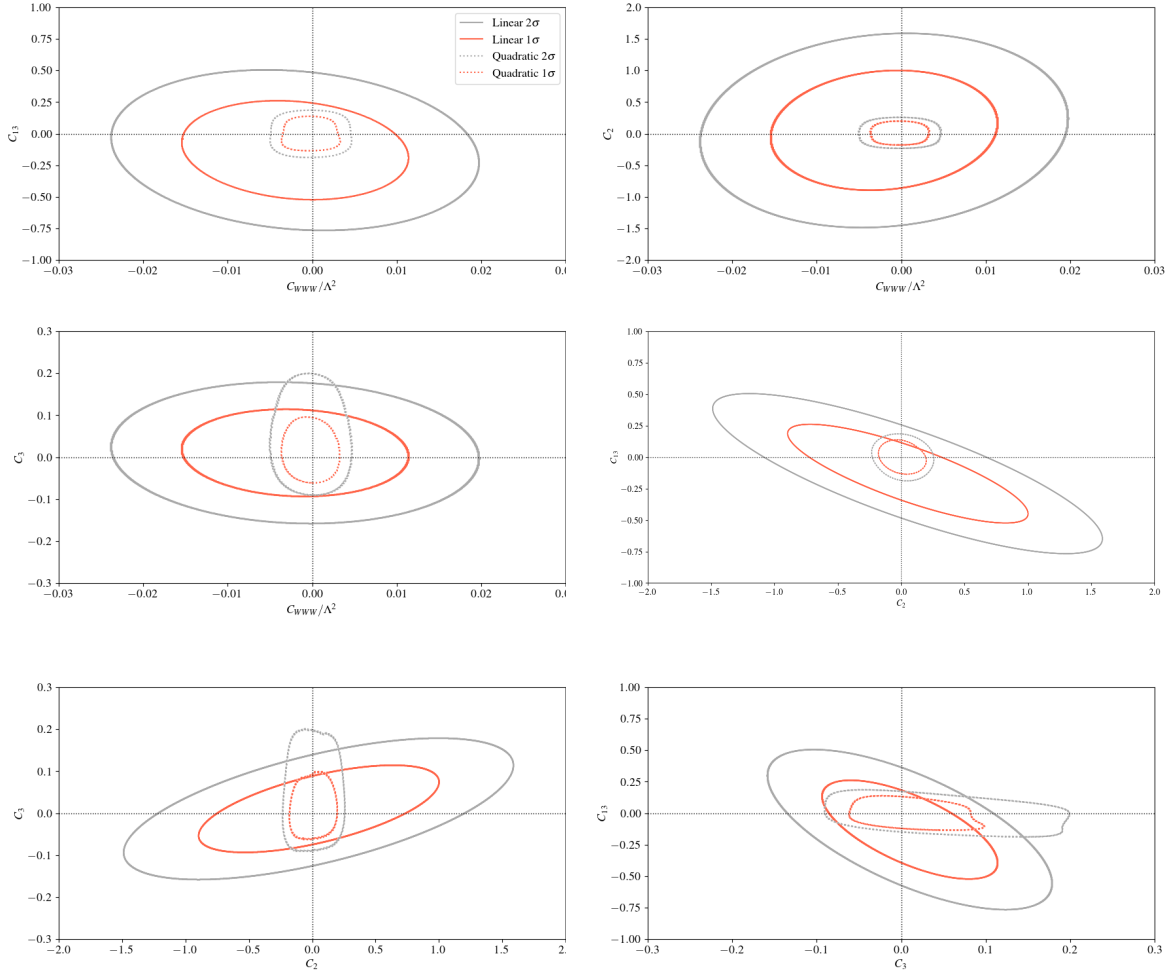


Figure 5.7: Two dimension marginalized projections of  $\Delta\chi^2$  for the Wilson coefficients  $c_{WWW}$ ,  $c_2$ ,  $c_3$ , and  $c_{13}$ , as indicated in the panels after marginalizing over the remaining fit parameters. The results are shown for the analysis including only the linear contribution of the Wilson coefficients (solid curves) as well as up to quadratic contributions (dashed curves).

Looking at the confidence regions in Figure 5.7, we notice that the correlations present in the linear case are broken in the quadratic analysis. Moreover, the bounds in the latter are stronger by a factor of 4-5.

In the linear fit, we can see that  $c_2$ ,  $c_3$ , and  $c_{13}$  are strongly correlated due to their corrections to the  $ZWW$  and  $\gamma WW$  vertices in equation (4.61). This is also an important information to take into account in the fit procedure as it is shown in the Table 5.4. When we contrast the individual fit with the marginalized one, we realized the importance of the correlation among the Wilson coefficients to determinate the bounds in the linear analysis. Only the coefficient  $c_{WWW}$  suffers a small change from the individual to the marginalized results since it is not very

correlated with the remaining fit parameters. When we move to the quadratic case, the changes are not very significant because all the correlations are practically broken.

In Tables 5.5 and 5.6, we display the 95% C.L. range for the Wilson coefficients where we only included two parameters in the fit. When the confidence interval was obtained for one, the other was marginalized. As predicted, in the analysis considering also the quadratic contributions of the Wilson coefficients all the confidence intervals are basically the same, as shown in Table 5.6. Meanwhile, in Table 5.5 we see that the operators  $c_2$  and  $c_{13}$  play a significant role in each others confidence interval, but they still differ by a factor of  $\sim 1.3$  from the actual confidence interval shown in the last column. Also from Table 5.5, the coefficient  $c_3$  only has a confidence interval close to the one in the last column when we take into account both parameters  $c_2$  and  $c_{13}$ . This discussion is important to highlight that when performing the analysis, if the correlations among the fit parameters are not considered, the obtained bounds may be more stringent than they actually are.

Coefficients	Parameter considered in the fit (95% C.L. range)				
	$c_2$	$c_3$	$c_{13}$	$c_{WWW}/\Lambda^2$	All
$c_2$	[-0.89, 0.52]	[-0.92, 0.51]	[-0.93, 0.97]	[-0.90, 0.52]	[-1.18, 1.28]
$c_3$	[-0.11, 0.08]	[-0.11, 0.08]	[-0.10, 0.11]	[-0.11, 0.09]	[-0.13, 0.15]
$c_{13}$	[-0.48, 0.24]	[-0.41, 0.18]	[-0.38, 0.16]	[-0.38, 0.17]	[-0.64, 0.38]
$c_{WWW}/\Lambda^2$	[-0.020, 0.013]	[-0.020, 0.014]	[-0.019, 0.015]	[-0.020, 0.014]	[-0.019, 0.015]

Table 5.5: 95% C.L. allowed range for the Wilson coefficients after marginalizing with respect to only one parameter. The results are shown only for the analysis including the linear contribution of the Wilson coefficients. The individual fit results are shown in the diagonal entries (gray entries) as well as the results taking into account all the parameters in the last column (gray entries) for comparison.

Coefficients	Parameter considered in the fit (95% C.L. range)				
	$c_2$	$c_3$	$c_{13}$	$c_{WWW}/\Lambda^2$	All
$c_2$	[-0.21, 0.23]	[-0.21, 0.23]	[-0.21, 0.23]	[-0.21, 0.23]	[-0.21, 0.23]
$c_3$	[-0.08, 0.16]	[-0.08, 0.16]	[-0.08, 0.15]	[-0.08, 0.16]	[-0.08, 0.15]
$c_{13}$	[-0.14, 0.15]	[-0.16, 0.16]	[-0.13, 0.15]	[-0.13, 0.15]	[-0.16, 0.16]
$c_{WWW}/\Lambda^2$	[-0.0043, 0.0040]	[-0.0044, 0.0040]	[-0.0043, 0.0040]	[-0.0044, 0.0041]	[-0.0043, 0.0040]

Table 5.6: 95% C.L. allowed range for the Wilson coefficients after marginalizing with respect to only one parameter. The results are shown only for the analysis including up to the quadratic contribution of the Wilson coefficients. The individual fit results are shown in the diagonal entries (gray entries) as well as the results taking into account all the parameters in the last column (gray entries) for comparison.

As we mentioned before, the operator  $\mathcal{P}_{13}$  is the only one that has no linear sibling. The impact of its respective Wilson coefficient is shown in Figures 5.8 and in Table 5.7, where we

compare the confidence regions and intervals in the case we take into account its contributions to the one we do not.

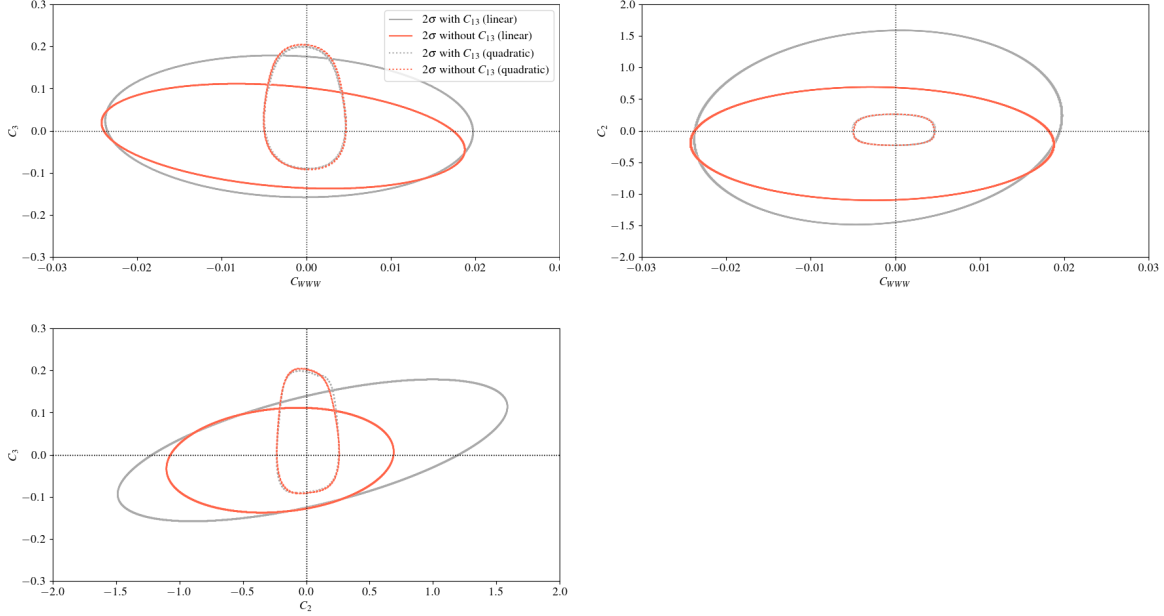


Figure 5.8: Two dimension marginalized projections for the Wilson coefficients  $c_2$ ,  $c_3$ , and  $c_{WWW}$ , as indicated in the panels after marginalizing over the remaining fit parameters, including (gray curves) and not (red curves) the coefficient  $c_{13}$ . The results are shown for the analysis including only the linear contribution of the Wilson coefficients (solid lines) as well as up to quadratic contributions (dashed lines).

Coefficients	95% C.L. range			
	Linear		Quadratic	
	Without $c_{13}$	With $c_{13}$	Without $c_{13}$	With $c_{13}$
$c_2$	[-0.92, 0.51]	[-1.18, 1.28]	[-0.21, 0.23]	[-0.21, 0.23]
$c_3$	[-0.11, 0.09]	[-0.13, 0.15]	[-0.08, 0.16]	[-0.08, 0.15]
$c_{WWW}/\Lambda^2$	[-0.020, 0.015]	[-0.019, 0.015]	[-0.0044, 0.0040]	[-0.0043, 0.0040]

Table 5.7: Allowed 95% C.L. range for the Wilson coefficients  $c_2$ ,  $c_3$ , and  $c_{WWW}$  after marginalizing over the remaining fit parameters. The results are shown including and not the coefficient  $c_{13}$  on the fit.

As shown in Figures in 5.8 and in Table 5.7, in the linear case the  $c_{13}$  has a significant impact in the operators  $c_2$  and  $c_3$ , while it is obsolete for the coefficient  $c_{WWW}$ . In contrast, in the analysis considering also the quadratic contributions of the Wilson coefficients, the confidence regions and intervals are basically the same since all the correlations are broken.

Also, we followed the same procedure as [11] and we obtained the Fisher information for the coefficients in our analysis. The Fisher information is basically a way to compare the sensitivity brought in by different datasets in a given EFT coefficient. For a specific dataset, the Fisher matrix takes the following form

$$I_{ij}(\vec{c}) = -E \left[ \frac{\partial^2 \ln f(\vec{\mu}|\vec{c})}{\partial c_i \partial c_j} \right], \quad (5.14)$$

where  $E$  stands for expectation value and  $\ln f(\vec{\mu}|\vec{c})$  is the logarithm of the likelihood among the observables  $\mu_i$  and the assumed true values of the Wilson coefficients  $\vec{c}$ . For the case where the data is Gaussian distributed with a correlation matrix  $V$  and the analysis is performed only at the linear order in the Wilson coefficients,

$$\mu_i = \mu_i^{\text{SM}} + \sum_j \alpha_i^j c^j + \mathcal{O}(c^2), \quad (5.15)$$

the Fisher matrix becomes

$$I = H^T V^{-1} H, \quad (5.16)$$

with  $H_{im} \equiv \alpha_i^m$ . The Fisher information compares the diagonal entries among different datasets. Our results are shown in Figure 5.9. In each column we have the diagonal values of the Fisher matrix. We choose to normalize the lines to 100, so we can identify which dataset has the dominant constraints on a given Wilson coefficient. For the dataset CMS  $WW$  0j the computation of the Fisher matrix was done numerically since in this specific case we have a Poisson distribution.

A few interesting observations can be made from the Figure 5.9. First, in the linear and in the quadratic case, the  $WW$  pair production datasets are the most important ones to set bounds on the coefficients  $c_2$  and  $c_{13}$ . This is also one way to explain their high correlation, because their bounds practically comes from the same datasets. However, for the coefficient  $c_3$ , the most important ones are the  $WZ$  pair productions, and for the coefficient  $c_{WWW}$  are the vector boson fusion for  $Z$ 's and the  $W\gamma$  pair production. In the quadratic case, the dataset CMS  $W\gamma$  becomes the most important one to set the bounds on the coefficient  $c_{WWW}$ . This dataset in particular uses kinematic distributions designated to avoid the cancellation among the SM and anomalous amplitude. The name of the technique is called Interference Resurrection [87], which we applied in our analysis. The impact of the vector boson fusion dataset, ATLAS  $Zjj$ , decreases by a factor of  $\sim 9$  in the quadratic analysis for the coefficient  $c_{WWW}$ .

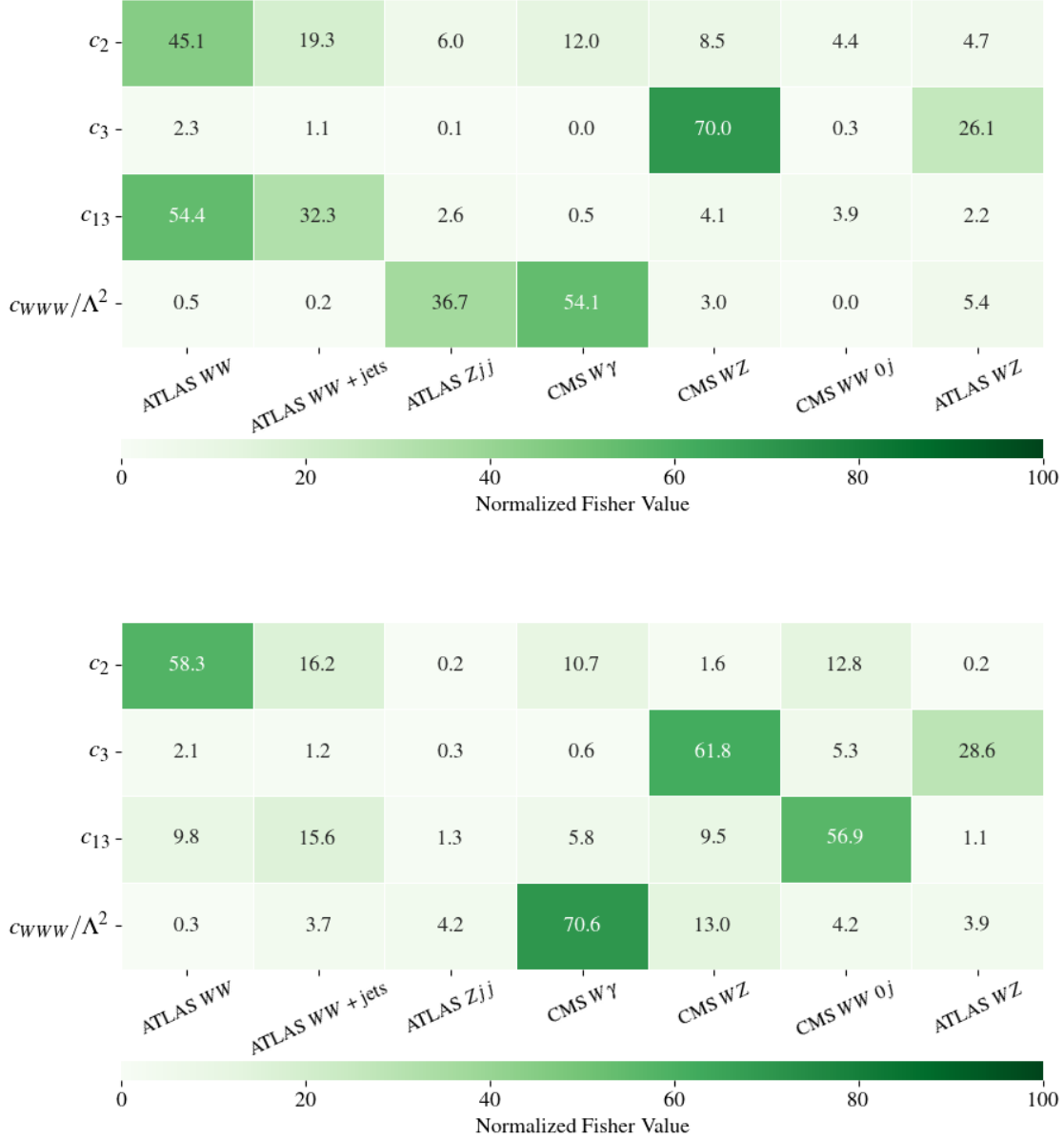


Figure 5.9: Normalized Fisher Value for the Wilson coefficients that affect TGV. Results for the analysis where we included only the linear (above) and up to the quadratic (below) contribution of the Wilson coefficients. The entries are normalized in such a way that the sum of the diagonal elements of the Fisher matrix for a specific Wilson coefficient is 100.

Lastly, when we performed the fit at linear order, the  $\Delta\chi^2$  takes the form

$$\Delta\chi^2 = \sum_{i=1}^N (f_i - f_{i,0}) V_{ij}^{-1} (f_j - f_{j,0}), \quad (5.17)$$



with  $V^{-1}$  being the covariance matrix among the Wilson coefficients  $f_i$  with the best-fit values denoted by  $f_{i,0}$

$$V_{ij} = \sigma_i \sigma_j \rho_{ij}. \quad (5.18)$$

The  $\sigma_i$  denotes the uncertainties and  $\rho$  the correlation matrix. For the Wilson coefficients affecting the TGC we present an approximate covariance matrix, because we neglected the dataset CMS  $WW 0j$  since it follows a Poisson distribution. The correlation matrix, the best-fit values, and the uncertainties are shown in Table 5.8.

		$c_2$	$c_3$	$c_{13}$	$c_{WWW}$
	b.f.	-0.10	-0.0023	-0.081	-0.0022
	$\sigma$	0.64	0.070	0.26	0.0090
$\rho$	$c_2$	1.000	0.626	-0.811	0.121
	$c_3$	0.626	1.000	-0.679	-0.079
	$c_{13}$	-0.811	-0.679	1.000	-0.157
	$c_{WWW}/\Lambda^2$	0.121	-0.079	-0.157	1.000

Table 5.8: Approximate best-fit values, uncertainties, and correlation matrix for the analysis including only the linear contribution of the Wilson coefficients  $c_2$ ,  $c_3$ ,  $c_{13}$ , and  $c_{WWW}$ .

The results shown in this section are also available in [8]. A few slight differences appeared in the confidence intervals for the analysis taking into account only the linear contribution of the Wilson coefficients. We assign these differences to fluctuations in the Monte-Carlo simulations in the interference among the SM and the anomalous contribution. In summary, our conclusion agrees with the one in [8]: no tension with the SM is found in the gauge bosons self-interactions.

### 5.3.2 Higgs constraints

The Higgs analysis was performed taking into account only the linear contribution of the Wilson coefficients. When the fit is performed only at linear order in the Wilson coefficients and all datasets follow a Gaussian distribution, we can obtain the confidence regions and intervals using analytical formulas. Meanwhile, in [8] the analysis was carried out also considering the quadratic contributions. We emphasize that in the latter more datasets were considered as well as some correlations among the CMS datasets. Here, these correlations have been neglected and we show our results for a smaller class of datasets. Nevertheless, our conclusions are the same, but we will mention the results from [8] as well. Following the same reasoning we used in the TGC results, we neglected effective operators leading to anomalous interactions among the gauge bosons and fermions, and we focus our study on the 11 effective operators from (5.13).

The one dimensional projections of the  $\Delta\chi_{\text{Higgs}}^2$  are shown in Figures 5.10 and 5.11, while the 95% C.L. allowed range is displayed in Table 5.9.

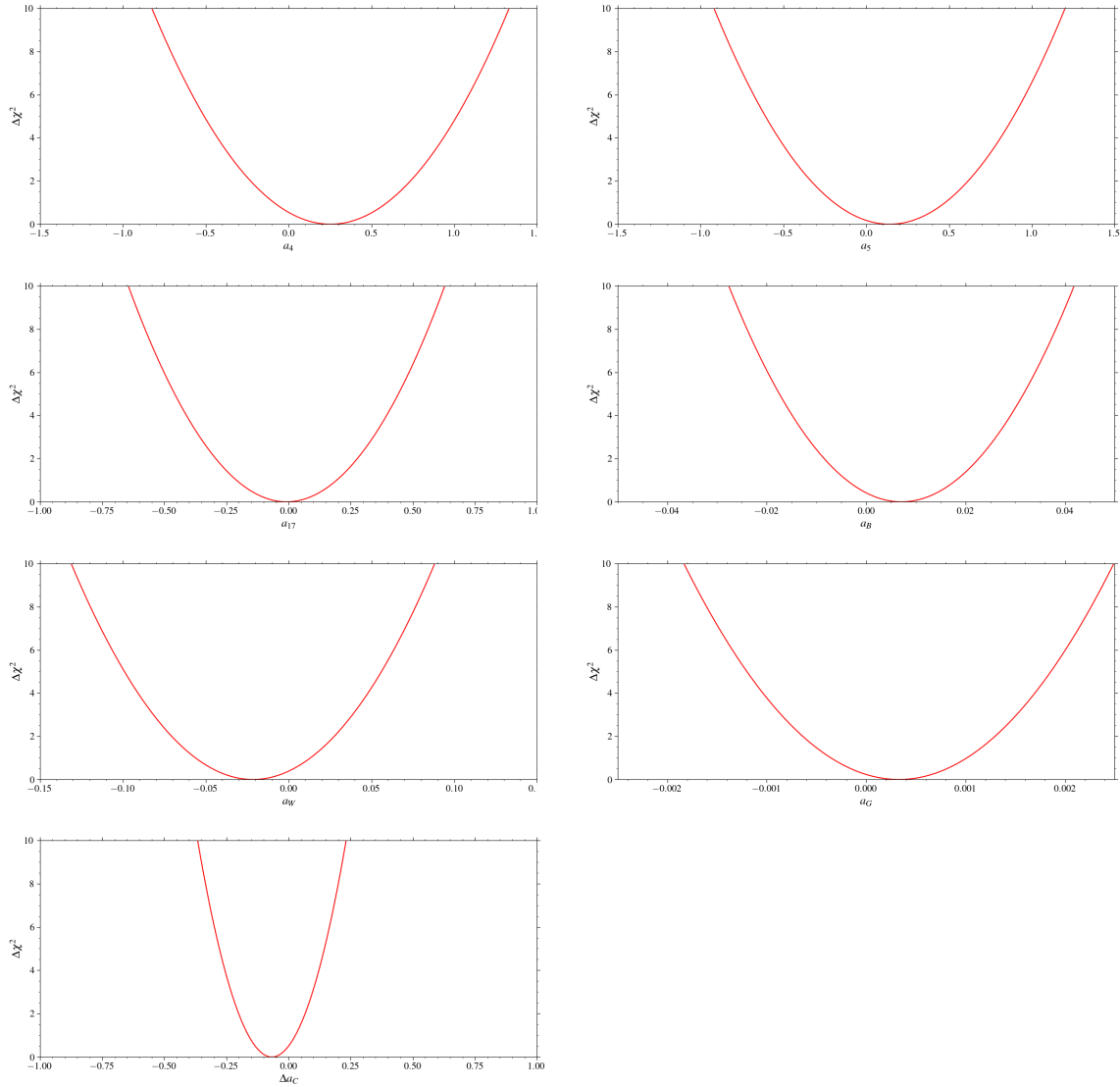


Figure 5.10: One dimension marginalized projections of  $\Delta\chi^2$  for the Wilson coefficients  $a_4$ ,  $a_5$ ,  $a_{17}$ ,  $a_B$ ,  $a_W$ ,  $a_G$ , and  $\Delta a_C$ , as indicated in the panels after marginalizing over the remaining fit parameters. The results are shown for the analysis including only the linear contribution of the Wilson coefficients.

First, we noticed that the results are compatible with the SM at 95% C.L.. Also, when comparing the marginalized with the individual intervals, we see a drastic change in the coefficients  $a_4$ ,  $a_5$ ,  $a_{17}$ ,  $a_B$ ,  $a_W$ , and  $\Delta a_C$ , because the correlations among them were neglected in the individual fit. As we saw in the TGC case, this emphasizes the importance of taking into account

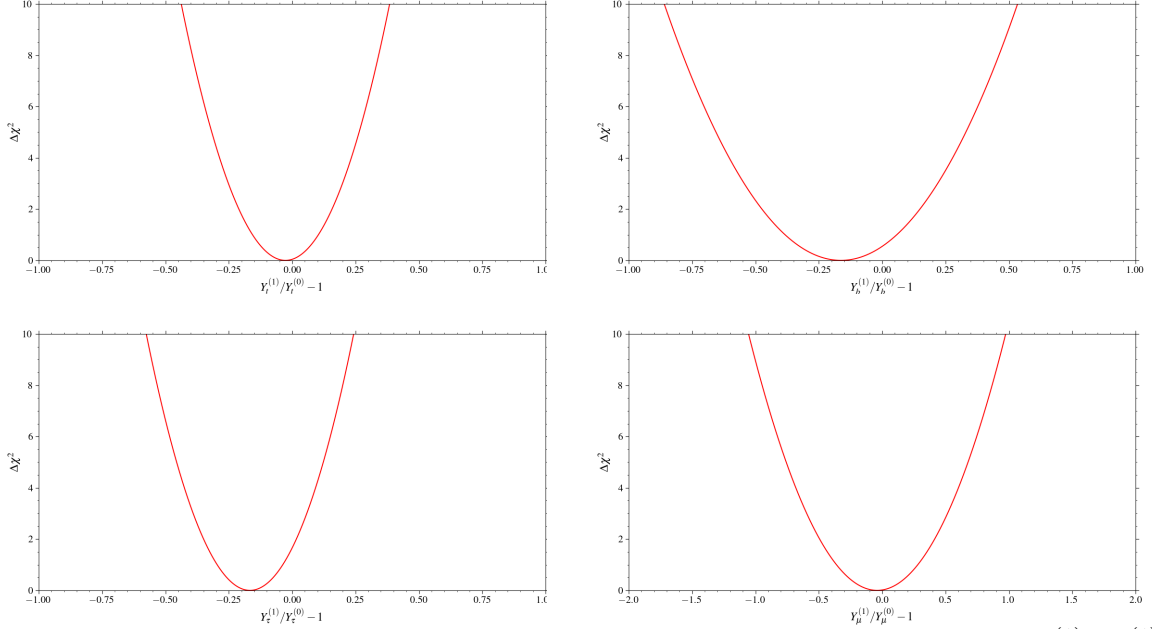


Figure 5.11: One dimension marginalized projections for the Yukawa couplings  $Y_t^{(1)}$ ,  $Y_b^{(1)}$ ,  $Y_\tau^{(1)}$ , and  $Y_\mu^{(1)}$ , as indicated in the panels after marginalizing over the remaining fit parameters. The results are shown for the analysis including only the linear contribution of the Wilson coefficients.

Coefficients	95 % C.L.	
	Individual	Marginalized
$a_4$	[-0.002, 0.12]	[-0.41, 0.92]
$a_5$	[-0.003, 0.26]	[-0.52, 0.80]
$a_{17}$	[-0.02, 0.13]	[-0.40, 0.39]
$a_B$	[-0.00035, 0.00062]	[-0.014, 0.029]
$a_W$	[-0.001, 0.002]	[-0.089, 0.047]
$\Delta a_C$	[-0.07, 0.04]	[-0.25, 0.12]
$a_G$	[-0.0003, 0.0005]	[-0.0010, 0.0017]
$Y_t^{(1)}/Y_t^{(0)} - 1$	[-0.08, 0.04]	[-0.28, 0.23]
$Y_b^{(1)}/Y_b^{(0)} - 1$	[-0.04, 0.12]	[-0.60, 0.27]
$Y_\tau^{(1)}/Y_\tau^{(0)} - 1$	[-0.25, 0.07]	[-0.42, 0.09]
$Y_\mu^{(1)}/Y_\mu^{(0)} - 1$	[-0.59, 0.48]	[-0.67, 0.59]

Table 5.9: 95 % Confidence Level for the parameters in the fit. The analysis was made including only the linear contribution of the Wilson coefficients.

the full correlations in the global fit. In special, the operator  $\mathcal{P}_{17}$  is the only one with no linear sibling. This operator plays an important role in our analysis because it is correlated with the bosonic operators as shown in Figure 5.12.

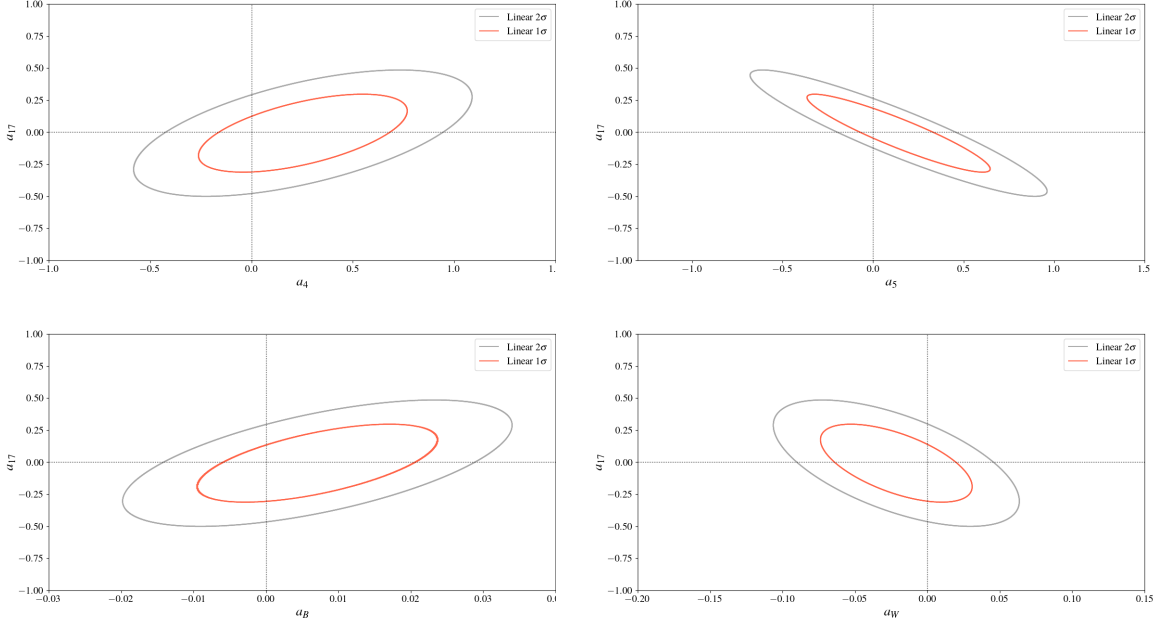


Figure 5.12: Two dimension marginalized projections for the Wilson coefficients  $a_{17}$ ,  $a_4$ ,  $a_5$ ,  $a_B$ , and  $a_W$ , as indicated in the panels after marginalizing over the remaining fit parameters. The results are shown for the analysis including only the linear contribution of the Wilson coefficients.

Here we must summarize some important results from [8] when the analysis is performed also taking into account the quadratic contributions of the Wilson coefficients. In [8], we took into account more datasets. The ones that are present in [8], but absent in Table 5.3 are displayed in Table 5.10. A few of the effective interactions can lead to a change of sign of the SM couplings. As a consequence, degenerated regions in the parameter space are possible as we show in Figure 5.13. This happens, for example, with the Yukawas  $Y_f^{(1)}$  and to the coupling  $\Delta a_C$ . In [8], we concluded that using the LHC Run 2 data, the dominant source of degeneracy remaining are those related to the Yukawas couplings  $Y_f^{(1)}$  for  $f = b, \tau$  and  $\mu$ . Also, we showed that the degeneracy for  $\Delta a_C$  is mainly broken by the data concerning the Higgs  $tH$  production mode, which receives contribution from  $HV\bar{V}$  and  $Ht\bar{t}$  vertices while only the first changes the sign for  $\Delta a_C \sim 2$ . The Higgs-top Yukawa vertex does not change sign because it also enters in the Higgs production by gluon fusion and the degeneracy can be eliminated by the STXS data. Lastly, another source of degeneracy is related to a sign change in the SM effective coupling  $H\gamma\gamma$  induced by loop effects. A linear combination of the operators  $\mathcal{P}_W$  and  $\mathcal{P}_B$  corrects the  $H\gamma\gamma$  coupling,

$$-\frac{1}{4}G_{SM}^{\gamma\gamma} + \frac{1}{2v}(a_B c^2 + a_W s^2), \quad (5.19)$$

where  $G_{SM}^{\gamma\gamma} \simeq 3.3 \times 10^{-2}$  is the one-loop SM contribution and  $s$  and  $c$  denotes the sine and cosine of the weak angle. When we performed the analysis taking in to account also the quadratic contributions of the Wilson coefficients, quasi-degenerate solutions were found as shown in Figure (5.14).

Name	Channel	Distribution	# bins	Data set	Int. Lum.
CMS-GGPMAX	$H \rightarrow \gamma\gamma$	STXS	17	CMS at 13 TeV	137 $fb^{-1}$ [88]
CMS-005	$H \rightarrow ZZ, b\bar{b}, \tau^+\tau^-, W^+W^- (ggH, VBF, ttH)$	SS	16	CMS at 13 TeV	137 $fb^{-1}$ [83]

Table 5.10: Data used for the Higgs analysis in [8], but absent in Table 5.3.

We also show the Fisher information in Figure 5.15. Among the datasets, the ATLAS-053 plays an important role in constraining most part of our parameters. This was expected since it is the one that contains most complete information about the correlation of different Higgs production modes. Moreover, we noticed that the datasets measuring the  $h \rightarrow Z\gamma$  decay, ATLAS- $Z\gamma$  and CMS-019, are important for the coefficients  $a_4$ ,  $a_5$ , and  $a_{17}$  since they modify the  $HZ\gamma$  coupling as shown in (4.66). For the Higgs-muon Yukawa coupling, the dominant dataset is ATLAS- $\mu\mu$  since it measures  $h \rightarrow \mu\mu$  decay. The same situation occurs with the coupling  $Y_\tau^{(1)}$ , most of the constraint comes from the CMS-010 dataset since it measures the  $h \rightarrow \tau\tau$  decay.

The correlation matrix, the uncertainties, and best-fit values for the coefficients in our analysis are gathered in Table 5.11.

		$a_4$	$a_5$	$a_{17}$	$a_B$	$a_W$	$a_G$	$\Delta a_C$	$\frac{Y_t^{(1)}}{Y_t^{(0)}} - 1$	$\frac{Y_b^{(1)}}{Y_b^{(0)}} - 1$	$\frac{Y_\tau^{(1)}}{Y_\tau^{(0)}} - 1$	$\frac{Y_\mu^{(1)}}{Y_\mu^{(0)}} - 1$
	b.f.	0.25	0.14	-0.0079	0.0071	-0.0215	0.0003	-0.07	-0.03	-0.16	-0.17	-0.04
	$\sigma$	0.34	0.34	0.20	0.0109	0.0347	0.0007	0.09	0.13	0.22	0.13	0.32
$\rho$	$a_4$	1.000	-0.409	0.573	0.987	-0.991	0.004	-0.472	0.007	-0.348	-0.393	0.208
	$a_5$	-0.409	1.000	-0.917	-0.394	0.403	-0.041	0.033	-0.195	-0.080	0.199	-0.042
	$a_{17}$	0.573	-0.917	1.000	0.601	-0.601	0.104	-0.326	0.141	-0.186	-0.360	0.140
	$a_B$	0.987	-0.394	0.601	1.000	-0.999	0.026	-0.568	-0.019	-0.443	-0.454	0.239
	$a_W$	-0.991	0.403	-0.601	-0.999	1.000	-0.022	0.539	0.005	0.409	0.430	-0.228
	$a_G$	0.004	-0.041	0.104	0.026	-0.022	1.000	-0.021	0.713	-0.068	-0.038	-0.009
	$\Delta a_C$	-0.472	0.033	-0.326	-0.568	0.539	-0.021	1.000	0.340	0.872	0.638	-0.322
	$\frac{Y_t^{(1)}}{Y_t^{(0)}} - 1$	0.007	-0.195	0.141	-0.019	0.005	0.713	0.340	1.000	0.496	0.290	-0.099
	$\frac{Y_b^{(1)}}{Y_b^{(0)}} - 1$	-0.348	-0.080	-0.186	-0.443	0.409	-0.068	0.872	0.496	1.000	0.690	-0.306
	$\frac{Y_\tau^{(1)}}{Y_\tau^{(0)}} - 1$	-0.393	0.199	-0.360	-0.454	0.430	-0.038	0.638	0.290	0.690	1.000	-0.253
	$\frac{Y_\mu^{(1)}}{Y_\mu^{(0)}} - 1$	0.208	-0.042	0.140	0.239	-0.228	-0.009	-0.322	-0.099	-0.306	-0.253	1.000

Table 5.11: Best-fit values, uncertainties, and correlation matrix for the analysis including only the linear contribution of the Wilson coefficients.

Since we have the covariance matrix for the Wilson coefficients, we can translate our results

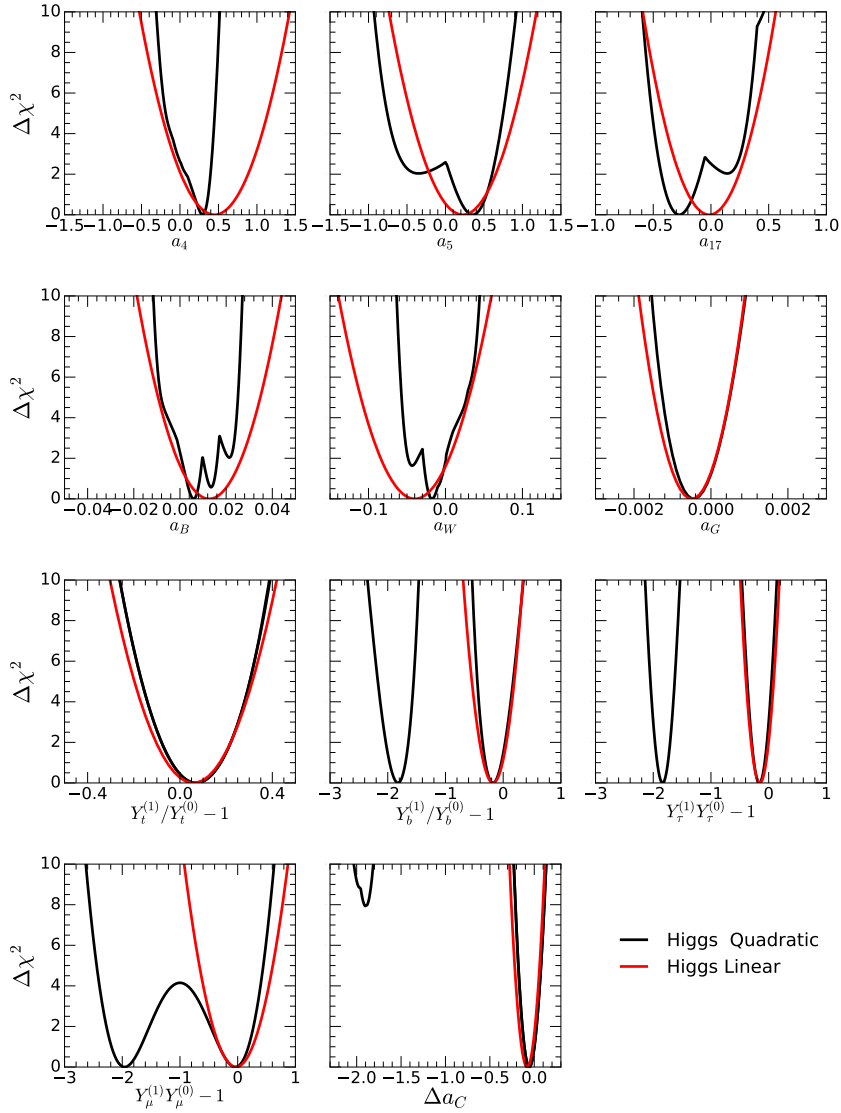


Figure 5.13:  $\Delta\chi^2$  as a function of the Wilson coefficients  $a_4$ ,  $a_5$ ,  $a_{17}$ ,  $a_B$ ,  $a_W$ ,  $a_G$ ,  $Y_t^{(1)}$ ,  $Y_b^{(1)}$ ,  $Y_\tau^{(1)}$ ,  $Y_\mu^{(1)}$ , and  $\Delta a_C$  as indicated in the panels after marginalizing over the remaining fit parameters. The red (black) line stands for the analysis considering the linear (and quadratic) contributions of the Wilson coefficients. Results extracted from [8].

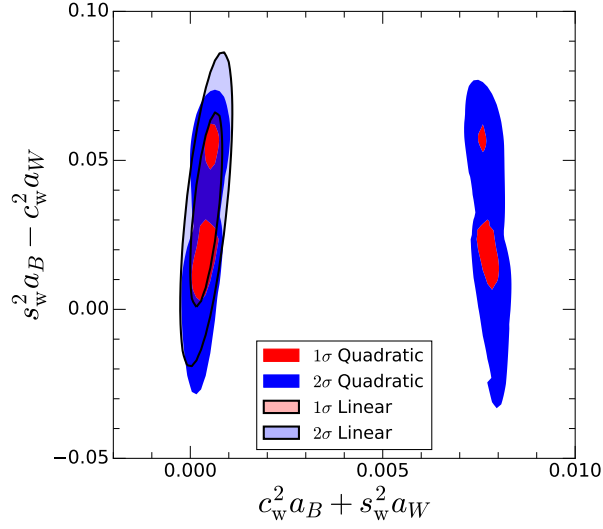


Figure 5.14:  $1\sigma$  and 95% CL (2dof) allowed regions from the Higgs analysis for the combinations  $c_W^2 a_B + s_W^2 a_W$  and  $s_W^2 a_B - c_W^2 a_W$ . The results are shown for the analysis including only the linear contributions of the Wilson coefficients (lighter regions) as well as up to quadratic contributions (darker regions). Results extracted from [8].

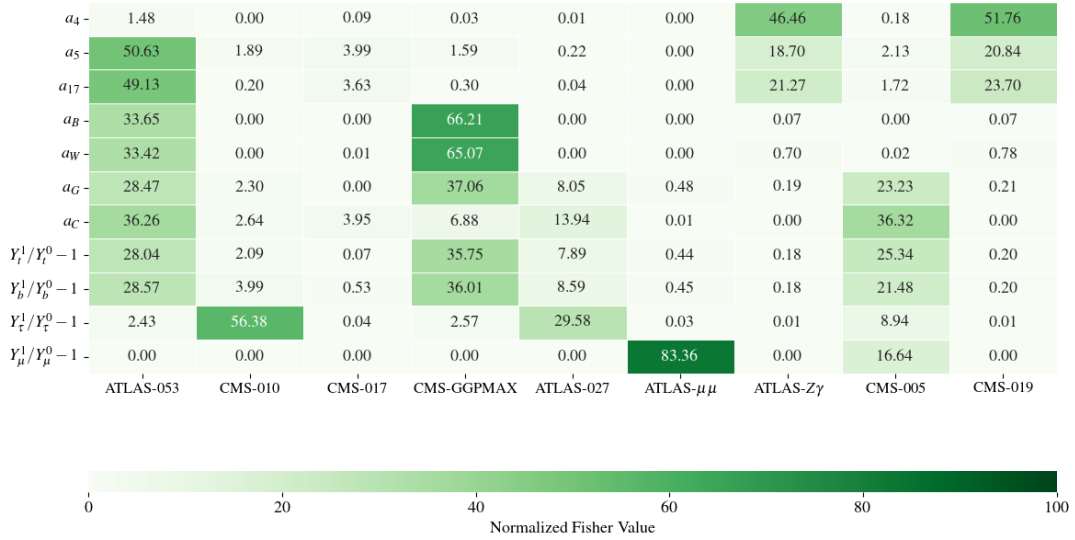


Figure 5.15: Normalized Fisher Value for the Wilson coefficients that affect the Higgs couplings. Results for the analysis where we included only the linear anomalous contribution. The entries are normalized in such a way that the sum of the diagonal elements of the Fisher matrix for a specific Wilson coefficient is 100.

to observables. In particular, we can obtain the covariance matrix for observables of the type

$$\sigma_l = \sigma_l^{\text{SM}} + \sum_i \sigma_l^{A,i} c^i + \mathcal{O}(c^2), \quad (5.20)$$

with  $c$  being the Wilson coefficients. The analytical expression for the covariance matrix among the  $\sigma_i$ 's is

$$\text{cov}(\sigma_l, \sigma_m) = \sum_{i,j=1}^N \sigma_l^{A,i} V^{ij} \sigma_m^{A,j}, \quad (5.21)$$

with  $V$  being the covariance matrix among the Wilson coefficients.

We use the expression above to obtain the correlation matrix among the Higgs branching ratios, Figure 5.16, and also for the cross-section for the different Higgs production modes normalized the total production cross-section, Figure 5.17.

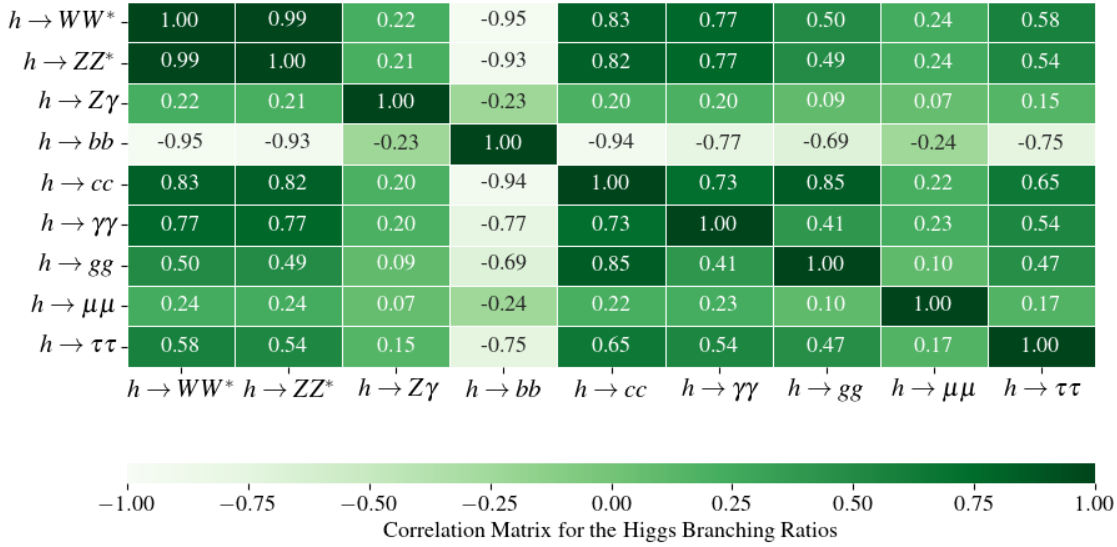


Figure 5.16: Correlation Matrix for the Higgs Branching Ratios. Results for the analysis where we included only the linear anomalous contribution.

The one-dimensional marginalized projections of  $\Delta\chi^2$  for the Higgs Branching Ratios (BRs) are shown in Figure 5.18. Looking to the two-dimensional projections in Figure 5.19, we see that the  $\text{BR}(H \rightarrow ZZ^*)$  and  $\text{BR}(H \rightarrow WW^*)$  are highly correlated, since we have the same Wilson coefficients affecting the same vertices  $HZZ$  and  $HWW$  as we show in equation (4.66). In special, the coefficient  $\Delta a_C$  plays an important role because it affects the couplings  $g_{HZZ}^{(3)}$  and  $g_{HWW}^{(3)}$  in the same form. Also, we see that the SM prediction for the  $\text{BR}(H \rightarrow Z\gamma)$  is more than  $1\sigma$  away from our best-fit value. This happens because the SS measured we used as an input in our fit is almost  $1\sigma$  away from the SM prediction. Lastly, the  $\text{BR}(H \rightarrow \gamma\gamma)$  and  $\text{BR}(H \rightarrow ZZ^*)$  are correlated since the coefficients  $a_B$  and  $a_W$  affect both vertices  $H\gamma\gamma$  and  $HZZ$ . In particular, the Higgs decaying to photons data is very important to constrain the coefficients  $a_B$  and  $a_W$ . As a result, both parameters are almost total anti-correlated, *i.e* their correlation is -0.999.



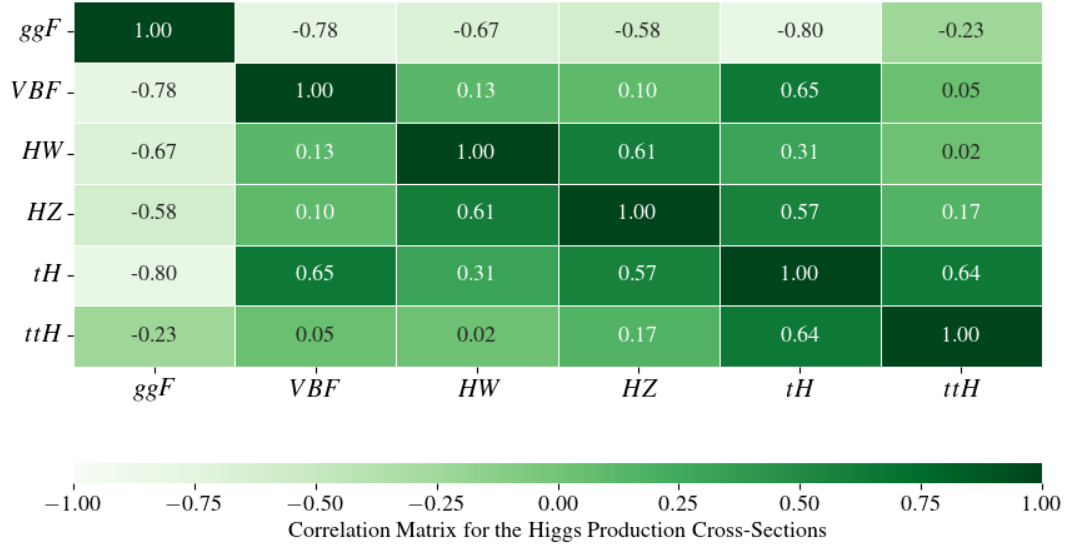


Figure 5.17: Correlation Matrix for the Higgs Production Cross-Sections normalized by the total production cross-section. Results for the analysis where we included only the linear anomalous contribution.

The one- and two- dimensional projections of the  $\Delta\chi^2$  for the Higgs production modes are shown in Figure 5.20. The same effects that have appeared in the BR confidence regions are present here. The cross-sections  $\sigma(HW)$  and  $\sigma(HZ)$  are correlated since we have the same Wilson coefficients affecting the vertices  $HW$  and  $HZ$ , *e.g.*  $\Delta a_C$ . The cross-sections  $\sigma(ggF)$ , Higgs production by gluon fusion, and  $\sigma(ttH)$ , Higgs production with top quarks, are correlated since the top-quark Yukawa  $Y_t^{(1)}$  enters in both processes.

Finally, we translated the bounds to two observables: the SS for the Higgs decaying to muons ( $\mu(H \rightarrow \mu\mu)$ ) and for the SS of the Higgs decaying to two gauge bosons ( $\mu(H \rightarrow Z\gamma)$ ). The one- and two- dimensional projections are displayed in Figure 5.21. Note that our best-fit value for the SS of  $H \rightarrow Z\gamma$  is close to the ATLAS SS data, which shows that, although the branching ratio for  $H \rightarrow Z\gamma$  is away from the SM prediction, our SS result is compatible with the data.

Lastly, we noticed that our conclusions agree with the ones in [8]. Our results show no tension with the SM within  $2\sigma$ . As we discussed in [8] and we briefly mentioned before, the Higgs kinematic distributions are important to remove some degenerate solutions when the fit is performed taking into account also the quadratic contributions of the Wilson coefficients.

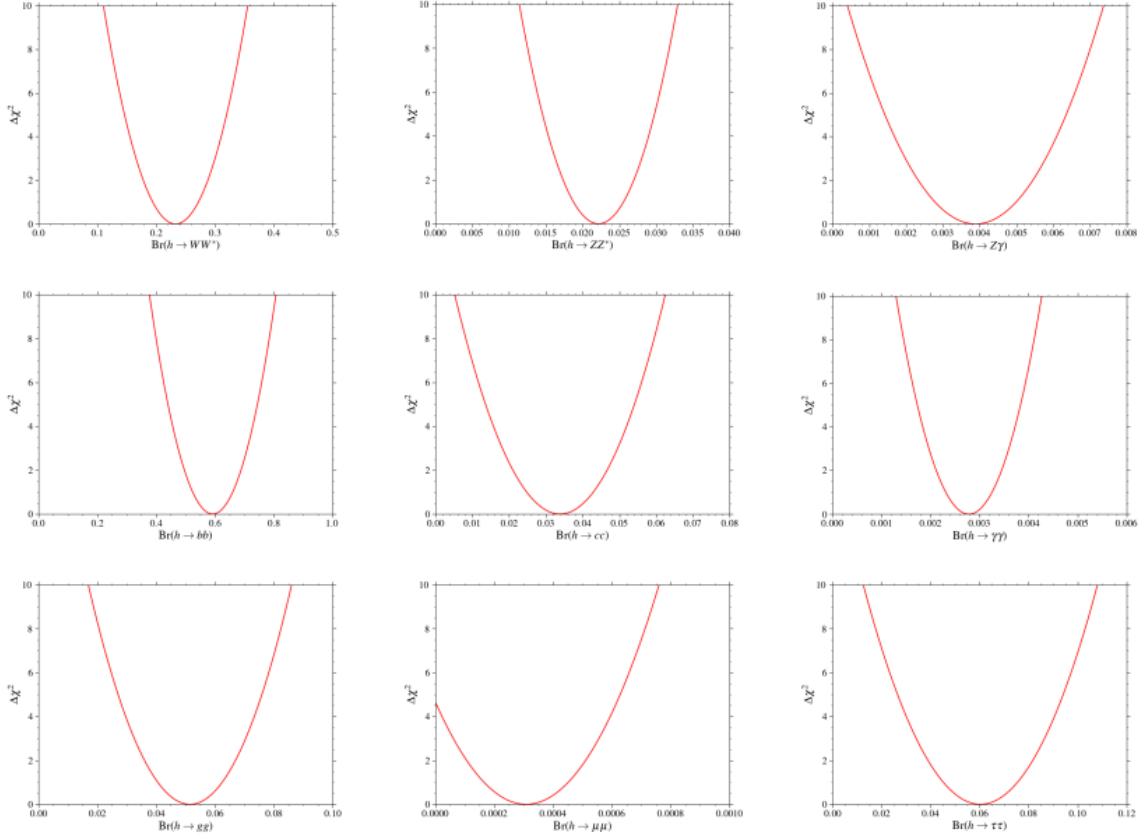


Figure 5.18: One-dimensional marginalized projection of the  $\Delta\chi^2$  for the Higgs branching ratios (BRs).

## 5.4 Discussion and conclusion

In this dissertation we present the analyses of the LHC data on gauge boson pair production and vector boson fusion as well as Higgs observables using the HEFT. Our results show no tension with the SM predictions. For the TGC couplings observables we had 4 effective operators, while for the Higgs observables we had 11. Also, for the latter we used the Higgs kinematic distributions in the form of STXS together with the SS data. In summary, the  $\chi^2$  values for the TGC and Higgs observables evaluated at the SM prediction give

$$\begin{aligned}\chi_{\text{TGC, SM}}^2 &= 64.8, \quad 73 \text{ observables,} \\ \chi_{\text{Higgs, SM}}^2 &= 69.7, \quad 68 \text{ observables.}\end{aligned}\tag{5.22}$$

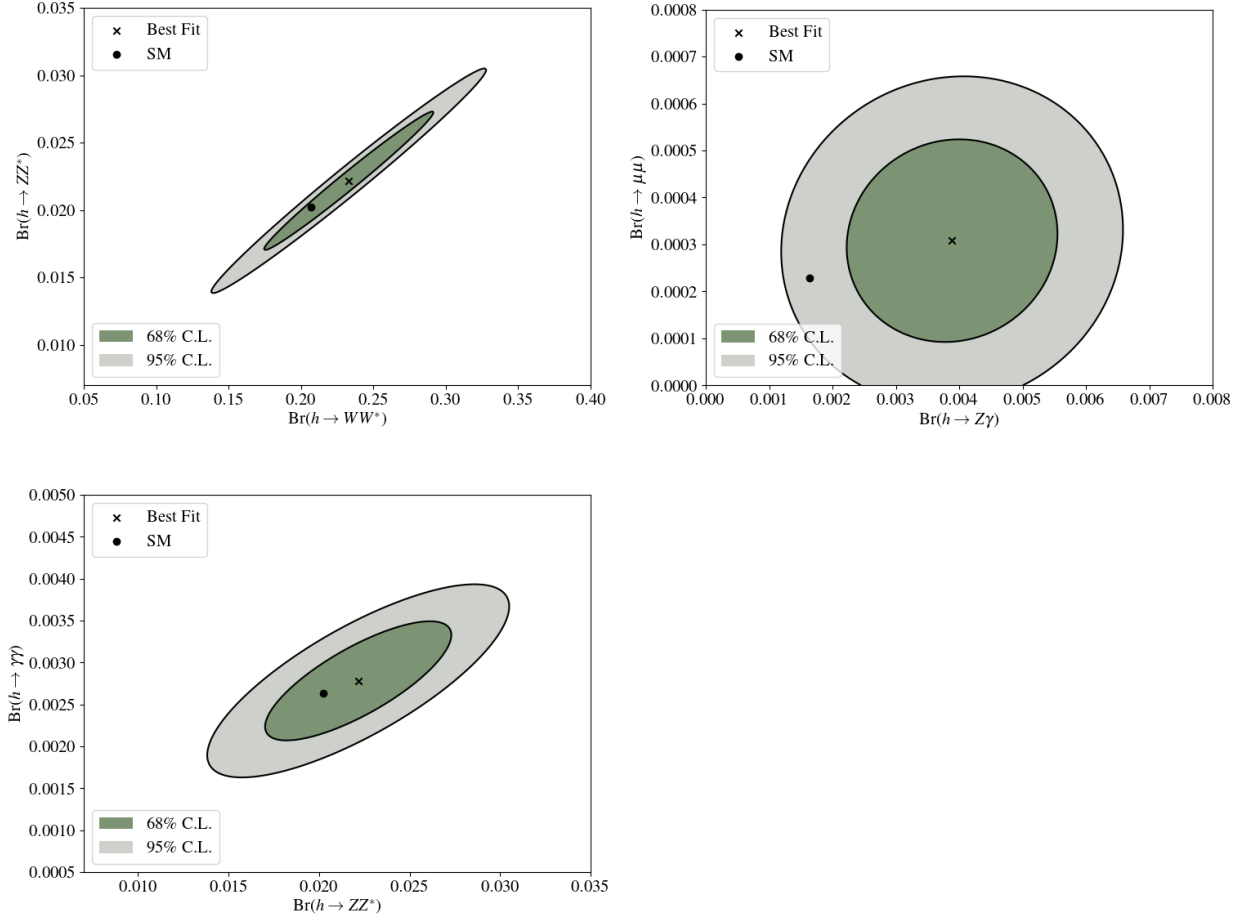


Figure 5.19: Two dimension marginalized projections for the Higgs Branching Ratios  $\text{BR}(H \rightarrow ZZ^*)$ ,  $\text{BR}(H \rightarrow WW^*)$ , and  $\text{BR}(H \rightarrow Z\gamma)$ , as indicated in the panels after marginalizing over the remaining fit parameters.

Meanwhile, evaluating at our best-fit values, we obtain

$$\begin{aligned} \chi_{\min, \text{TGC Linear [Quadratic]} }^2 &= 64.1[64.2], \quad 73 \text{ observables \& 4 coefficients,} \\ \chi_{\min, \text{Higgs Linear}}^2 &= 62.0, \quad 68 \text{ observables \& 11 coefficients.} \end{aligned} \quad (5.23)$$

As we said previously, in the HEFT we are allowed to make the analysis of the TGC and Higgs data separately since we do not account a Higgs bosons doublet in the construction of the EFT. This is not possible in the SMEFT for instance. In Chapter 4.4, we defined 4 variables that are useful to study the correlations present in the TGC and Higgs data. In Figure 5.22, we present their one-dimension projections for the  $\Delta\chi^2$ , and in Figure 5.23 we present the respective confidence regions. This analysis was performed only taking into account the linear

contribution of the Wilson coefficients.

In particular, the  $\Delta$ 's value should be zero in the linear realization of the SM gauge symmetry, and the  $\Sigma$ 's should be proportional to the Wilson coefficients  $f_B$  and  $f_W$  from the HISZ basis [9]. In summary, using data gathered from the LHC Run 2 concerning TGC observables and Higgs observables in the form of STXS and SS, we learn that, at the present, it is not possible to distinguish between the two possible scenarios for the Higgs nature.

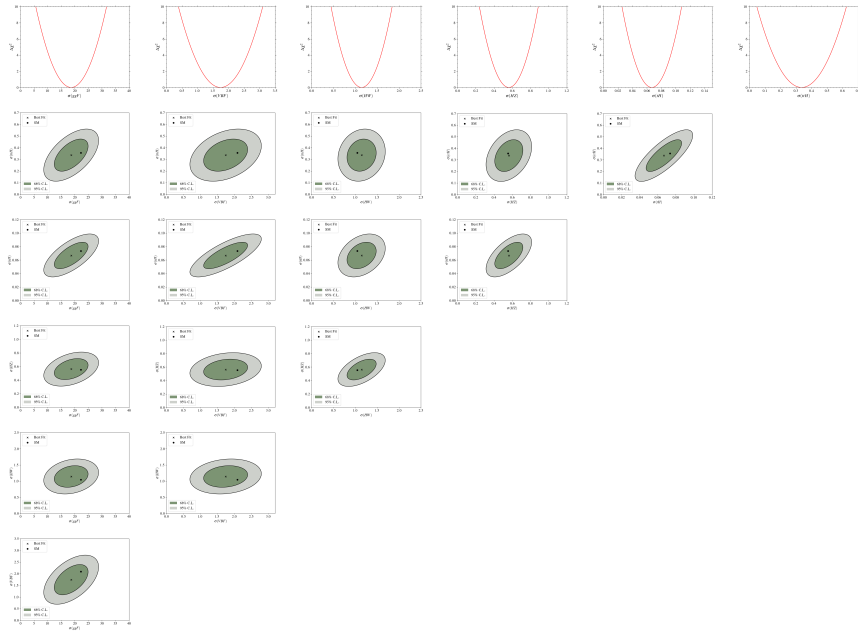


Figure 5.20: One- and two- dimensional marginalized projections of the  $\Delta\chi^2$  for the Higgs production cross sections as indicated on the panels.

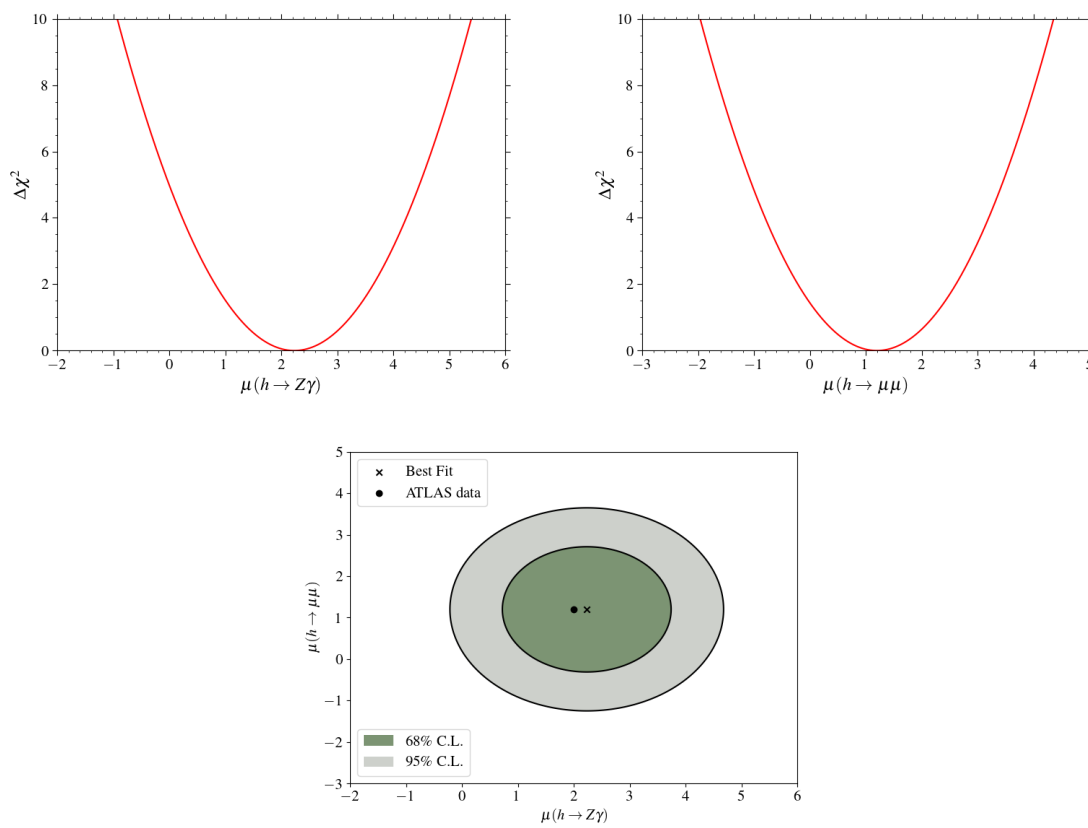


Figure 5.21: One dimension projection and two dimensional confidence regions for the SS of  $H \rightarrow \mu\mu$  and  $H \rightarrow Z\gamma$ .

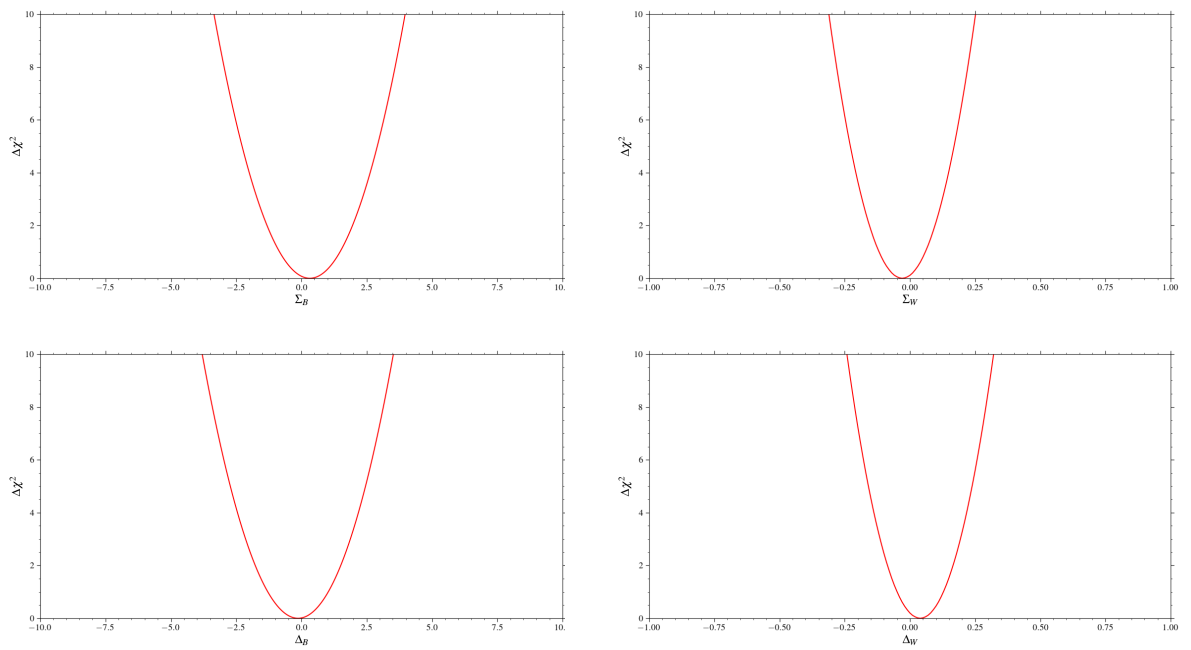


Figure 5.22: One dimension projection for the variables  $\Sigma_B$ ,  $\Sigma_W$ ,  $\Delta_B$ , and  $\Delta_W$  after marginalizing with respect to the fit parameters. The results are shown for the analysis including only the linear contribution for the Wilson coefficients.

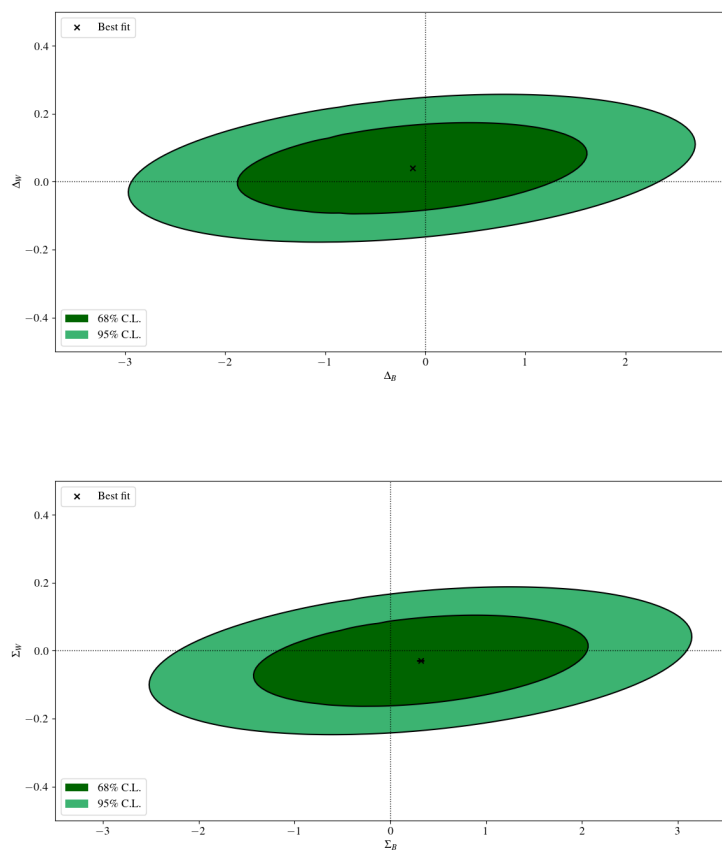


Figure 5.23: Two dimension confidence region for the variables  $\Delta_B$  and  $\Delta_W$  after marginalizing with respect to the fit parameters. The results are shown for the analysis including only the linear contribution for the Wilson coefficients.



---

# CONCLUSIONS

As we discussed at the beginning of the dissertation, one of the ways to encode possible deviations presented in the data gathered from the LHC Collaborations is using EFTs. In this work, we mentioned two parametrizations, the SMEFT, and the HEFT. Both of them can accommodate possible indirect signals of new physics, but they differ on how the SM gauge symmetry is realized at low-energies on the scalar sector. The first one assumes a linear realization of the symmetry, ensuring symmetry relations among the observed Higgs boson and the Goldstone bosons from the EWSB. Meanwhile, the latter considers a non-linear realization, and such relations are absent. Investigating how the symmetry is realized at low-energies has the potential to rule out some extensions of the SM. For instance, if the symmetry is non-linearly realized it may be an indication that the new physics is strongly coupled [89].

This dissertation was divided in two parts. The first one was responsible for introducing the basic concepts regarding EFTs, followed by a discussion of the SM, SMEFT, and HEFT. In the second part, we provided an analysis of the TGCs and Higgs observables in terms of the HEFT.

Our analysis had 15 parameters, 4 of them affecting TGCs and 11 affecting Higgs physics. For the TGCs we used all available data from the LHC Run 2 concerning diboson production of  $WZ$ ,  $WW$ , and  $W\gamma$  pairs as well as the vector boson fusion in the production of  $Z$ 's. For the Higgs observables we used the most recent Higgs kinematic distributions in the form of STXS as well as total SS. The TGC analysis was carried out at linear order and also up to the quadratic order in the Wilson coefficients, while for the Higgs analysis the fit was performed only at linear order.

Our analysis shows no tension with the SM within  $2\sigma$ . Moreover, we pointed out that, with the current data, is not possible to distinguish among the two possible realizations of the SM gauge symmetry in the scalar sector. Nevertheless, our work contains the most up-to-date analy-

sis of the LHC data in terms of the HEFT and we were also able to improve the existent bounds in the literature, as we summarized in [8].

---

# BIBLIOGRAPHY

- [1] Georges Aad et al. “Observation of a new particle in the search for the Standard Model Higgs boson with the ATLAS detector at the LHC”. In: *Phys. Lett. B* 716 (2012), pp. 1–29. DOI: [10.1016/j.physletb.2012.08.020](https://doi.org/10.1016/j.physletb.2012.08.020). arXiv: [1207.7214](https://arxiv.org/abs/1207.7214) [hep-ex].
- [2] Serguei Chatrchyan et al. “Observation of a New Boson at a Mass of 125 GeV with the CMS Experiment at the LHC”. In: *Phys. Lett. B* 716 (2012), pp. 30–61. DOI: [10.1016/j.physletb.2012.08.021](https://doi.org/10.1016/j.physletb.2012.08.021). arXiv: [1207.7235](https://arxiv.org/abs/1207.7235) [hep-ex].
- [3] A. Arbey and F. Mahmoudi. “Dark matter and the early Universe: a review”. In: *Prog. Part. Nucl. Phys.* 119 (2021), p. 103865. DOI: [10.1016/j.pnpnp.2021.103865](https://doi.org/10.1016/j.pnpnp.2021.103865). arXiv: [2104.11488](https://arxiv.org/abs/2104.11488) [hep-ph].
- [4] R. D. Peccei. “The Strong CP problem and axions”. In: *Lect. Notes Phys.* 741 (2008). Ed. by Markus Kuster, Georg Raffelt, and Berta Beltran, pp. 3–17. DOI: [10.1007/978-3-540-73518-2\\_1](https://doi.org/10.1007/978-3-540-73518-2_1). arXiv: [hep-ph/0607268](https://arxiv.org/abs/hep-ph/0607268).
- [5] Michael Dine. “Naturalness Under Stress”. In: *Ann. Rev. Nucl. Part. Sci.* 65 (2015), pp. 43–62. DOI: [10.1146/annurev-nucl-102014-022053](https://doi.org/10.1146/annurev-nucl-102014-022053). arXiv: [1501.01035](https://arxiv.org/abs/1501.01035) [hep-ph].
- [6] Miguel G. Folgado and Veronica Sanz. “On the Interpretation of Nonresonant Phenomena at Colliders”. In: *Adv. High Energy Phys.* 2021 (2021), p. 2573471. DOI: [10.1155/2021/2573471](https://doi.org/10.1155/2021/2573471). arXiv: [2005.06492](https://arxiv.org/abs/2005.06492) [hep-ph].
- [7] Ilaria Brivio and Michael Trott. “The Standard Model as an Effective Field Theory”. In: *Phys. Rept.* 793 (2019), pp. 1–98. DOI: [10.1016/j.physrep.2018.11.002](https://doi.org/10.1016/j.physrep.2018.11.002). arXiv: [1706.08945](https://arxiv.org/abs/1706.08945) [hep-ph].

- [8] Oscar J. P. Eboli, M. C. Gonzalez-Garcia, and Matheus Martines. “Electroweak Higgs effective field theory after LHC run 2”. In: *Phys. Rev. D* 105.5 (2022), p. 053003. DOI: [10.1103/PhysRevD.105.053003](https://doi.org/10.1103/PhysRevD.105.053003). arXiv: [2112.11468](https://arxiv.org/abs/2112.11468) [hep-ph].
- [9] Eduardo da Silva Almeida et al. “Electroweak legacy of the LHC run II”. In: *Phys. Rev. D* 105.1 (2022), p. 013006. DOI: [10.1103/PhysRevD.105.013006](https://doi.org/10.1103/PhysRevD.105.013006). arXiv: [2108.04828](https://arxiv.org/abs/2108.04828) [hep-ph].
- [10] J. de Blas et al. “Global analysis of electroweak data in the Standard Model”. In: (Dec. 2021). arXiv: [2112.07274](https://arxiv.org/abs/2112.07274) [hep-ph].
- [11] Jacob J. Ethier et al. “Combined SMEFT interpretation of Higgs, diboson, and top quark data from the LHC”. In: *JHEP* 11 (2021), p. 089. DOI: [10.1007/JHEP11\(2021\)089](https://doi.org/10.1007/JHEP11(2021)089). arXiv: [2105.00006](https://arxiv.org/abs/2105.00006) [hep-ph].
- [12] John Ellis et al. “Top, Higgs, Diboson and Electroweak Fit to the Standard Model Effective Field Theory”. In: *JHEP* 04 (2021), p. 279. DOI: [10.1007/JHEP04\(2021\)279](https://doi.org/10.1007/JHEP04(2021)279). arXiv: [2012.02779](https://arxiv.org/abs/2012.02779) [hep-ph].
- [13] I. Brivio et al. “The complete HEFT Lagrangian after the LHC Run I”. In: *Eur. Phys. J. C* 76.7 (2016), p. 416. DOI: [10.1140/epjc/s10052-016-4211-9](https://doi.org/10.1140/epjc/s10052-016-4211-9). arXiv: [1604.06801](https://arxiv.org/abs/1604.06801) [hep-ph].
- [14] I. Brivio et al. “Disentangling a dynamical Higgs”. In: *JHEP* 03 (2014), p. 024. DOI: [10.1007/JHEP03\(2014\)024](https://doi.org/10.1007/JHEP03(2014)024). arXiv: [1311.1823](https://arxiv.org/abs/1311.1823) [hep-ph].
- [15] C. P. Burgess. “Intro to Effective Field Theories and Inflation”. In: (Nov. 2017). arXiv: [1711.10592](https://arxiv.org/abs/1711.10592) [hep-th].
- [16] David B. Kaplan. “Five lectures on effective field theory”. In: Oct. 2005. arXiv: [nuc1-th/0510023](https://arxiv.org/abs/nuc1-th/0510023).
- [17] Riccardo Penco. “An Introduction to Effective Field Theories”. In: (June 2020). arXiv: [2006.16285](https://arxiv.org/abs/2006.16285) [hep-th].
- [18] H. Georgi. “Effective field theory”. In: *Ann. Rev. Nucl. Part. Sci.* 43 (1993), pp. 209–252. DOI: [10.1146/annurev.ns.43.120193.001233](https://doi.org/10.1146/annurev.ns.43.120193.001233).
- [19] Gustavo Burdman. *Quantum Field Theory*. 2020. URL: <http://fma.if.usp.br/~burdman/QFT1/qft1index.html>.
- [20] Matthew D. Schwartz. *Quantum Field Theory and the Standard Model*. Cambridge University Press, Mar. 2014. ISBN: 978-1-107-03473-0, 978-1-107-03473-0.
- [21] Timothy Cohen. “As Scales Become Separated: Lectures on Effective Field Theory”. In: *PoS TASI2018* (2019), p. 011. arXiv: [1903.03622](https://arxiv.org/abs/1903.03622) [hep-ph].

- [22] Timothy Cohen, Xiaochuan Lu, and Zhengkang Zhang. “Functional Prescription for EFT Matching”. In: *JHEP* 02 (2021), p. 228. DOI: [10.1007/JHEP02\(2021\)228](https://doi.org/10.1007/JHEP02(2021)228). arXiv: [2011.02484](https://arxiv.org/abs/2011.02484) [hep-ph].
- [23] C. P. Burgess. *Introduction to Effective Field Theory*. Cambridge University Press, Dec. 2020. ISBN: 978-1-109-04804-0, 978-0-521-19547-8. DOI: [10.1017/9781139048040](https://doi.org/10.1017/9781139048040).
- [24] John C. Collins. *Renormalization: An Introduction to Renormalization, The Renormalization Group, and the Operator Product Expansion*. Vol. 26. Cambridge Monographs on Mathematical Physics. Cambridge: Cambridge University Press, 1986. ISBN: 978-0-521-31177-9, 978-0-511-86739-2. DOI: [10.1017/CBO9780511622656](https://doi.org/10.1017/CBO9780511622656).
- [25] C. G. Bollini and J. J. Giambiagi. “Dimensional Renormalization: The Number of Dimensions as a Regularizing Parameter”. In: *Nuovo Cim. B* 12 (1972), pp. 20–26. DOI: [10.1007/BF02895558](https://doi.org/10.1007/BF02895558).
- [26] Gerard 't Hooft and M. J. G. Veltman. “Regularization and Renormalization of Gauge Fields”. In: *Nucl. Phys. B* 44 (1972), pp. 189–213. DOI: [10.1016/0550-3213\(72\)90279-9](https://doi.org/10.1016/0550-3213(72)90279-9).
- [27] Michael E. Peskin and Daniel V. Schroeder. *An Introduction to quantum field theory*. Reading, USA: Addison-Wesley, 1995. ISBN: 978-0-201-50397-5.
- [28] Brian Henning, Xiaochuan Lu, and Hitoshi Murayama. “How to use the Standard Model effective field theory”. In: *JHEP* 01 (2016), p. 023. DOI: [10.1007/JHEP01\(2016\)023](https://doi.org/10.1007/JHEP01(2016)023). arXiv: [1412.1837](https://arxiv.org/abs/1412.1837) [hep-ph].
- [29] Claudius G. Krause. “Higgs Effective Field Theories - Systematics and Applications”. PhD thesis. Munich U., 2016. DOI: [10.5282/edoc.19873](https://doi.org/10.5282/edoc.19873). arXiv: [1610.08537](https://arxiv.org/abs/1610.08537) [hep-ph].
- [30] Jeremy Bernstein. “Spontaneous symmetry breaking, gauge theories, the Higgs mechanism and all that”. In: *Rev. Mod. Phys.* 46 (1 Jan. 1974), pp. 7–48. DOI: [10.1103/RevModPhys.46.7](https://doi.org/10.1103/RevModPhys.46.7). URL: <https://link.aps.org/doi/10.1103/RevModPhys.46.7>.
- [31] Jeffrey Goldstone, Abdus Salam, and Steven Weinberg. “Broken Symmetries”. In: *Phys. Rev.* 127 (3 Aug. 1962), pp. 965–970. DOI: [10.1103/PhysRev.127.965](https://doi.org/10.1103/PhysRev.127.965). URL: <https://link.aps.org/doi/10.1103/PhysRev.127.965>.

- [32] Sheldon L. Glashow. “Partial-symmetries of weak interactions”. In: *Nuclear Physics* 22.4 (1961), pp. 579–588. ISSN: 0029-5582. DOI: [https://doi.org/10.1016/0029-5582\(61\)90469-2](https://doi.org/10.1016/0029-5582(61)90469-2). URL: <https://www.sciencedirect.com/science/article/pii/0029558261904692>.
- [33] Steven Weinberg. “A Model of Leptons”. In: *Phys. Rev. Lett.* 19 (21 Nov. 1967), pp. 1264–1266. DOI: [10.1103/PhysRevLett.19.1264](https://doi.org/10.1103/PhysRevLett.19.1264). URL: <https://link.aps.org/doi/10.1103/PhysRevLett.19.1264>.
- [34] Abdus Salam. “Weak and Electromagnetic Interactions”. In: *Conf. Proc. C* 680519 (1968), pp. 367–377. DOI: [10.1142/9789812795915\\_0034](https://doi.org/10.1142/9789812795915_0034).
- [35] Peter W. Higgs. “Broken Symmetries and the Masses of Gauge Bosons”. In: *Phys. Rev. Lett.* 13 (16 Oct. 1964), pp. 508–509. DOI: [10.1103/PhysRevLett.13.508](https://doi.org/10.1103/PhysRevLett.13.508). URL: <https://link.aps.org/doi/10.1103/PhysRevLett.13.508>.
- [36] F. Englert and R. Brout. “Broken Symmetry and the Mass of Gauge Vector Mesons”. In: *Phys. Rev. Lett.* 13 (9 Aug. 1964), pp. 321–323. DOI: [10.1103/PhysRevLett.13.321](https://doi.org/10.1103/PhysRevLett.13.321). URL: <https://link.aps.org/doi/10.1103/PhysRevLett.13.321>.
- [37] S. Schael et al. “Precision electroweak measurements on the  $Z$  resonance”. In: *Phys. Rept.* 427 (2006), pp. 257–454. DOI: [10.1016/j.physrep.2005.12.006](https://doi.org/10.1016/j.physrep.2005.12.006). arXiv: [hep-ex/0509008](https://arxiv.org/abs/hep-ex/0509008).
- [38] S. Schael et al. “Electroweak Measurements in Electron-Positron Collisions at W-Boson-Pair Energies at LEP”. In: *Phys. Rept.* 532 (2013), pp. 119–244. DOI: [10.1016/j.physrep.2013.07.004](https://doi.org/10.1016/j.physrep.2013.07.004). arXiv: [1302.3415](https://arxiv.org/abs/1302.3415) [hep-ex].
- [39] John F. Gunion et al. *The Higgs Hunter’s Guide*. Vol. 80. 2000.
- [40] W. Buchmuller and D. Wyler. “Effective Lagrangian Analysis of New Interactions and Flavor Conservation”. In: *Nucl. Phys. B* 268 (1986), pp. 621–653. DOI: [10.1016/0550-3213\(86\)90262-2](https://doi.org/10.1016/0550-3213(86)90262-2).
- [41] Steven Weinberg. “Baryon- and Lepton-Nonconserving Processes”. In: *Phys. Rev. Lett.* 43 (21 Nov. 1979), pp. 1566–1570. DOI: [10.1103/PhysRevLett.43.1566](https://doi.org/10.1103/PhysRevLett.43.1566). URL: <https://link.aps.org/doi/10.1103/PhysRevLett.43.1566>.
- [42] Christopher Arzt. “Reduced effective Lagrangians”. In: *Phys. Lett. B* 342 (1995), pp. 189–195. DOI: [10.1016/0370-2693\(94\)01419-D](https://doi.org/10.1016/0370-2693(94)01419-D). arXiv: [hep-ph/9304230](https://arxiv.org/abs/hep-ph/9304230).

- [43] B. Grzadkowski et al. “Dimension-Six Terms in the Standard Model Lagrangian”. In: *JHEP* 10 (2010), p. 085. DOI: [10.1007/JHEP10\(2010\)085](https://doi.org/10.1007/JHEP10(2010)085). arXiv: [1008.4884](https://arxiv.org/abs/1008.4884) [hep-ph].
- [44] Kaoru Hagiwara et al. “Probing nonstandard bosonic interactions via W boson pair production at lepton colliders”. In: *Nucl. Phys. B* 496 (1997), pp. 66–102. DOI: [10.1016/S0550-3213\(97\)00208-3](https://doi.org/10.1016/S0550-3213(97)00208-3). arXiv: [hep-ph/9612268](https://arxiv.org/abs/hep-ph/9612268).
- [45] K. Hagiwara et al. “Low energy effects of new interactions in the electroweak boson sector”. In: *Phys. Rev. D* 48 (5 Sept. 1993), pp. 2182–2203. DOI: [10.1103/PhysRevD.48.2182](https://doi.org/10.1103/PhysRevD.48.2182). URL: <https://link.aps.org/doi/10.1103/PhysRevD.48.2182>.
- [46] G. F. Giudice et al. “The Strongly-Interacting Light Higgs”. In: *JHEP* 06 (2007), p. 045. DOI: [10.1088/1126-6708/2007/06/045](https://doi.org/10.1088/1126-6708/2007/06/045). arXiv: [hep-ph/0703164](https://arxiv.org/abs/hep-ph/0703164).
- [47] Celine Degrande. “A basis of dimension-eight operators for anomalous neutral triple gauge boson interactions”. In: *JHEP* 02 (2014), p. 101. DOI: [10.1007/JHEP02\(2014\)101](https://doi.org/10.1007/JHEP02(2014)101). arXiv: [1308.6323](https://arxiv.org/abs/1308.6323) [hep-ph].
- [48] Celine Degrande et al. “Effective Field Theory: A Modern Approach to Anomalous Couplings”. In: *Annals Phys.* 335 (2013), pp. 21–32. DOI: [10.1016/j.aop.2013.04.016](https://doi.org/10.1016/j.aop.2013.04.016). arXiv: [1205.4231](https://arxiv.org/abs/1205.4231) [hep-ph].
- [49] Rodrigo Alonso et al. “Renormalization Group Evolution of the Standard Model Dimension Six Operators III: Gauge Coupling Dependence and Phenomenology”. In: *JHEP* 04 (2014), p. 159. DOI: [10.1007/JHEP04\(2014\)159](https://doi.org/10.1007/JHEP04(2014)159). arXiv: [1312.2014](https://arxiv.org/abs/1312.2014) [hep-ph].
- [50] Ilaria Brivio. “SMEFTsim 3.0 — a practical guide”. In: *JHEP* 04 (2021), p. 073. DOI: [10.1007/JHEP04\(2021\)073](https://doi.org/10.1007/JHEP04(2021)073). arXiv: [2012.11343](https://arxiv.org/abs/2012.11343) [hep-ph].
- [51] Tyler Corbett et al. “Robust Determination of the Higgs Couplings: Power to the Data”. In: *Phys. Rev. D* 87 (2013), p. 015022. DOI: [10.1103/PhysRevD.87.015022](https://doi.org/10.1103/PhysRevD.87.015022). arXiv: [1211.4580](https://arxiv.org/abs/1211.4580) [hep-ph].
- [52] Stefan Scherer. “Introduction to chiral perturbation theory”. In: *Adv. Nucl. Phys.* 27 (2003). Ed. by John W. Negele and E. W. Vogt, p. 277. arXiv: [hep-ph/0210398](https://arxiv.org/abs/hep-ph/0210398).
- [53] S. Coleman, J. Wess, and Bruno Zumino. “Structure of Phenomenological Lagrangians. I”. In: *Phys. Rev.* 177 (5 Jan. 1969), pp. 2239–2247. DOI: [10.1103/PhysRev.177.2239](https://doi.org/10.1103/PhysRev.177.2239). URL: <https://link.aps.org/doi/10.1103/PhysRev.177.2239>.

- [54] Curtis G. Callan et al. “Structure of Phenomenological Lagrangians. II”. In: *Phys. Rev.* 177 (5 Jan. 1969), pp. 2247–2250. DOI: [10.1103/PhysRev.177.2247](https://doi.org/10.1103/PhysRev.177.2247). URL: <https://link.aps.org/doi/10.1103/PhysRev.177.2247>.
- [55] F. Feruglio. “The Chiral approach to the electroweak interactions”. In: *Int. J. Mod. Phys. A* 8 (1993), pp. 4937–4972. DOI: [10.1142/S0217751X93001946](https://doi.org/10.1142/S0217751X93001946). arXiv: [hep-ph/9301281](https://arxiv.org/abs/hep-ph/9301281).
- [56] Gilberto Colangelo and Gino Isidori. “An Introduction to ChPT”. In: *Frascati Phys. Ser.* 18 (2000). Ed. by G. Panzeri, pp. 333–376. arXiv: [hep-ph/0101264](https://arxiv.org/abs/hep-ph/0101264).
- [57] W. K. Tung. *GROUP THEORY IN PHYSICS*. 1985.
- [58] Steven Weinberg. *The quantum theory of fields. Vol. 2: Modern applications*. Cambridge University Press, Aug. 2013. ISBN: 978-1-139-63247-8, 978-0-521-67054-8, 978-0-521-55002-4.
- [59] Steven Weinberg. “Phenomenological Lagrangians”. In: *Physica A: Statistical Mechanics and its Applications* 96.1 (1979), pp. 327–340. ISSN: 0378-4371. DOI: [https://doi.org/10.1016/0378-4371\(79\)90223-1](https://doi.org/10.1016/0378-4371(79)90223-1). URL: <https://www.sciencedirect.com/science/article/pii/0378437179902231>.
- [60] Morad Aaboud et al. “Search for heavy resonances decaying into  $WW$  in the  $e\nu\mu\nu$  final state in  $pp$  collisions at  $\sqrt{s} = 13$  TeV with the ATLAS detector”. In: *Eur. Phys. J. C* 78.1 (2018), p. 24. DOI: [10.1140/epjc/s10052-017-5491-4](https://doi.org/10.1140/epjc/s10052-017-5491-4). arXiv: [1710.01123](https://arxiv.org/abs/1710.01123) [[hep-ex](https://arxiv.org/abs/1710.01123)].
- [61] Georges Aad et al. “Measurements of  $W^+W^- + \geq 1$  jet production cross-sections in  $pp$  collisions at  $\sqrt{s} = 13$  TeV with the ATLAS detector”. In: *JHEP* 06 (2021), p. 003. DOI: [10.1007/JHEP06\(2021\)003](https://doi.org/10.1007/JHEP06(2021)003). arXiv: [2103.10319](https://arxiv.org/abs/2103.10319) [[hep-ex](https://arxiv.org/abs/2103.10319)].
- [62] “Measurement of  $W^\pm Z$  production cross sections and gauge boson polarisation in  $pp$  collisions at  $\sqrt{s} = 13$  TeV with the ATLAS detector”. In: (July 2018).
- [63] Georges Aad et al. “Differential cross-section measurements for the electroweak production of dijets in association with a  $Z$  boson in proton–proton collisions at ATLAS”. In: *Eur. Phys. J. C* 81.2 (2021), p. 163. DOI: [10.1140/epjc/s10052-020-08734-w](https://doi.org/10.1140/epjc/s10052-020-08734-w). arXiv: [2006.15458](https://arxiv.org/abs/2006.15458) [[hep-ex](https://arxiv.org/abs/2006.15458)].
- [64] “ $W^\pm\gamma$  differential cross sections and effective field theory constraints at  $\sqrt{s} = 13$  TeV”. In: (2021).
- [65] “Measurement of the  $pp \rightarrow WZ$  inclusive and differential cross sections, polarization angles and search for anomalous gauge couplings at  $\sqrt{s} = 13$  TeV”. In: (2021).



- [66] Albert M Sirunyan et al. “ $W^+W^-$  boson pair production in proton-proton collisions at  $\sqrt{s} = 13$  TeV”. In: *Phys. Rev. D* 102.9 (2020), p. 092001. DOI: [10.1103/PhysRevD.102.092001](https://doi.org/10.1103/PhysRevD.102.092001). arXiv: [2009.00119](https://arxiv.org/abs/2009.00119) [hep-ex].
- [67] Johan Alwall et al. “MadGraph 5 : Going Beyond”. In: *JHEP* 06 (2011), p. 128. DOI: [10.1007/JHEP06\(2011\)128](https://doi.org/10.1007/JHEP06(2011)128). arXiv: [1106.0522](https://arxiv.org/abs/1106.0522) [hep-ph].
- [68] Neil D. Christensen and Claude Duhr. “FeynRules - Feynman rules made easy”. In: *Comput. Phys. Commun.* 180 (2009), pp. 1614–1641. DOI: [10.1016/j.cpc.2009.02.018](https://doi.org/10.1016/j.cpc.2009.02.018). arXiv: [0806.4194](https://arxiv.org/abs/0806.4194) [hep-ph].
- [69] Adam Alloul et al. “FeynRules 2.0 - A complete toolbox for tree-level phenomenology”. In: *Comput. Phys. Commun.* 185 (2014), pp. 2250–2300. DOI: [10.1016/j.cpc.2014.04.012](https://doi.org/10.1016/j.cpc.2014.04.012). arXiv: [1310.1921](https://arxiv.org/abs/1310.1921) [hep-ph].
- [70] Torbjörn Sjöstrand et al. “An introduction to PYTHIA 8.2”. In: *Comput. Phys. Commun.* 191 (2015), pp. 159–177. DOI: [10.1016/j.cpc.2015.01.024](https://doi.org/10.1016/j.cpc.2015.01.024). arXiv: [1410.3012](https://arxiv.org/abs/1410.3012) [hep-ph].
- [71] J. de Favereau et al. “DELPHES 3, A modular framework for fast simulation of a generic collider experiment”. In: *JHEP* 02 (2014), p. 057. DOI: [10.1007/JHEP02\(2014\)057](https://doi.org/10.1007/JHEP02(2014)057). arXiv: [1307.6346](https://arxiv.org/abs/1307.6346) [hep-ex].
- [72] Andrew Fowlie. “LHCO\_reader: A new code for reading and analyzing detector-level events stored in LHCO format”. In: (Oct. 2015). arXiv: [1510.07319](https://arxiv.org/abs/1510.07319) [hep-ph].
- [73] G. Cowan. *Statistical data analysis*. 1998. ISBN: 978-0-19-850156-5.
- [74] G. L. Fogli et al. “Getting the most from the statistical analysis of solar neutrino oscillations”. In: *Phys. Rev. D* 66 (2002), p. 053010. DOI: [10.1103/PhysRevD.66.053010](https://doi.org/10.1103/PhysRevD.66.053010). arXiv: [hep-ph/0206162](https://arxiv.org/abs/hep-ph/0206162).
- [75] D. de Florian et al. “Handbook of LHC Higgs Cross Sections: 4. Deciphering the Nature of the Higgs Sector”. In: 2/2017 (Oct. 2016). DOI: [10.23731/CYRM-2017-002](https://doi.org/10.23731/CYRM-2017-002). arXiv: [1610.07922](https://arxiv.org/abs/1610.07922) [hep-ph].
- [76] Matthew D. Schwartz. “TASI Lectures on Collider Physics”. In: *Proceedings, Theoretical Advanced Study Institute in Elementary Particle Physics : Anticipating the Next Discoveries in Particle Physics (TASI 2016): Boulder, CO, USA, June 6-July 1, 2016*. Ed. by Rouven Essig and Ian Low. 2018, pp. 65–100. DOI: [10.1142/9789813233348\\_0002](https://doi.org/10.1142/9789813233348_0002). arXiv: [1709.04533](https://arxiv.org/abs/1709.04533) [hep-ph].
- [77] “Interpretations of the combined measurement of Higgs boson production and decay”. In: (Oct. 2020).

- [78] “Measurement of Higgs boson production in the decay channel with a pair of  $\tau$  leptons”. In: (2020).
- [79] “Measurement of Higgs boson production in association with a W or Z boson in the  $H \rightarrow WW$  decay channel”. In: (2021).
- [80] “A combination of measurements of Higgs boson production and decay using up to  $139 \text{ fb}^{-1}$  of proton–proton collision data at  $\sqrt{s} = 13 \text{ TeV}$  collected with the ATLAS experiment”. In: (Aug. 2020).
- [81] Georges Aad et al. “A search for the dimuon decay of the Standard Model Higgs boson with the ATLAS detector”. In: *Phys. Lett. B* 812 (2021), p. 135980. DOI: [10.1016/j.physletb.2020.135980](https://doi.org/10.1016/j.physletb.2020.135980). arXiv: [2007.07830](https://arxiv.org/abs/2007.07830) [hep-ex].
- [82] Georges Aad et al. “A search for the  $Z\gamma$  decay mode of the Higgs boson in  $pp$  collisions at  $\sqrt{s} = 13 \text{ TeV}$  with the ATLAS detector”. In: *Phys. Lett. B* 809 (2020), p. 135754. DOI: [10.1016/j.physletb.2020.135754](https://doi.org/10.1016/j.physletb.2020.135754). arXiv: [2005.05382](https://arxiv.org/abs/2005.05382) [hep-ex].
- [83] “Search for the Higgs boson decay to  $Z\gamma$  in proton-proton collisions at  $\sqrt{s} = 13 \text{ TeV}$ ”. In: (2021).
- [84] Valentin Hirschi and Olivier Mattelaer. “Automated event generation for loop-induced processes”. In: *JHEP* 10 (2015), p. 146. DOI: [10.1007/JHEP10\(2015\)146](https://doi.org/10.1007/JHEP10(2015)146). arXiv: [1507.00020](https://arxiv.org/abs/1507.00020) [hep-ph].
- [85] Céline Degrande et al. “Automated one-loop computations in the standard model effective field theory”. In: *Phys. Rev. D* 103.9 (2021), p. 096024. DOI: [10.1103/PhysRevD.103.096024](https://doi.org/10.1103/PhysRevD.103.096024). arXiv: [2008.11743](https://arxiv.org/abs/2008.11743) [hep-ph].
- [86] Andy Buckley et al. “Rivet user manual”. In: *Comput. Phys. Commun.* 184 (2013), pp. 2803–2819. DOI: [10.1016/j.cpc.2013.05.021](https://doi.org/10.1016/j.cpc.2013.05.021). arXiv: [1003.0694](https://arxiv.org/abs/1003.0694) [hep-ph].
- [87] Giuliano Panico, Francesco Riva, and Andrea Wulzer. “Diboson interference resurrection”. In: *Phys. Lett. B* 776 (2018), pp. 473–480. DOI: [10.1016/j.physletb.2017.11.068](https://doi.org/10.1016/j.physletb.2017.11.068). arXiv: [1708.07823](https://arxiv.org/abs/1708.07823) [hep-ph].
- [88] Albert M Sirunyan et al. “Measurements of Higgs boson production cross sections and couplings in the diphoton decay channel at  $\sqrt{s} = 13 \text{ TeV}$ ”. In: *JHEP* 07 (2021), p. 027. DOI: [10.1007/JHEP07\(2021\)027](https://doi.org/10.1007/JHEP07(2021)027). arXiv: [2103.06956](https://arxiv.org/abs/2103.06956) [hep-ex].

- [89] Christopher T. Hill and Elizabeth H. Simmons. “Strong Dynamics and Electroweak Symmetry Breaking”. In: *Phys. Rept.* 381 (2003). [Erratum: *Phys.Rept.* 390, 553–554 (2004)], pp. 235–402. DOI: [10 . 1016 / S0370 - 1573 \(03 \) 00140 - 6](https://doi.org/10.1016/S0370-1573(03)00140-6). arXiv: [hep - ph / 0203079](https://arxiv.org/abs/hep-ph/0203079).